DEVELOPMENT OF A HEAT RECOVERY SYSTEM FOR A 250 KW FLUIDIZED BED GASIFICATION SYSTEM FUELED BY COTTON GIN TRASH

A Dissertation

by

WALTER OOSTHUIZEN

Submitted to the Office of Graduate and Professional Studies of
Texas A&M University
in partial fulfillment of the requirements for the degree of

DOCTOR OF PHILOSOPHY

Chair of Committee,	Sergio C. Capareda
Committee Members,	Ronald E. Lacey
	Calvin B. Parnell
	Jerald A. Caton
Head of Department,	Stephen W. Searcy

December 2018

Major Subject: Biological and Agricultural Engineering

ABSTRACT

Disposing of cotton gin trash (CGT) at gins has been an issue for decades. Instead of a waste byproduct, CGT can be utilized as a sustainable fuel for fluidized bed gasification (FBG). The overall objective of this project was to design and evaluate a FBG system, capable of supplying 250 kW_e of electricity, for commercial manufacturing. Additional research was needed for a heat recovery system (HRS) such that the system could be classified as cogeneration. Two sources of waste heat from the FBG system were identified as syngas and generator exhaust gases. Design of multiple counter-flow heat exchangers heated ambient air to supply thermal energy to gins to reduce fuel usage, resulting in yearly economic savings.

A small-scale heat exchanger was evaluated for syngas cooling, where gasification tests revealed that a fouling layer reduced heat transfer by 30% to 50%. Tar thermal conductivity was estimated to be 0.03 $W\ m^{-1}\ K^{-1}$, which reduced relative errors of heat capture modeling to below 10%. A large-scale heat exchanger was evaluated for correcting a heat transfer model, where relative errors of heat capture were also reduced to below 10%. An HRS model was developed to predict operational characteristics by varying number of heat exchangers. Reducing temperature of both hot gas streams to below 200°C required 17 heat exchangers. Supplying the required air flow rate for a stripper gin resulted in 10 heat exchangers. Conclusions from a cotton drying model and economics analysis revealed that optimal number of heat exchangers were four to five when average thermal demand of natural gas gins was about 0.16 $GJ\ bale^{-1}$, while propane gins were identified as ideal candidates. Five heat exchangers were recommended as the HRS design specifically for the 250 kW_e FBG system, where total heat capture was 260 kW_{th}, overall system efficiency was 21%, and heat capture conversion was 1800 $kJ\ kg_{CGT}^{-1}$.

DEDICATION

To my soon to be fiancée, Karli Gold, for motivating and encouraging me throughout my graduate studies. To my mother, Ingrid Oosthuizen, for the endless and life-long support. To my goddaughter, Jocelynn Briggs, for always inspiring me. To my grandfather, Jurgen Schulz, for teaching me how to pave my path to success. To my father, Johan, and brothers, Jurgen, Johan, and Chris. To my family friends, Stephanie Wolfram and Ana Mier y Teran.

ACKNOWLEDGEMENTS

I would like to thank my committee chair, Dr. Sergio Capareda, for the guidance throughout my Ph.D. career. Also, Dr. Calvin Parnell, Dr. Ronald Lacey, and Dr. Jerald Caton, my committee members, for their support and contribution to my work.

A special thanks to Kelley Green, Aaron Nelson, Dr. Robert Hardin, and Dr. Paul Funk for their knowledgeable insight regarding cotton ginning and drying. I'd also like to thank Richard Epting and Joaquin Cavazos for the excellent fabrication of heat exchangers.

I'd like to extend my gratitude to Joe Thomas with Lummus Corporation for the financial support of this project and prior gasification projects. My five-year journey with the gasification projects has definitely been an enjoyable and learning experience.

CONTRIBUTORS AND FUNDING SOURCES

Contributors

This work was supported by a dissertation committee consisting of Dr. Sergio Capareda, committee chair, Dr. Ronald Lacey and Dr. Parnell of the BAEN Department, and Dr. Jerald Caton of the MEEN Department.

Data provided for Chapter III were provided by Kelley Green from Texas Cotton Ginners' Association. Data provided for Chapter IV was provided by Dr. Paul Funk from USDA ARS. All work for this dissertation was completed independently by the student with the supervision of Dr. Sergio Capareda.

Funding Sources

Financial support for lab equipment and supplies for the entirety of the research was provided by Lummus Corporation.

NOMENCLATURE

ANOVA	Analysis of Variance
ASTM	American Society for Testing and Materials
BC	Base Case
bph	Bales Per Hour
CGT	Cotton Gin Trash
CHP	Combined Heat and Power
EPA	Environmental Protection Agency
ER	Equivalence Ratio
FBG	Fluidized Bed Gasification
HHV	Higher Heating Value
HP	High Pressure
HRS	Heat Recovery System
IROR	Investor's Rate of Return
IRR	Internal Rate of Return
kW_e	Kilowatt (electrical power)
kW_{th}	Kilowatt (thermal power)
LHV	Lower Heating Value
LMTD	Log Mean Temperature Difference
MC	Moisture Content
MW_e	Megawatt (electrical power)
NCC	National Cotton Council

NG	Natural Gas
NPV	Net Present Value
P	Propane
PBP	Payback Period
TCGA	Texas Cotton Ginners' Association
USDA	United States Department of Agriculture
VFD	Variable Frequency Drive
ε-NTU	Effectiveness Number of Transfer Units

TABLE OF CONTENTS

LIST OF FIGURES

Page

LIST OF TABLES

Page

CHAPTER I

INTRODUCTION

BACKGROUND

Disposal of Cotton Gin Wastes

The United States is one of the world's leaders in cotton production. In 2016, cotton gins in the United States ginned over 17 million bales of cotton (USDA, 2016) and production was expected to increase by 5% for 2017-2018 (NCC, 2018). The ginning industry plays a vital role for cotton between harvest and final product. Once harvested from the field, seed cotton gets transported to a cotton gin to be cleaned. Burs, sticks, leaves, and other organic matter, also known as cotton gin trash (CGT), gets separated from cotton lint at the gin before the lint is pressed into a bale and shipped to a textile mill or other location. Harvest method affects how much CGT is in a bale of seed cotton. A picker, stripper with a cleaner, or stripper without a cleaner typically has about 70, 180, or 360 kg (150, 400, or 800 lb) of CGT per bale, respectively (Parnell, 1977). The number of bales processed varies by gin; some cotton gins process up to or over 100,000 bales in a given season which results in thousands of tons of accumulated CGT. In most cases, the CGT is a waste product that cost the gin $20 - $50 per ton to dispose of properly.

Incineration of CGT at gin yards was once common practice but no longer permitted due to federal and state air quality regulations. First attempts at a solution were to combust the gin trash to utilize heat for drying, where 30% heat recovery from CGT was estimated to sustain average gin thermal demand (McCaskill et al., 1977). Although promising, CGT has a low eutectic point that results in significant slagging and fouling of ash at the high temperatures of

combustion. Operating combustors for a period of time would eventually be ceased due to the buildup and clogging of "clinkers" (Buffler, 1977). Therefore, combusting CGT was impractical from an operating standpoint due to high maintenance and frequent cleaning of combustion systems.

Other means of disposing CGT have been redistributing the biomass back to fields and as an animal feed supplement, but the value of these methods is decreasing (Thomas et al., 2018). However, CGT is a biomass that has a heating value of about 16.28 MJ kg^{-1} and can be utilized as fuel for a fluidized bed gasification (FBG) system for heat and power generation.

Gasification

Gasification is a partial combustion process that converts a biomass into a low calorific value synthesis gas (syngas) in which the syngas can be combusted in a generator for electricity generation. Since the 1980's, researchers at AgriLife Research at Texas A&M University have conducted studies with CGT as a fuel for FBG (LePori and Soltes, 1981; Capareda, 1990). Initially, the syngas was combusted in a fire-tube boiler to produce steam to power a turbine. However, the high capital cost of steam turbines made the method unfeasible. The FBG system was further matured through the development of autonomous control instrumentation and extensive engine testing (Maglinao, 2009; Maglinao, 2013). In addition, a gas clean-up system has been implemented to properly remove the tars from the syngas before the syngas is combusted in the generator. The system has been developed into a fully mobile unit, shown in Figure 1, which requires no external power supply and is ready for field demonstration at cotton gins (Capareda and Maglinao, 2018).

Figure 1. Trailer mounted, fully mobile FBG unit.

The electrical power generation of the FBG system has been established, but in order for the system to be classified as combined heat and power (CHP) or cogeneration, waste heat needed to be captured from the system and efficiently utilized. Sources of waste heat from the gasification system include cooling exhaust gases from the generator and cooling the hot syngas through a series of heat exchangers. Thermal energy conversion processes, such as combustion and gasification, provide a substantial potential of waste heat energy due to the elevated reaction temperatures. However, in order to justify implementing equipment for heat capture, there must be a demand for the thermal energy. Cotton gins generally use heated air at temperatures between 150°C and 180°C for pneumatically conveying and drying the incoming seed cotton (Anthony and Mayfield, 1944). Flow rate and temperature of heated air are two critical factors when reducing the moisture content (MC) of seed cotton such that the cotton can be cleaned efficiently in the gin (Laird and Baker, 1996). Utilizing waste heat in the form of heated air for seed cotton drying illustrates that a heat recovery system from the FBG system can potentially

reduce or potentially replace natural gas or propane. This cogeneration aspect establishes more attraction for cotton gins, especially from an economic standpoint since about 25% of ginning costs are from purchasing electrical and thermal energy (Funk and Hardin, 2017).

Implementing FBG systems would allow cotton gins to be energy independent (Figure 2). Harvested seed cotton gets transported to a cotton gin where gin trash and cottonseed are separated from cotton lint. Cotton lint is pressed into bales for transportation and marketing to textile mills and cottonseed is sold for animal feed or oil extraction, while gin trash accumulates near the gin. Utilizing gin trash as the fuel for the gasification power plant supplies both heat and electricity back to the gin. A continuous operation could be sustained given that sufficient amount of waste from seed cotton is transported to the gin. A special note should be taken that the capacity of gins in Texas varies significantly, from as low as 8 bales per hour (bph) up to 126 bph (Kelley Green and Aaron Nelson, TCGA, personal communication, 19 April 2016). Therefore, size of gasification power plants would vary for each gin.

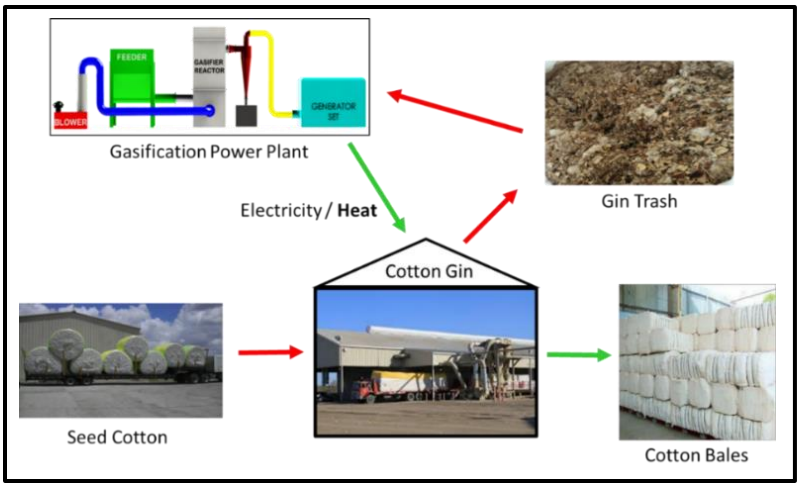

Figure 2. Process flow of a cotton gin with FBG power plant. Given that sufficient trash from harvested seed cotton is transported to the gin, the FBG power plant can continuously supply heat and electricity to power machinery and dry cotton.

Heat Recovery from Gasification

Wang et al. (2015) evaluated a combined cooling, heating, and power biomass gasification system where incorporating a heat exchanger increased overall efficiency by up to 5%. Nwokolo et al. (2016) suggested capturing waste heat from the surface of the cyclone separator since it's the first stage downstream of the gasifier. Thapa et al. (2017) conducted a study in which a double pipe heat exchanger was implemented downstream of a gasifier to decrease tar concentration in the syngas. They concluded that the tar collection efficiency was significantly improved by cooling syngas before the tar was removed. Francois et al. (2013) modeled a 10 MW_e CHP gasification power plant and concluded that net overall efficiencies of 66% can be achieved. A similar overall efficiency was reported by Skorek-Osikowska et al. (2014) where researchers concluded that economic viability of CHP gasification power plants is strongly influenced by current energy prices and "green" incentives. Baina et al. (2015)

investigated the effects of thickness and thermal conductivity of deposit materials on heat exchanger performance from syngas combustion in an externally-fired gas turbine. They concluded that thermal conductivity of deposits of 0.1 W m^{-1} K^{-1} and lower decreases the performance of heat exchange.

The initial step towards designing the heat recovery system (HRS) for the 250 kW_e FBG system was to identify sources of waste heat from the gasification process and methods of heat capture. Syngas was obviously the first source as this is the gas produced from the reactor, typically at temperatures of around 700°C (1300°F). A general process diagram of the FBG system is displayed in Figure 3. Before syngas is combusted in a generator, syngas must be cleaned and cooled. Cyclones separate biochar particulates from the syngas while a scrubber removes tars. Syngas is typically cooled through the chiller before the scrubber to around 15°C (60°F) before entering the generator. The large temperature difference, 700°C to 15°C, of syngas suggested that there was a potential of waste heat recovery. Implementing an HRS to capture the perceived "free" energy from syngas became an attractive option to the industry.

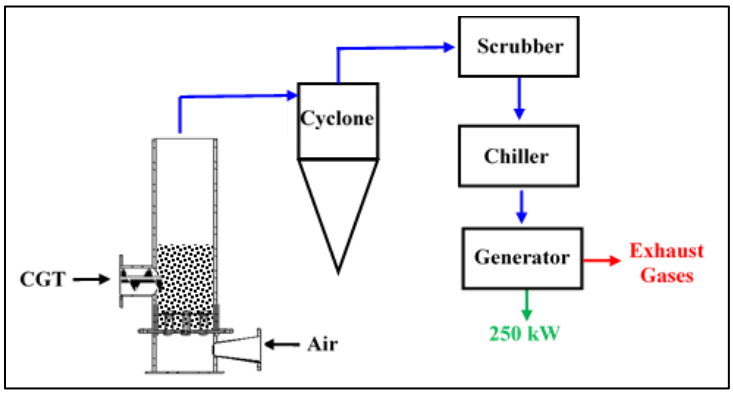

Figure 3. General process flow of syngas for the 250 kW_e FBG system. Syngas must be cleaned and cooled before combusting in a generator to sustainably generate electricity.

One obstacle in implementing an HRS was placement of heat exchangers. Initially, placing the heat exchangers immediately downstream of the gasifier was favored since at this location the syngas would have the highest temperature. However, there were concerns that the heat exchangers would negatively affect the performance of cyclones. High capture efficiency of cyclones are experienced at a range of optimal inlet velocities (Parnell, 1996). Reductions and variations of syngas temperature would ultimately equate to variations in flow rate and gas velocity at the inlet of cyclones. Also, a fouling layer could potentially build up within the cyclone, further reducing cyclone performance. Therefore, placement of heat exchangers for syngas cooling were concluded to be placed immediately downstream of the cyclones.

Corrosion, erosion, and fouling are major concerns when determining the design, material selection, and performance of a heat exchanger (Schaafhausen et al., 2015). Since sulfur is typically present in biomass, H_2S and COS can be present in the syngas. Alkali species are also common. The main contaminant of syngas is tars, which are higher hydrocarbons that condense as syngas gets cooled. Temperature of tar condensation (dew point) can be expected to be below 250°C (Kiel et al., 2004). Cooling syngas has the potential of creating a fouling layer, which is a consequence of tar condensation that results in buildup of tars and fine biochar. The fouling layer has two main effects for heat exchangers: an increased pressure drop and variation in thermal performance (Hesselgreaves, 2002).

From the 250 kW_e FBG system, cooling syngas from 700°C to 150°C would provide an estimated 230 kW_{th} of thermal energy. According to the Texas Cotton Ginners' Association (TCGA) 2016 annual energy survey (TCGA, 2010 - 2017), waste heat from syngas would provide about 70% of the average thermal demand. Therefore, additional heat must be captured

from the FBG to meet the average demand. Additional sources of waste heat include combusting syngas and utilizing generator exhaust gases.

Combusting syngas to provide additional heat for cotton gins implied that additional CGT be fed into the gasifier during operation and thus, more syngas such that electricity generation were not hindered. Sixto (1999) designed and evaluated a staged combustion system that reduced nitrogen oxide emissions to below EPA limits, which revealed that syngas combustion was a viable method for producing and supplying heat. However, incorporating a combustion and control system would be needed. This approach was ultimately deemed unnecessary, especially since hot gases were produced from the generator. Generator exhaust gases were a readily available source of waste heat that did not require additional equipment besides heat exchangers.

The primary benefit of utilizing generator exhaust gases would be such that feeding additional CGT was not required. Since air mixes with syngas in the generator, higher flow rates of exhaust gases could potentially supply higher rates of heat capture than syngas. A challenge of utilizing exhaust gases was that indirect heating with heat exchangers were also needed to capture waste heat. If generator exhausts were used directly for seed cotton drying, the maximum temperature of gases exposed to cotton would be limited to between 150°C and 180°C to prevent scorching. This would mean that generator exhausts would have to be cooled down from around 540°C (1000°F) before being efficiently utilized. In addition, quality of cotton fibers would be in jeopardy since combustion of syngas in a generator produces an unpleasant odor.

OBJECTIVES

The overall objective of the gasification project was to design and evaluate a 250 kW_e FBG system, fueled by CGT, for commercial manufacturing. Purpose of the 250 kW_e system

was to perform on-site field demonstrations at a cotton gin to supply both electrical and thermal energy to power machinery and reduce / replace fuel usage, respectively. Gins would become energy self-sufficient and independent by utilizing a readily available energy source since the CGT biomass already is transported to the gin with the harvested seed cotton. Benefits of implementing FBG systems at gins expands beyond supplying energy to a gin. Utilizing heat and power would offset purchasing electricity and fuel, resulting in economic savings for gins. In addition, the issue of properly disposing CGT becomes resolved, which also saves money.

Objectives presented in this dissertation were to conduct the necessary experimental research for the development of an HRS model for the 250 kW_e FBG such that the system would be classified as cogeneration. Implementation of heat exchangers to convert waste heat from syngas and generator exhausts to heated air would supply gins with thermal energy for drying seed cotton or for other processes. With a designed HRS, a technical and economical analysis were performed to demonstrate the effectiveness and feasibility of the system.

CHAPTER II

EVALUATION OF HEAT EXCHANGE FROM COOLING SYNGAS

INTRODUCTION

Two main sources of waste heat from the 250 kW_e FBG system were identified to be syngas and generator exhausts. Captured waste heat needed to be in the form of heated air such that thermal energy would be beneficial for cotton gins. Several configurations of heat transfer were investigated, which included counter-flow and parallel-flow double-pipe heat exchangers, along with shell and tube heat exchangers. Due to the concern of deposit build up from syngas and generator exhausts, shell and tube heat exchangers were determined to be maintenance intensive due to bends and duct constrictions. Also, higher air pressure differentials would be experienced through shell and tube heat exchangers. Between counter-flow and parallel-flow heat exchangers, counter-flow heat exchangers have higher heat transfer efficiencies, as shown in Figure 4. For parallel-flow heat exchangers, the outlet temperature of cold fluid becomes limited by the outlet temperature of the hot fluid. In contrast, the outlet temperature of the cold fluid can exceed the temperature of the hot fluid for counter-flow configurations.

Heat transfer through a double pipe heat exchanger is fundamentally illustrated as a hollow cylinder, displayed in Figure 5. Typically, the hot fluid flows through the inner pipe while the cooling fluid flows in the annulus. When the fluids are at different temperatures, a temperature gradient exists in which heat transfers from the hot to cold fluid through the walls of the pipe, otherwise known as conduction. Fourier's Law for thermal conduction states that heat transfer is proportionally perpendicular to the temperature gradient, illustrated in equation 1.

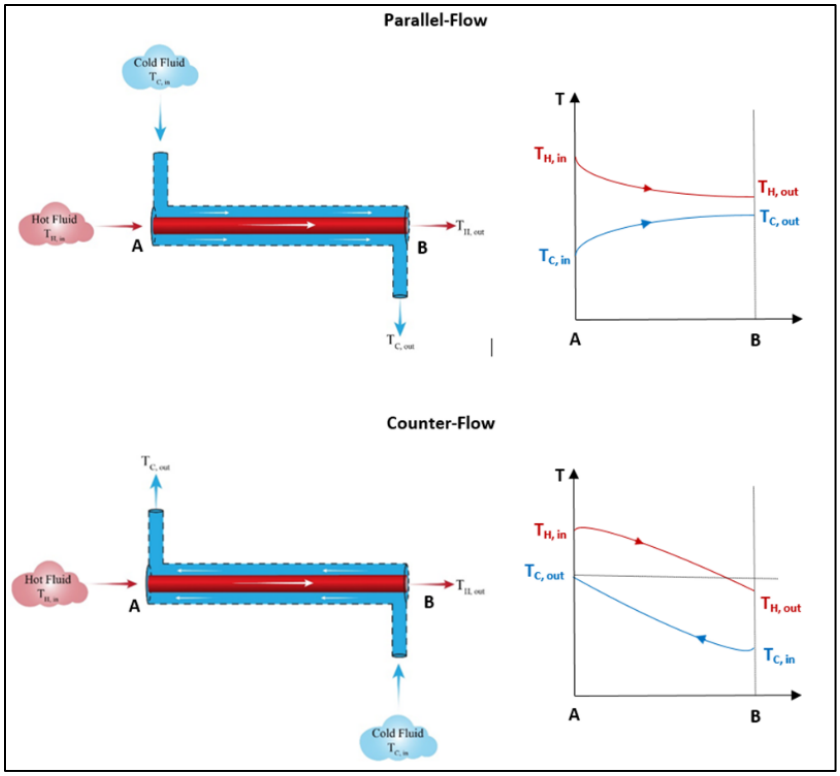

Figure 4. Comparison between parallel-flow and counter-flow heat exchangers. Counter-flow heat exchangers are more efficient since the outlet temperature of outlet cold fluid can exceed the outlet temperature of hot fluid.

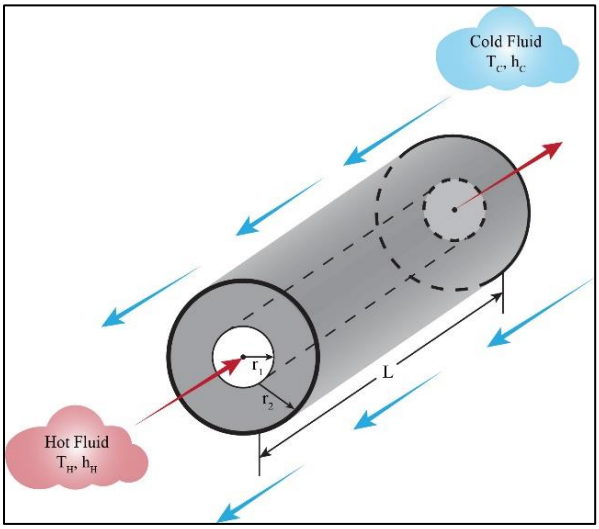

Figure 5. Radial conduction of heat transfer for a hollow cylinder.

$$\vec{q} = -k\nabla T \quad (1)$$

where $\vec{q}$ is heat flux (W m^{-2}), k is material thermal conductivity (W m^{-1} K^{-1}), and ∇T is temperature gradient (K m^{-1}). The negative proportion in equation 1 indicates that heat transfers from higher to lower temperature.

Two popular methods of designing and modeling heat exchangers are log mean temperature difference method (LMTD) and effectiveness number of transfer units (ε-NTU) (Henderson et al., 1997). Each method has a unique analysis of heat exchange. LMTD is useful when the inlet and outlet temperatures of both fluids are known and can be used to estimate either the heat transfer rate or effective surface area. The ε-NTU method is useful when estimating overall heat transfer rate and outlet temperatures of fluids based upon inlet temperatures and effective surface area. Modeling heat exchange by applying the ε-NTU method can be carried out to estimate the performance of a heat exchanger (Baina et al., 2015; Bergman and Lavine, 2011).

The purpose of this study was to evaluate heat transfer of a counter-flow, double pipe heat exchanger for syngas cooling from a pilot-scale FBG system. The ε-NTU method was applied to estimate heat transfer based upon properties of hot and cold gases, along with pre-determined dimensions of the heat exchanger. Initially, propane exhaust gases were utilized as the hot gas to act as the control for experiments. The heat exchanger was evaluated by varying both inlet hot gas temperature and inlet ambient air flow to acquire data for heat transfer model corrections. Once corrected, the heat exchanger was evaluated by cooling syngas to determine and estimate the effect of the fouling layer on overall heat transfer in the model.

Objectives

The goal of this chapter was to design a small-scale, counter-flow double pipe heat exchanger that matched the size of a readily available pilot-scale fluidized bed gasifier. Specific objectives were to:

- Develop a preliminary model for the design of a counter-flow, double pipe heat exchanger and evaluate performance using propane exhausts as hot gas,
- Determine method of higher efficiency by comparing heat transfer of a non-finned and finned double pipe heat exchanger, and
- Evaluate heat transfer from cooling syngas during gasification and incorporate the effect of the fouling layer into the heat transfer model.

MATERIALS AND METHODS

Heat Exchanger Model

The ε-NTU method (Bergman and Lavine, 2011) was applied to develop a model for the counter-flow, double pipe heat exchanger used throughout this project. The model defined an effectiveness (ε) of a heat exchanger as the ratio of theoretical heat transfer rate to a thermodynamically possible maximum heat transfer rate (equation 2).

$$\varepsilon = \frac{q_{th}}{q_{max}} \tag{2}$$

where ε is heat exchanger effectiveness (dimensionless), q_{th} is theoretical heat transfer (W), and q_{max} is maximum heat transfer (W).

Maximum heat transfer rate, q_{max}, was calculated by assuming an infinitely long heat exchanger where one of the gases experiences a maximum temperature differential, or the temperature difference between the inlets of both gases. Minimum heat capacity rate, instead of the maximum, was used since this gas would experience the maximum temperature differential. Maximum heat transfer rate was determined by taking the product of maximum temperature differential and minimum heat capacity rate (equation 3).

$$q_{max} = C_{min}(T_{H,i} - T_{c,i}) \tag{3}$$

where C_{min} is minimum heat capacity rate (W K^{-1}), T is temperature (K), and H, C, i are subscripts for hot gas, cold gas, and inlet, respectively.

Number of transfer units, *NTU*, is a non-dimensional measure of the size of a heat exchanger and is defined as the ratio of overall conductance, also known as heat exchanger thermal capacity, to minimum heat capacity rate, or $UA\ C_{min}^{-1}$. Overall conductance was estimated by taking the reciprocal of the summation of thermal resistances (equation 4).

$$UA = \frac{1}{R_H + R_C + R_{wall} + R_{foul}} = \frac{1}{\frac{1}{(hA)_H} + \frac{1}{(hA)_C} + R_{wall} + R_{foul}} \tag{4}$$

where UA is heat exchanger thermal capacity (W K^{-1}), R is thermal resistance (K W^{-1}), h is gas convection coefficient (W m^{-2} K^{-1}), A is effective surface area (m^2), and *wall*, *foul* are subscripts for pipe wall and fouling layer, respectively. Thermal resistances of the wall and fouling layers were calculated by assuming radial conduction for a cylindrical wall (equation 5).

$$R_{wall,foul} = \frac{\ln(r_2/r_1)}{2\pi Lk} \tag{5}$$

where r_2 is outer radius (m), r_1 is inner radius (m), and L is length of cylinder (m).

In order to determine gas convection coefficients for both hot and cold gases (h_H and h_C), assumptions of initial parameters were defined. These parameters included inlet temperatures of

hot and cold gases, flow rates of gases, diameters of inner and outer pipes, and length of heat exchanger. Based upon the temperatures of each gas, specific heat, viscosity, Prandtl number, and conductivity were estimated. Reynolds number (*Re*) was calculated for the hot gas in the inner pipe and cooling air in the annulus. Nusselt's number was correlated to Reynolds and Prandtl number through the Dittus-Boelter equation (Winterton, 1998). Nusselt's number for each gas was used to determine convection coefficients (equation 6).

$$h = Nu\ \frac{k}{D} \tag{6}$$

where *Nu* is Nusselt number (dimensionless) and *D* is pipe diameter (m). The hydraulic diameter (D_h) was used in place of pipe diameter (*D*) for for calculations of Reynolds number and convection coefficient for cooling air in the annulus. Hydraulic diameter was calculated by taking the difference between the outer pipe's inner diameter and inner pipe's outer diameter.

Heat capacity rate ratio, C_r, was the ratio of minimum to maximum heat capacity rates ($C_{min}\ C_{max}^{-1}$) of the hot and cold gases. Heat capacity rates were obtained by taking the product of the mass flow rate and specific heat of each respective gas. Since outlet temperatures of both gases were not initially known, the effectiveness of the heat exchanger was estimated with the use of C_r and *NTU* when $C_r < 1$ (equation 7).

$$\varepsilon = \frac{1-\exp[-NTU(1-C_r)]}{1-C_r\exp[-NTU(1-C_r)]} \tag{7}$$

where *NTU* is number of transfer units (dimensionless).

With calculated values of ε and q_{max}, q_{th} was estimated from equation 2. Assuming that all of the heat transfers from hot to cold gases with no heat loss, outlet temperatures were estimated with equation 8.

$$q_{th} = \dot{m}_H c_{p,H}\left(T_{H,i} - T_{H,o}\right) = \dot{m}_C c_{p,C}(T_{C,o} - T_{C,i}) \tag{8}$$

where $\dot{m}$ is mass flow rate (g s^{-1}), c_p is specific heat (J g^{-1} K^{-1}), and o is a subscript for outlet.

Iterative computations were performed to recalculate convection coefficients of hot and cold gases based upon the average of inlet and outlet temperatures. Because the properties of both gases change within the heat exchanger, initial *UA* values may not have been correct. Therefore, several iterations were performed until the average gas properties became relatively consistent for an approximate estimate of *UA*.

Finned and Non-finned Heat Exchanger

Extended surfaces, or fins, can provide a means of additional heat transfer at the same length of heat exchanger by increasing the effective surface area. A simple fin model was developed (Bergman and Lavine, 2011; Lee and Bae, 2008) to determine optimal dimensions, such as thickness and length, of longitudinal fins. An iterative process was performed that resulted in highest possible heat transfer given dimension constraints of the heat exchanger. Since fins could potentially present conduction resistance, however, heat transfer experiments were conducted with a finned and non-finned pipe of the same pipe size for heat transfer comparison.

Due to the concern of corrosion from the products of gasification, 304L stainless steel was the material of choice for the heat exchanger. Although stainless steel has a lower thermal conductivity compared to other metals commonly used for heat exchangers, such as aluminum and copper, stainless steel has shown to be reliable for countless hours of gasification. Threaded pipe caps were bored out to allow the inner pipe to pass through the outer tube of the heat exchanger (Figure 6). This allowed the heat exchanger to be interchangeable between the finned and non-finned pipe. Due to the dimensions of the fins, there was a potential that air flowing

through the heat exchanger would travel the path of least resistance and therefore not be exposed to some surfaces of the fins. For this reason, two air inlets were implemented into the design of the heat exchanger to induce turbulence. A tee-section fitting was connected to the bottom of the heat exchanger since tars could significantly condense when operating the heat exchanger during gasification.

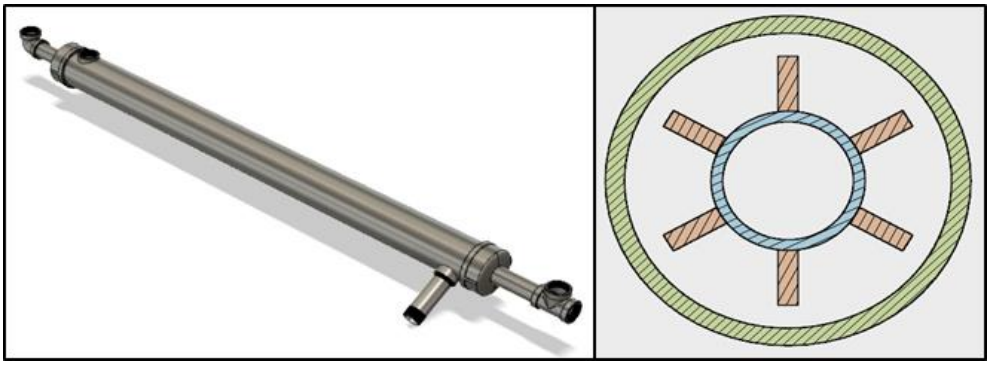

Figure 6. Design of small-scale heat exchanger and cross sectional view of fins. The inner pipe was interchangeable to test both a finned and non-finned pipe.

Experimental set up of heat exchanger tests can be seen in the schematic in Figure 7. A compressor blower was used to supply air through a propane burner and heat exchanger while radial fans were used to supply ambient cooling air. Propane exhaust gases were assumed an adequate surrogate for generator exhausts. Orifice meters were used to measure the flow rates of air supplied by the compressor and fans. Thermocouples were placed at the exhaust gas inlet, exhaust gas outlet, and air outlet of the heat exchanger. Ambient temperature was measured for

the air inlet. All piping was wrapped with ultra-high temperature ceramic fiber insulation to minimize heat losses to the environment.

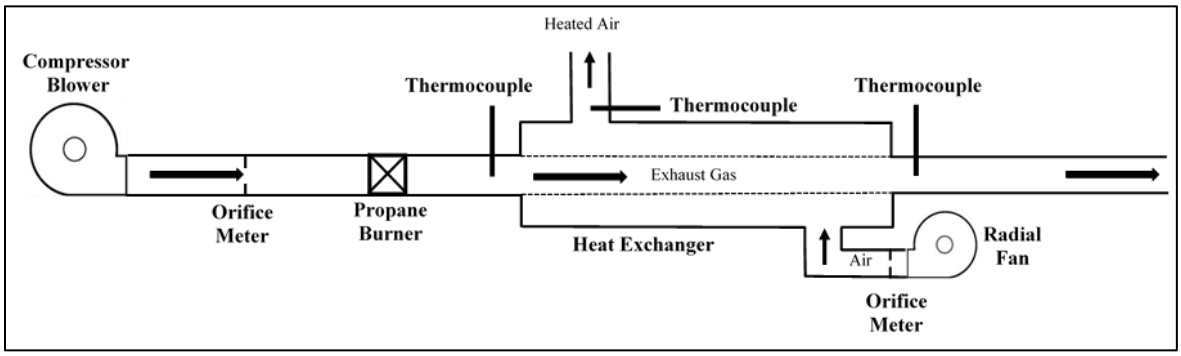

Figure 7. Experimental set up of small-scale heat exchanger. Exhaust gas and air temperature differentials were measured with thermocouples, while orifice meters measured flow rates.

Barometric pressure, relative humidity, and ambient temperature were recorded from the National Weather Service's website to calculate the density of moist air during tests. Temperatures were measured with K-Type thermocouple probes connected to Jenco temperature displays (Model 765, Jenco Quality Instruments, San Diego, CA). The compressor blower was a Sutorbilt positive displacement compressor (Type L, Gardner Denver, Quincy, Illinois), while the radial fans were heavy duty blowers (Model HP33P, Blowers LLC, Elmhurst, IL). Volumetric flow rates were measured with orifice meters that were calibrated with a laminar flow element (Model Z50MC2-2, Meriam Process Technologies, Cleveland, OH). Differential pressures were measured with Magnehelic gauges (Series 2000, Dwyer Instruments, Michigan City, IN).

Volumetric flow rates supplied by both the compressor blower and radial fans were calculated using the orifice meter equation (Henderson et al., 1997). Mass flow rate was calculated by taking the product of volumetric flow rate and density of air. The mass flow rate of the exhaust gases was assumed equal to that of the air supplied by the blower since the addition of propane, by mass, was negligible. The flow rate of exhaust gas was held constant and similar to that expected of the syngas from gasification throughout all tests. Heat transfer rate was calculated using equation 9.

$$q_{act} = \dot{m} c_p \Delta T \quad (9)$$

where q_{act} is actual heat transfer (W) and ΔT is gas temperature differential (K). Specific heats for the exhaust gas and air were estimated from the average temperature between the inlets and outlets.

Prior operation of the pilot-scale FBG system revealed that the mass flow of syngas ranged between 0.64 and 0.68 kg min^{-1} under certain operating parameters. Therefore, a similar flow rate of propane exhaust gas was used for testing. Heat exchanger performance was evaluated by varying the flow rate of ambient air and exhaust inlet temperature independently. Three air flow rates of 1.4, 2.1, and 2.8 m^3 min^{-1} (50, 75, and 100 ft^3 min^{-1}) were selected while maintaining a constant flow and inlet temperature of exhaust gas at 538°C ± 28°C (1000°F ± 50°F). The heat exchanger was also evaluated by varying the inlet temperature of the propane exhaust gases. Temperatures of 427°C and 704°C ± 28°C (800°F and 1300°F ± 50°F) were selected while maintaining an ambient air flow rate of 2.8 m^3 min^{-1}. Each test consisted of one hour in which data was collected every three minutes. Before each test was initiated, the inlet temperature of the propane exhaust gases was allowed to stabilize for ten minutes without flow of ambient air. Air temperature differential, heat transfer rates, and heat exchanger effectiveness

were averaged from the time series when the system was in steady state for all replicates. Steady state was defined when the change in heat capture was less than or equal to 1%. The effectiveness of the heat exchanger was determined by taking the ratio of actual heat captured to maximum heat transfer (q_{max}). Heat release was defined as the heat transfer rate of exhaust gas, while heat captured was defined as the heat transfer rate of air.

Once all data were collected, the ε-NTU model for the heat exchanger was corrected by applying an average *UA* correction factor, or F_{UA} (Baina et al., 2015). This correction factor was calculated by taking the ratio of actual *UA* to initial theoretical UA for each combination of inlet exhaust temperature and air flow. Actual *UA* was computed by determining C_r and ε for each data point during steady state, in which equation 6 was rearranged to calculate actual *NTU*. With the incorporation of F_{UA}, the corrected model revealed the relative errors of heat capture and effectiveness between model and actual data.

Statistical Analysis

Design of experiments for the heat exchanger with propane exhaust gases was structured with a single factor design, with the factors being type of heat exchanger, exhaust temperature, and ambient air flow rate. Each factor was evaluated independently. Type of heat exchanger had two levels (finned and non-finned), while exhaust temperature and air flow rate had three levels (427°C, 538°C, 704°C and 1.4, 2.1, 2.8 m^3 min^{-1}, respectively). Measured responses for each test were inlet and outlet temperatures of exhaust gases and air. Calculated responses for statistical analysis were average air temperature differential, heat captured, and heat exchanger effectiveness while the system was in steady state. Two replicates for each test were performed since standard deviations between each test were minimal. A randomized complete block design

was performed to minimize experimental variability of atmospheric air properties. A statistical program (Design Expert 8, Stat-Ease, Minneapolis, MN) was used to perform an analysis of variance (ANOVA) for the effect each factor had on the responses where a significance level (α) of 0.05 was selected.

Confidence intervals were also evaluated for each combination of air flow and exhaust temperature for non-finned heat exchanger heat capture results. Data between replicates were combined to calculate the mean heat capture. Alpha was selected as 0.01 that resulted in 99% confidence intervals. The corresponding z-value for the intervals was 2.58.

Evaluation of Heat Exchanger during Gasification

Gasification experiments were conducted on a pilot-scale, FBG system (Figure 8) with CGT as the biomass fuel. The diameter of the gasifier was 0.15 m (6 in.). A positive displacement compressor connected to a variable frequency drive (VFD) controller supplied air to fluidize the bed material. Refractory calcined mullite was the bed material in the gasifier that had a reported particle density and mean particle diameter of 2.6 g cm^{-3} and 818 µm, respectively. The CGT fuel was stored in an enclosed feed hopper and fed to the reactor with a 0.1 m (4 in.) diameter screw auger connected to an AC controller. Downstream of the gasifier, a 0.08 m (3 in.) diameter tube cyclone separated biochar particles from syngas. At the exit of the cyclone, the heat exchanger was used to cool the syngas and heat ambient air. Once the syngas passed through the heat exchanger, the gas flowed through an orifice meter and then flared off to the atmosphere.

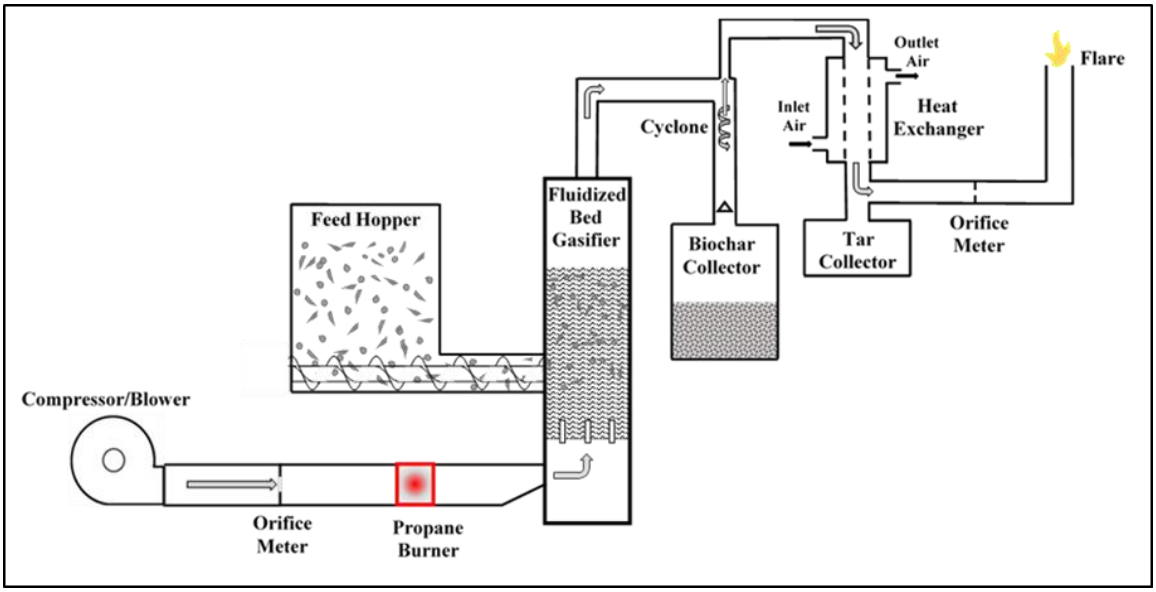

Figure 8. Components and process flow of pilot-scale FBG system. The heat exchanger was placed downstream of the cyclone to evaluate performance while cooling syngas.

CGT Processing and Preparation

The CGT biomass used for gasification was acquired from a cotton gin located in Colorado City, Texas. The trash was composed of sticks, leaves, burs, soil, and lint. Due to the inconsistent composition of raw CGT, there was non-uniform feeding through the screw auger in the pilot scale FBG system. Therefore, a hammer mill was used to grind the CGT in to smaller particles so that the CGT could be fed into the gasifier at a constant, steady rate.

Prior to gasification tests, the feed rate of CGT was calibrated with the motor speed driving the screw conveyor. A tachometer was equipped to digitally display the rotational speed of the motor. Gin trash was placed in the feed hopper and conveyed through the auger at preset motor speeds and known time durations. Time and weight of CGT conveyed out were recorded

to calculate the average feed rate at each motor speed. A linear correlation between feed rate and motor speed was developed to approximate feed rate during gasification.

The heating value and moisture content (MC), in wet basis, of CGT were determined prior to gasification to ensure smooth operation. Higher heating value analysis was carried out using Parr isoperibol bomb calorimeter following ASTM D5865 (Standard Test Method for Gross Calorific Value of Coal and Coke). Samples of CGT were weighed before and after being placed in a convection oven when determining MC following ASTM E871 (Standard Method for Moisture Analysis of Particulate Wood Fuels). Three samples of CGT were independently evaluated for each standard.

Gasification Experimental Procedure

Before the gasification reaction began, the propane burner was used to preheat the bed material to about 540°C (1000°F) while being fluidized. Once this temperature was reached, the burner was turned off, air adjusted to the target air flow rate, and CGT feed rate initiated such that the air-to-fuel ratio was 1.4 kg_{air} kg_{CGT}^{-1}. This A/F ratio caused the temperature within the gasifier to continue to increase. The feed rate was incrementally increased until an equilibrium, steady state temperature of about 700°C was sustained, typically at an equivalence ratio (ER) of around 0.20 (Maginlao et al., 2015). Sufficient time was allowed to ensure that the system was operating in a continuous and sustainable manner before initiating heat exchanger tests.

Once steady state gasification was reached, the radial fans were turned on to evaluate the performance of the heat exchanger. Air flow rates of 1.4 and 2.8 m^3 min^{-1} were selected to collect data of heat exchange between syngas and ambient air. Each flow rate was evaluated for a minimum of 30 minutes. Three glass jars were connected to the bottom of the heat exchanger;

one for when the heat exchanger was not being operated and one for each air flow rate. Purpose of the glass jars were to trap and measure the amount of tars if they significantly condensed within the heat exchanger.

Performance of the heat exchanger was evaluated similar to that of the propane exhaust tests. Heat transfer rate, q_{act}, was calculated for both syngas and air using equation 9. Inlet and outlet temperatures of both syngas and air were measured to determine temperature differentials. Averages of the inlet and outlet temperatures were used to estimate the specific heat of each gas. Volumetric flow rates were determined by measuring the pressure drop across orifices.

Comparison of heat exchange between propane exhaust gas and syngas was done to incorporate a method of modeling heat capture from syngas cooling. Since there is a lack of tar thermal conductivity in literature, especially from agricultural biomass gasification, the comparison led to the estimation of thermal resistance of the fouling layer from the developed model. The two main components of thermal fouling during gasification were tars and fine biochar. With a measured thickness of each layer, the thermal conductivity of tar was estimated. Thermal conductivity of fine biochar was assumed as 0.079 W m^{-1} K^{-1} (Usowics et al., 2016).

Energy Analysis of Pilot-Scale FBG

Based upon the data collected from this study and syngas properties from Maglinao et al. (2015), an analysis of useful energy fractions from gasifying CGT was performed. A summary of necessary assumptions is presented in Table 1. Specific heat was estimated for syngas and generator exhausts by assuming both gases as heated air. Total useful energy was determined as the sum of electrical power, heat captured from syngas, and heat captured from exhaust gases. Conversion efficiency of electricity was taken as the ratio of input energy to output electrical

power, where input energy was the product of mass flow and heating value of CGT. Conversion efficiency of heat capture was calculated as the ratio of total potential heat capture to input energy, where total heat capture was sensible heat reduction in exhaust gases and syngas.

Table 1. Assumptions of syngas and generator exhaust properties for energy analysis.

Initial Syngas Temperature	704	°C
Final Syngas Temperature	150	°C
Air-to-Fuel Ratio in Generator	1	$kg_{air}\ kg_{syngas}^{-1}$
Generator Efficiency	20	%
Exhaust Initial Temperature	538	°C
Exhaust Final Temperature	150	°C

RESULTS AND DISCUSSION

Non-finned Heat Exchanger Performance

A heat rate plot can be seen in Figure 9, which showed a similar trend between all tests. Before each test was initiated by supplying ambient air, heat energy from exhaust gases was stored within the heat exchanger's material. This resulted in higher heat captured for about the first 30 minutes of each test. However, the heat captured decreased while the heat released increased as the two rates approached steady state conditions. Heat rates became relatively equal during steady state, which indicated that there were minimal heat losses within the heat exchanger and to the surroundings.

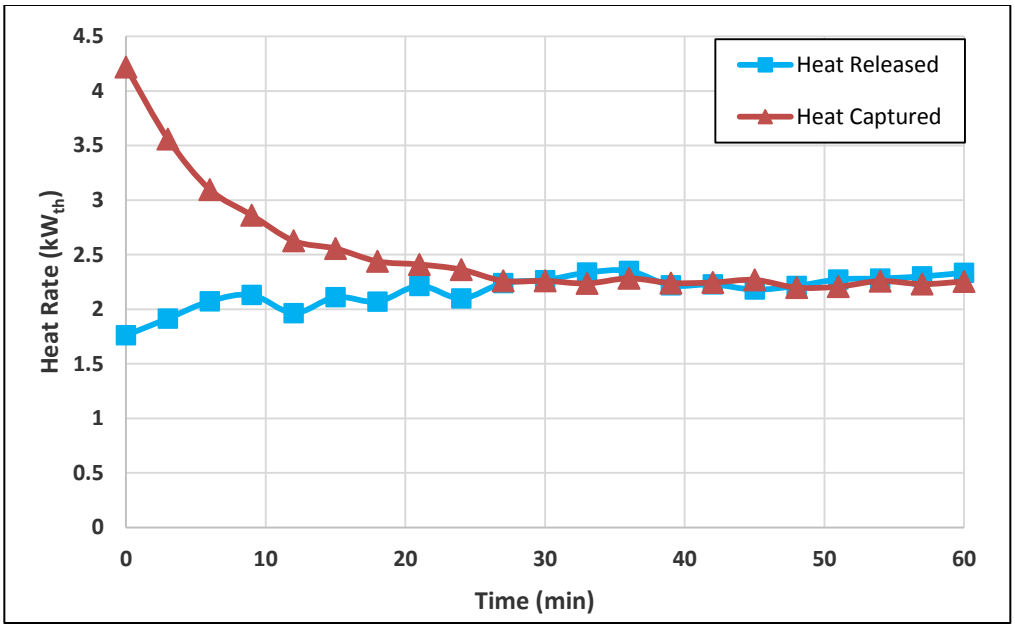

Figure 9. Heat rate plot for air flow rate of 2.1 m^3 min^{-1} for finned heat exchanger. Heat captured and released became approximately equal during steady state.

Summary of results for varying air flow rates are presented in Table 2. Ambient air inlet temperatures for all tests ranged between 16°C and 19°C (60°F and 66°F). The assumption was made that this range of inlet air temperatures had an insignificant effect on the overall performance of the heat exchanger for all replicates. As ambient air flow rate increased, air temperature differential decreased, i.e. outlet air temperature decreased. This was due to the residence time of the air flowing through the heat exchanger; longer residence times resulted in higher outlet temperatures. However, as air flow rate increased, heat captured by the air also increased even though the temperature differential decreased. From this observation, it appeared that flow rate of air outweighed the air temperature differential with respect to heat capture.

For varying inlet exhaust temperature tests, temperatures were varied at 427°C and 704°C while maintaining an ambient air flow rate of 2.8 m^3 min^{-1}. For exhaust inlet temperatures of 427°C

and 704°C, average heat capture was 2.0 and 3.5 kW_{th}, respectively while air temperature differential was 17°C and 44°C (62°F and 111°F), respectively. The actual effectiveness remained relatively constant between 0.42 and 0.43.

Table 2. Results of varying air flow on non-finned heat exchanger performance with exhaust inlet temperature of 538°C. Increasing air flow rate decreased air temperature differential but increased overall heat capture.

Ambient Air Flow Rate [m^3 min^{-1}]	Air Temperature Differential (Std. Dev.) [°C]	Heat Captured (Std. Dev.) [kW]	Effectiveness (Std. Dev.)
1.4	55 (1.6)	2.05 (0.05)	0.32 (0.010)
2.1	39 (1.4)	2.46 (0.07)	0.40 (0.011)
2.8	27 (1.12)	2.62 (0.04)	0.42 (0.010)

Results from varying air flow rate and inlet exhaust temperature were further analyzed to determine the percentage of total heat captured from the heat exchanger used in this study. Assuming that the propane exhausts were to be cooled to 150°C (300°F), the total potential sensible waste heat was around 4.6 kW_{th}. At air flow rates of 1.4, 2.1, and 2.8 m^3 min^{-1}, 45%, 54%, and 58% of the total heat was captured. For varying exhaust inlet temperatures at 427°C, 538°C, and 704°C, 63%, 58%, and 53% of the total waste heat was captured. These results indicated that two to three heat exchangers would have been required to capture the total waste heat.

For model corrections, average F_{UA} was calculated to be about 1.79, which revealed that the actual *UA* was almost doubled that of the initial theoretical. The correction factor was applied

to the model and a comparison between model and actual *UA* for the non-finned heat exchanger is shown in Table 3. Relative errors between the model and actual data ranged between 0.8% to 2.8% and 1.3% to 3.5% for heat capture and effectiveness, respectively. Since F_{UA} was calculated based upon actual data, relative errors were expected to be low. A special note should be taken that the value of F_{UA} is unique to conditions in this study, such as dimensions and configuration of the non-finned heat exchanger. From Table 3, *UA* displayed an increasing trend with both air flow and inlet exhaust temperature. Increasing inlet exhaust temperature had a near-linear relationship with *UA*, with an R^2 value of about 0.97. With increasing air flow rate, the rate of increase of *UA* diminished, indicating that increasing air flow above 2.8 $m^3\ min^{-1}$ resulted in *UA* becoming relatively constant at about 7 $W\ K^{-1}$.

Table 3. Model corrections for small-scale heat exchanger model. Relative errors of heat capture between the data and the corrected model were reduced to 3.5% and below.

Initial Parameters		Actual		Model		Relative Error	
Exhaust Inlet Temperature	Air Flow Rate	Heat Capture	UA	Heat Capture	UA	Heat Capture	Effectiveness
[°C]	[$m^3\ min^{-1}$]	[kW]	[$W\ K^{-1}$]	[kW]	[$W\ K^{-1}$]	[%]	[%]
427	2.8	2.0	6.7	2.0	6.9	1.2%	3.5%
704	2.8	3.5	7.4	3.6	7.2	1.3%	1.3%
538	2.8	2.6	6.9	2.7	7.1	1.3%	1.8%
538	1.4	2.0	5.1	2.0	5.1	0.8%	1.3%
538	2.1	2.5	6.4	2.4	6.2	2.8%	2.1%

Comparison of Finned and Non-finned Heat Exchanger

Average heat captured, along with uncertainty, from the non-finned heat exchanger was compared to that from the finned heat exchanger (Figure 10). For all variations of operating parameters of ambient air flow rate and inlet exhaust temperature, except at an ambient air flow rate of 1.4 m^3 min^{-1}, the average heat captured from the non-finned heat exchanger was greater than that of the finned heat exchanger by 9% to 11%. At an air flow rate of 1.4 m^3 min^{-1}, the average heat captured from the non-finned heat exchanger was about 2% lower than that of the finned. During testing of the non-finned heat exchanger at a flow rate of 1.4 m^3 min^{-1}, observations were made that the flow rate of air was unstable which could have been a consequence of the lower power input for the fans. This could account for the non-linear trend seen varying flow rate. Linear relationships with R^2 values greater than 0.99 were observed for all cases, except for non-finned varying flow. These linear trends demonstrated that heat capture can be estimated for specific conditions of air flow and exhaust inlet temperature, given that the flow rate of exhaust gas is similar to the value tested for this study.

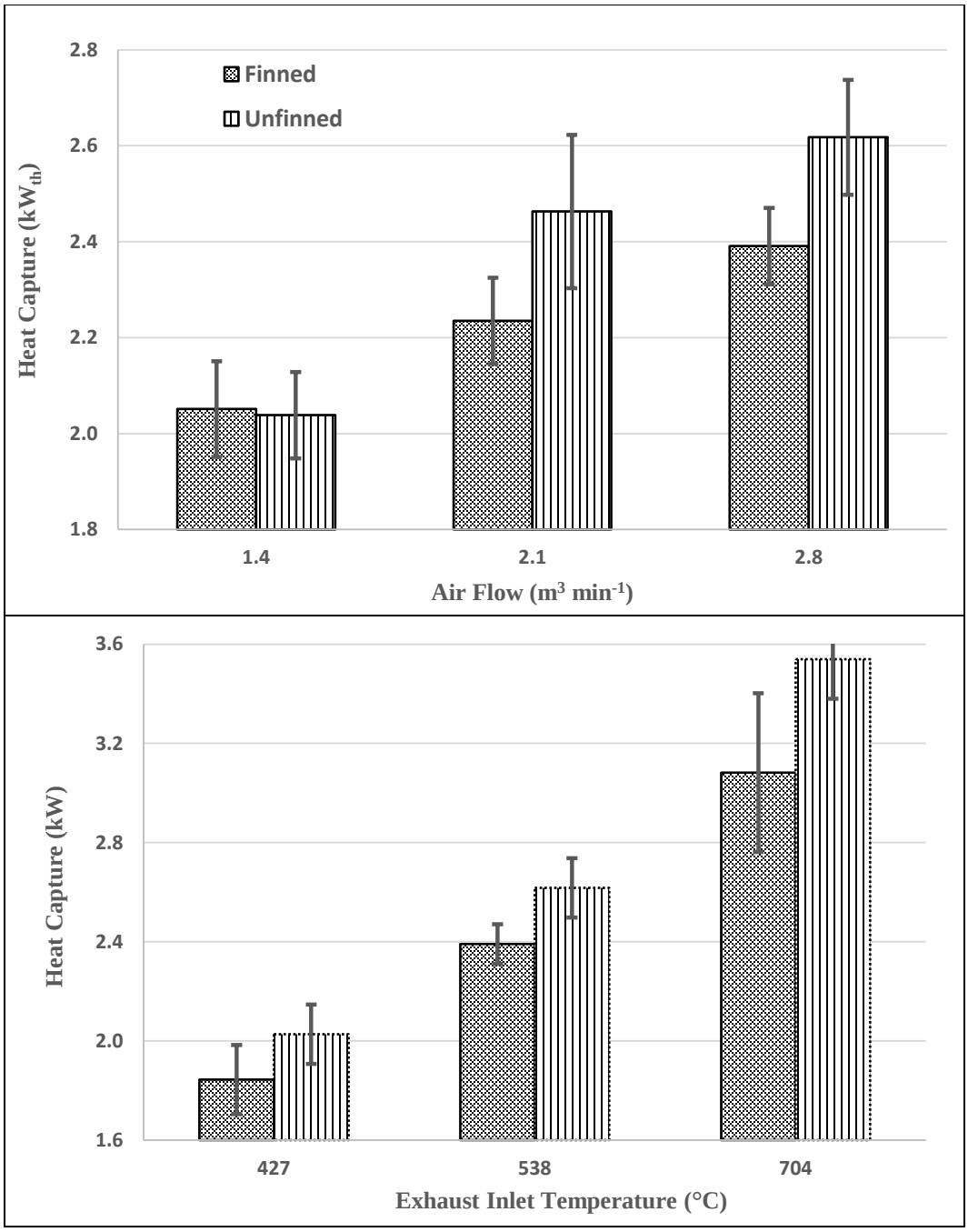

Figure 10. Comparison of finned and non-finned heat exchangers by varying air flow and exhaust inlet temperature. Non-finned heat exchanger provided up to 10% additional heat transfer than finned, except at an air flow rate of 1.4 m^3 min^{-1}.

Statistical Results

As expected, the results from ANOVA revealed that type of heat exchanger, air flow rate, and exhaust inlet temperature significantly affected air temperature differential and heat capture with low p-values of <0.001. Type of heat exchanger and air flow rate also significantly affected effectiveness with p-values of 0.002 and below. The low p-values indicated that the null hypothesis was rejected that means between levels were equal. Exhaust inlet temperature, however, did not significantly affect effectiveness where the p-value was approximately 0.49, in which case the null hypothesis failed to be rejected. A detailed summary of ANOVA results is displayed in Table 4.

Table 4. ANOVA table for statistical comparison between finned and non-finned heat exchangers. Low p-values between groups indicated heat transfer was significantly affected by type of heat exchanger.

Source of Variation	SS	df	MS	F	p-value	F crit
Groups	60.22	4	15.05	3811.8	1.13E-222	2.408
Interaction	1.88	4	0.47	118.8	1.25E-56	2.408
Total	65.73	259				

Results of the 99% confidence intervals are shown in Table 5. For each combination of exhaust temperature and air flow rate, sufficient experimental data of heat capture were within the upper and lower bounds of the confidence intervals. There was strong evidence that the collected data were near the mean heat capture for each combination, which was also concluded from the low standard deviations from Table 2.

Table 5. Confidence intervals (99%) for heat capture at each combination of air flow rate and exhaust temperature.

Exhaust Temperature [°C]	Air Flow Rate [m^3 min^{-1}]	Lower Bound [kW]	Upper Bound [kW]
427	2.8	1.99	2.05
704	2.8	3.50	3.58
538	2.8	2.59	2.65
538	1.4	2.02	2.07
538	2.1	2.43	2.50

Heat Exchanger Evaluation during Gasification

Average MC (wet basis) and average heating value of the CGT were 11.6% and 15.54 MJ kg^{-1} (6682 Btu lb^{-1}), respectively. Moisture content of the CGT was low enough such that additional drying was not needed before gasification. To ensure MC would not increase, the CGT was stored in a sealed barrel after being hammer milled until the biomass was ready for gasification tests. Heating value of the CGT was sufficient for smooth operation of the FBG.

Figure 11 shows the setup of heat exchanger during gasification operation. The non-finned heat exchanger was evaluated since heat transfer was expected to be higher compared to the finned. Due to the combination of low bulk density of hammer milled CGT and volume of the feed hopper, continuous operation of the gasifier was sustained between 40 to 50 minutes. Therefore, three full feed hoppers corresponded to first heating the system, second to testing an air flow rate of 2.8 m^3 min^{-1} through the heat exchanger, and third to testing an air flow rate of 1.4 m^3 min^{-1}. Time between refills of the feed hopper was between 5 to 10 minutes. An air flow rate of 2.8 m^3 min^{-1} was tested for 38 minutes, while 1.4 m^3 min^{-1} was tested for 30 minutes. The trend of heat rates for syngas and air were similar to that shown in Figure 9. Steady state of heat

transfer between the two gases was achieved at around 20 minutes of testing. Average heat capture for air flow rates of 1.4 and 2.8 m^3 min^{-1} were 0.74 and 1.31 kW_{th}, respectively. Inlet temperatures of syngas ranged between 400°C and 409°C (753°F and 768°F).

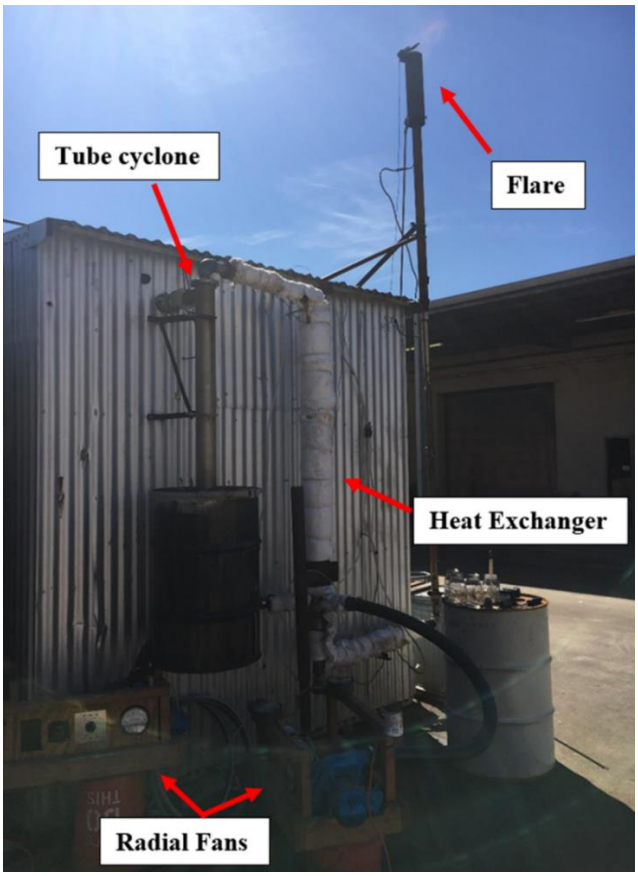

Figure 11. Set up of heat exchanger for syngas cooling during gasification.

The parameters of the heat exchanger during gasification were input into the corrected ε-NTU model to compare heat transfer between propane exhausts (control) and syngas under similar conditions. For air flow rates of 1.4 and 2.8 m^3 min^{-1}, theoretical heat transfer was 1.5

and 1.9 kW_{th}, respectively. Actual heat transfer was about 50% to 70% of theoretical, which indicated that the fouling layer of biochar and tar inhibited heat transfer. Average thermal conductivity of tars for 1.4 and 2.8 $m^3\ min^{-1}$ were calculated to be 0.022 and 0.039 $W\ m^{-1}\ K^{-1}$, respectively, with an overall average value of 0.03 $W\ m^{-1}\ K^{-1}$. Applying the overall average thermal conductivity of tar to the model, relative errors of heat capture were 3.1% and 9.2% for first and seconds tests, respectively. These low relative errors indicated that the overall average tar thermal conductivity was an adequate estimate for modeling syngas cooling.

Tar thickness was measured to be about 1 mm for the estimation of thermal conductivities for both tests. Biochar thickness was measured to be 9 mm at the completion of both tests, and a value of 3 mm was assumed for the first test of an air flow of 2.8 $m^3\ min^{-1}$. High thicknesses of biochar build up were a consequence of the low capture efficiency of the tube cyclone in the pilot scale system. However, the 250 kW_e FBG system comes equipped with a two stage cyclone cleaner, where build-up of char will not be as significant as the pilot system.

Total percentage of waste heat capture from the heat exchanger was estimated with the corrected ε-NTU model. The thickness of the fouling layer was adjusted to that estimated for the larger FBG system, which was 2 mm for each component. Assuming that syngas be cooled from 704°C to 150°C, the total potential sensible waste heat was 8.3 kW_{th}. Utilizing the model, the heat exchanger was expected to capture 34% of total waste heat in one pass at an ambient air flow rate of 2.8 $m^3\ min^{-1}$.

At the beginning of each gasification test, a glass mason jar was connected to the bottom of the heat exchanger to capture potential liquid tars. For all tests, insignificant amounts of tar were observed to be captured, while small amounts of biochar were captured for the duration of each test. During operation of the heat exchanger between all three tests, lowest outlet

temperature of syngas was 307°C (584°F) while highest was 325°C (617°F). This implied that tars from CGT syngas did not significantly condense at temperatures above 580K.

Energy Distribution from CGT Gasification

The distribution of theoretical electrical power, heat captured from syngas, and heat captured from generator exhaust gases is presented in Figure 12. Based upon the distribution, capturing heat from generator exhausts had the highest fraction of useful energy while capturing heat from syngas had the lowest. The total sensible waste heat was determined to be approximately 3450 kJ kg^{-1} of CGT, or 1750 kJ Nm^{-3} of syngas. This total was estimated through the summation of capturing waste heat from both generator exhausts and syngas to total input of CGT and flow of syngas. Conversion efficiency of energy from CGT to electricity was calculated to be around 10%, while efficiency to heat was about 20%. Therefore, by implementing a heat recovery system, the overall efficiency has the potential to be increased to approximately 30%.

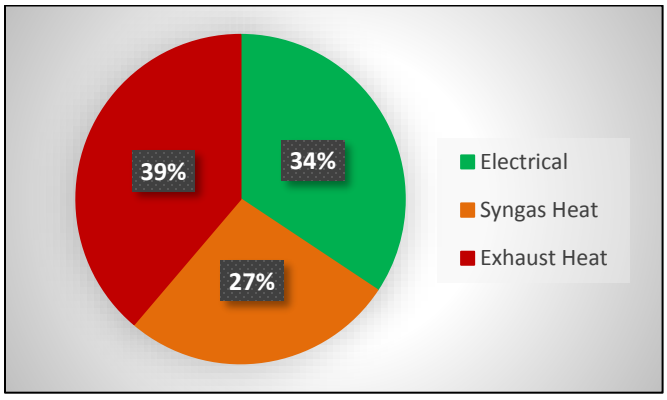

Figure 12. Distribution of useful energy from the pilot-scale FBG system. Exhaust gases contained the highest fraction of useful energy, while syngas contained the lowest.

CONCLUSIONS

A prototype counter flow, non-finned double pipe heat exchanger was designed and evaluated to capture waste heat from a pilot scale FBG system. The heat exchanger used in this study demonstrated that through one pass, up to 58% and 34% of total waste heat can be captured from generator exhaust and syngas, respectively, with effectiveness of up to approximately 0.42 and 0.33, respectively. Assuming that both gases were cooled to 150°C (300°F), the total sensible waste heat potential from gasifying CGT was 3450 kJ per kg of CGT, or 1750 kJ per Nm^3 of syngas, which would increase overall efficiency by around 20%. Heat exchanger thermal capacity displayed a linear increasing trend with increasing inlet exhaust temperature, while maximum *UA* was about 7 W K^{-1} with increasing air flow. Compared to a finned pipe of the same size and length, an non-finned double pipe heat exchanger provided up to 10% additional heat transfer, which demonstrated higher efficiency. Heat exchange during gasification tests performed for this study revealed the fouling layer reduced heat transfer by 30% to 50%. Tar thermal conductivity was estimated at 0.03 W m^{-1} K^{-1}, which reduced relative errors of heat capture to around 10% and below. In addition, liquid tars were not captured at temperatures of 307°C and above, which indicated that a tar trap did not need to be implemented in the first stage heat exchanger. Results from this study aided in the modeling of the HRS for the 250 kW_e FBG system.

CHAPTER III

DEVELOPMENT OF A HEAT RECOVERY SYSTEM MODEL

INTRODUCTION

Research and work presented in this chapter were used in conjunction to develop a heat recovery system (HRS) for the 250 kW_e fluidized bed gasification (FBG) system such that the system can be classified as cogeneration. Heat generated from the FBG has the potential to be captured and utilized in an efficient manner that benefits cotton gins, such as supplying heated air. Waste heat from syngas and generator exhausts could be captured in the form of heated air and used for drying incoming seed cotton at a gin. Thermal energy from the HRS would benefit gins by either reducing or replacing fuel usage that would otherwise be used for a burner.

The small-scale heat exchanger presented in Chapter II demonstrated several promising and informative aspects of capturing waste heat from generator exhausts and syngas. One major finding was that a non-finned heat exchanger provided up to 10% additional heat transfer than a finned heat exchanger at the same length and testing conditions. This was a consequence of using stainless steel as the material where the fins imposed conduction resistance. Another finding was that effectiveness of the heat exchanger reached up to 0.42, which was greater than the estimation of 0.27 from the initial effectiveness number of transfer units (ε-NTU) model. The high effectiveness revealed that the design of the heat exchanger provided an efficient means of capturing waste heat. Lastly, capturing waste heat from hot syngas caused tars to condense within the heat exchanger's surfaces, building a fouling layer of tars and fine biochar which reduced heat transfer by 30% to 50%. Modeling of heat transfer from syngas cooling produced an estimation of tar thermal conductivity of 0.03 $W\ m^{-1}\ K^{-1}$. Conclusions from experimental

results from the small-scale heat exchanger aided in the design of the large-scale heat exchanger and HRS.

The ε-NTU model that was developed and corrected in Chapter II revealed that relative errors of actual and theoretical heat capture could be reduced to 3.5% and below by incorporating a correction factor. This correction factor, F_{UA}, was established by averaging the ratios of actual to theoretical overall conductance (UA) for all tests. However, the value of F_{UA} may be specific to the dimensions of a heat exchanger and operational characteristics of fluids. Overall conductance is a function of surface area along with temperature and flow rate of both fluids. Therefore, a correction factor also needed to be established for the large-scale heat exchangers for the design of the HRS. This was accomplished by performing similar experiments to that presented in Chapter II.

Increasing effectiveness and efficiency of heat exchangers typically involves incorporating modifications, such as baffles. Baffles in heat exchangers are obstructions to the flow of fluids that induce turbulence, resulting in higher rates of heat transfer (Permatasari and Yusuf, 1977). However, increased heat transfer comes at an expense. Increasing turbulence causes a larger pressure differential, which equates to increasing power consumption by the device supplying the fluid. Therefore, the tradeoff between additional power consumption versus additional heat transfer must be compared and the economics evaluated. Since economic feasibility of FBG at cotton gins is relatively sensitive (Richardson et al., 2016), evaluation of baffles for heat exchangers for the HRS was not performed in this research.

In addition to baffles, type of material for heat exchangers also affects heat transfer due to the materials thermal conductance. Copper, aluminum, and black iron are among common materials for heat exchangers. Similar to baffles, the tradeoff between cost of material and

additional heat transfer must be evaluated. From the ε-NTU model for the small-scale heat exchanger, the thermal conductivity was varied to determine effect on overall heat transfer. Increasing conductivity to values for pure aluminum (237 W m^{-1} K^{-1}) and pure copper (400 W m^{-1} K^{-1}) (Bergman and Lavine, 2011) resulted in an insignificant increase in heat transfer of only up to 10 W. Type of material would also affect F_{UA} for heat transfer, which could be evaluated to correct another model. However, the corrosion resistance of common heat exchanger materials to the contaminants from FBG were unknown since there is lack of literature. For this reason, 304 stainless steel was used for the large-scale heat exchanger, guaranteeing long life of equipment.

In order to model the HRS for the 250 kW_e FBG system, the properties and characteristics of generator exhausts and syngas were evaluated. A preliminary analysis (Figure 13) of the FBG system was conducted to estimate the total waste heat potential from both hot gases. Data of syngas from cotton gin trash (CGT) gasification (Maglinao et al., 2015) was utilized to estimate properties and flow rates of syngas and CGT. Syngas data included gas yield, composition, and lower heating value (LHV). Assumptions of syngas combustion in the generator included a 20% electrical efficiency, initial exhaust gas temperature of 538°C (1000°F), and an air-to-fuel (A/F) ratio of 1 kg_{air} kg_{syngas}^{-1}. Potential sensible heat capture from cooling syngas and generator exhausts were 233 and 272 kW_{th}, respectively. By incorporating a heat recovery system for the gasifier, overall energy efficiencies can be increased from about 10% to approximately 30%.

Energy usage data of Texas cotton gins (TCGA, 2010 – 2017) was used to estimate the range of thermal demands for cotton gins. Assuming an electricity usage of 40 kW-hr $bale^{-1}$, the 250 kW_e FBG had the potential to supply a ginning capacity of about 6.25 bales per hour (bph). Annual comparisons between total potential heat capture from the 250 kW_e FBG system

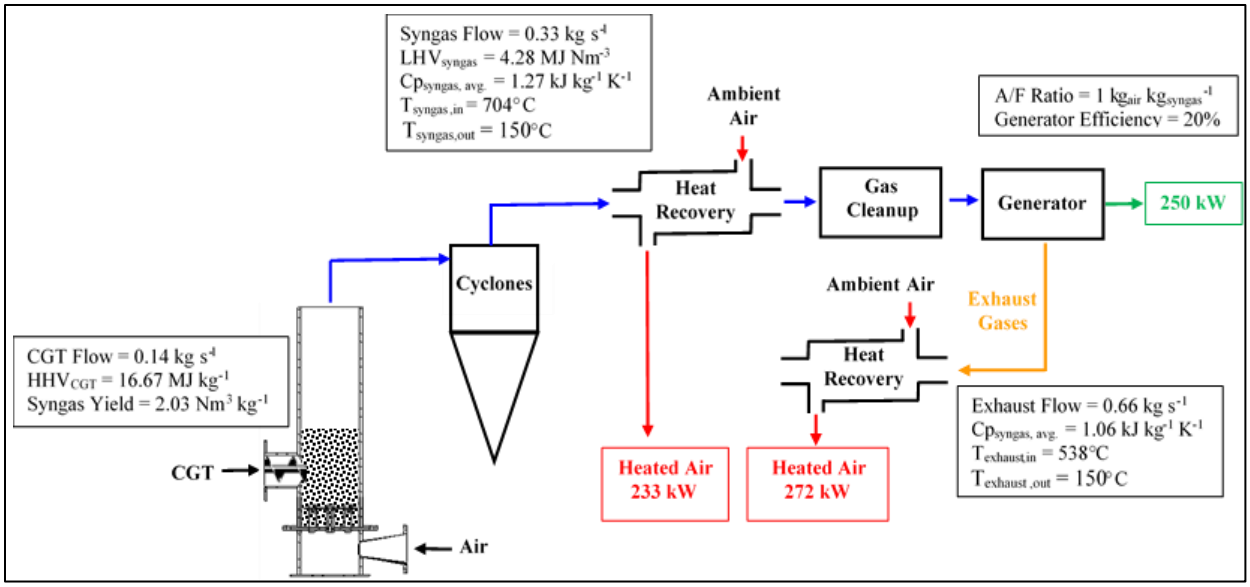

Figure 13. Preliminary analysis of heat capture from the 250 kW_e FBG system. An estimated 500 kW of thermal energy was available by cooling syngas and generator exhausts to 150°C.

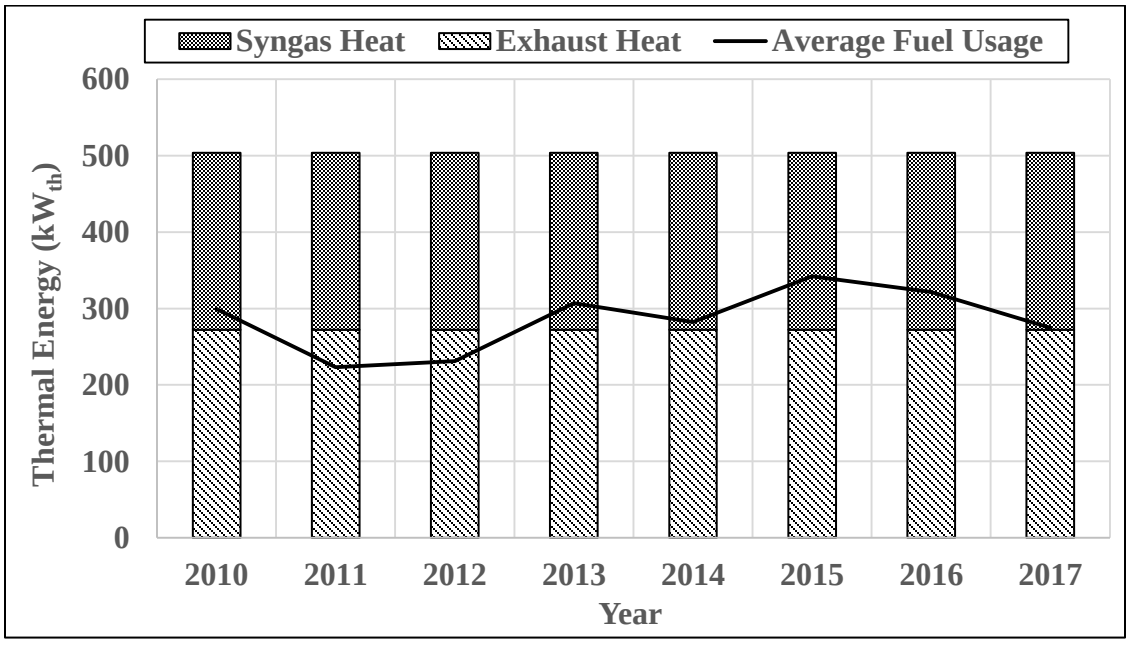

Figure 14. Comparison of potential thermal energy from FBG and Texas gin fuel usage. By scaling the FBG to supply an electrical capacity of 6 bph, waste heat from the FBG exceeded average fuel usage for all years. In some years, heat from generator exhausts alone could meet average thermal demand.

and Texas gin's average thermal demand is illustrated in Figure 14. For years 2011 and 2012, waste heat from generator exhausts alone were capable of supplying average demand. Capturing waste heat from both exhaust gases and syngas exceeded average fuel usage for all years, demonstrating that the HRS can replace a majority of natural gas or propane.

Two significant assumptions were made in the preliminary analysis of the 250 kW_e FBG system, which were the air-to-fuel (A/F) ratio of syngas combustion in the generator and the outlet temperature of generator exhausts. Although these two parameters could be estimated by referring to a generator manual, there was uncertainty since syngas has different characteristics when compared to natural gas or propane. These characteristics include heating value and chemical composition of gas. Therefore, experiments were conducted with the mobile unit FBG for a more accurate approximation of the generator exhaust's flow rate and temperature, which would result in a more accurate model for the HRS.

The primary function of the HRS model was to evaluate the overall heat capture based upon number of heat exchangers. For each heat exchanger, heat transfer and outlet temperatures of both gases were evaluated based upon inlet temperatures and mass flow rates. Since heat exchangers were in series, the outlet temperature of one heat exchanger was the inlet temperature for the following heat exchanger. As more heat exchangers were added to the HRS, overall heat capture increased but in a diminishing manner. This meant that outlet temperatures of heated air for each heat exchanger were not equal, and that a method for estimating the final temperature of mixed air from all heat exchangers was needed. An additional function of the model was to estimate the pressure differential of air flowing through each heat exchanger, which was to estimate power consumption for each blower. Therefore, the final model was capable of

estimating overall heat capture, temperature and flow of final mixed air, and total blower power consumption based upon a varying amount of heat exchangers.

Objectives

The objectives presented in this chapter were to acquire the necessary data for the construction of the HRS model for the 250 kW_e FBG system. Specific objectives were to:

- Estimate the flow rate and temperature of generator exhaust gases from syngas combustion for the 250 kW_e FBG system,
- Evaluate a heat exchanger for the 250 kW_e FBG to model accurate heat transfer, and
- Develop a HRS model and provide an initial design.

MATERIALS AND METHODS

Generator Exhaust Experimental Set Up

Experimental tests were performed to evaluate the effect that engine load had on the properties of syngas combustion in an IC engine / generator. Gasification experiments were conducted on the trailer mounted, mobile unit gasifier with CGT and wood chips (separately) as the biomass fuels. Properties of syngas combustion that were evaluated included flow rate and temperature of generator exhausts. Since the mobile FBG unit was equipped with a 30 kW_e generator (QT03015ANS, Generac Power Systems, Waukesha, WI) (Appendix A), correlations were established between percent engine load (%load), equivalence ratio (ER), and exhaust temperature. These correlations were used to estimate the characteristics of the exhaust gases for the 250 kW_e FBG system.

Schematic of the experimental set up for generator tests is shown in Figure 15. Syngas and air were mixed and combusted in the generator to produce exhausts. An orifice meter was placed upstream of the generator to measure the flow rate of syngas, while another orifice meter was implemented downstream of the generator in the exhaust duct. Thermocouples were attached to the orifice meters to measure the temperatures of both gases. The generator was equipped with a digital display that showed real-time electrical power.

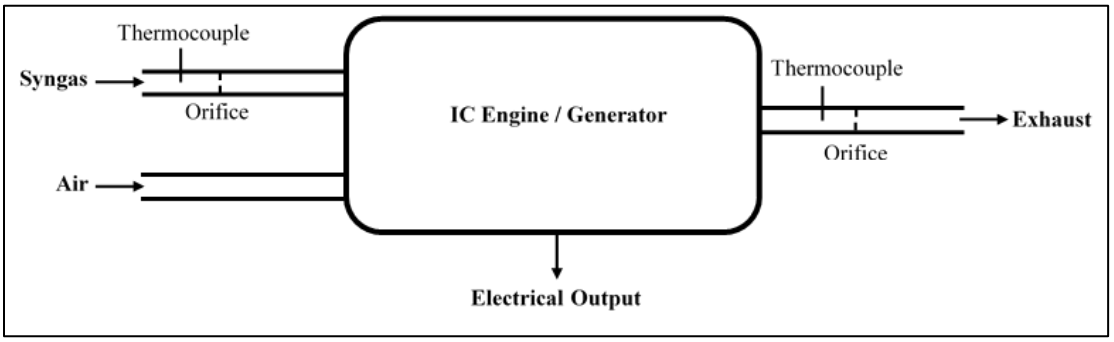

Figure 15. Experimental set up of generator exhaust tests. Orifice meters and thermocouples were placed in syngas and exhaust ducts to measure flow rate and temperature.

Experiments were categorized by varying load on the generator for each test. Since the generator was equipped with a digital display of electrical output, the power generated was recorded with each data point and correlated to a percent-load (%load) of the rated output of the generator. Three different loads on the generator corresponded to each test: no load (exercise cycle), low load, and high load. Low load for the generator was induced by powering the chiller and water pump for the gasifier, while high load was powering the chiller, water pump, and a

furnace. Due to the high consumption rate and limited amount of biomass fuel for the gasifier, each test was limited to 30 minutes where data were collected in one minute intervals.

Initially, the generator was fueled by methane while the gasification process was allowed to become in equilibrium and steady state. Once the syngas appeared to have a steady and healthy flare, the generator was manually weaned off methane into syngas. Data collection for the first test was initiated approximately five minutes after the generator was fueled by only syngas such that the temperature and flow rate of exhaust gases would stabilize. Data collection for subsequent tests were initiated once the desired load was induced on the generator. Data for all tests were collected when the generator was fueled solely by syngas.

Flow rate of syngas and exhaust gases were calculated by recording the temperature and pressure drop across the orifice meters. Temperature was used to calculate gas density with the use of the Ideal Gas Law, while flow rate was calculated through the orifice meter equation (equation 10).

$$\dot{V}_{orifice} = 3.478 * K * D_{orifice}{}^{2} \sqrt{\frac{\Delta P_{orifice}}{\rho_{air}}} \quad (10)$$

where $\dot{V}_{orifice}$ is orifice volumetric flow rate ($m^3\ s^{-1}$), K is orifice constant (dimensionless), $D_{orifice}$ is orifice diameter (m), $\Delta P_{orifice}$ is pressure drop across orifice (mm H_2O), and ρ_{air} is air density ($kg\ m^{-3}$). Orifice meters were calibrated with a laminar flow element (LFE) prior to testing to determine K.

Mass flow rate of air was calculated as the difference between flow rates of exhaust gases and syngas. Actual air-to-fuel (A/F) ratio was calculated by taking the ratio of mass flow rates of air to syngas. Based upon the reported composition of syngas (Maglinao et al., 2015), the molecular weight of syngas and stoichiometric A/F ratio of complete syngas combustion was

calculated to be approximately 27.6 kg $kmol^{-1}$ and 1.05 kg_{air} / kg_{syngas}, respectively. From actual and stoichiometric A/F ratios, *ER* was estimated with equation 11.

$$ER = \frac{(A/F)_{act}}{(A/F)_{stoich}} \quad (11)$$

where $(A/F)_{act}$ is actual A/F (dimensionless) and $(A/F)_{stoich}$ is stoichiometric A/F (dimensionless).

Exhaust gas temperature and flow rate for each test were plotted with the progression of time to visually display the range of values. Exhaust temperature and ER were plotted with %load where the average, minimum, maximum, and uncertainty were summarized for each test. These plots were utilized to determine the relationship that each response had with %load such that the properties of the exhaust gases could be extrapolated at rated load, or 100% load.

Statistical design of generator tests were structured as a randomized block design with one factor, where engine load was the single factor varied at 3 levels of no load, low load, and high load. Calculated responses to the tests were ER of syngas combustion and temperature of exhaust gases. For each response, null hypothesis (H_o) was determined that means were equal between levels, while alternative hypothesis (H_a) was that means were not equal. A single factor analysis of variance (ANOVA) was executed where a significance level (α) of 0.05 was used. Design Expert 8 was the statistical program used. Confidence intervals were also evaluated for both exhaust temperature and ER for each load. An alpha level of 0.01 corresponded to 99% confidence intervals where the z-value was 2.58.

Heat Exchanger Design and Experimental Procedure

Similar to the heat exchanger presented in Chapter II for the pilot scale FBG, a counter-flow, double pipe heat exchanger was selected for the 250 kW_e FBG system. The design of the

prototype heat exchanger (Figure 16) was carried out by first selecting the inner pipe as 4-inch pipe, which was the same size piping for the FBG system. The outer tube was selected to be 6-inch pipe to allow sufficient distance between the walls of both pipes. Overall length of heat exchange was 1.83 m (6 ft.), while inlet and outlet pipes were 3 inch pipe size. Five threaded couplings were implemented in the outer pipe of the heat exchanger such that thermocouples could be inserted to measure air temperature distribution as a function of length. Each coupling was spaced in increments of 0.3 m (12 in.) between the air inlet and outlet.

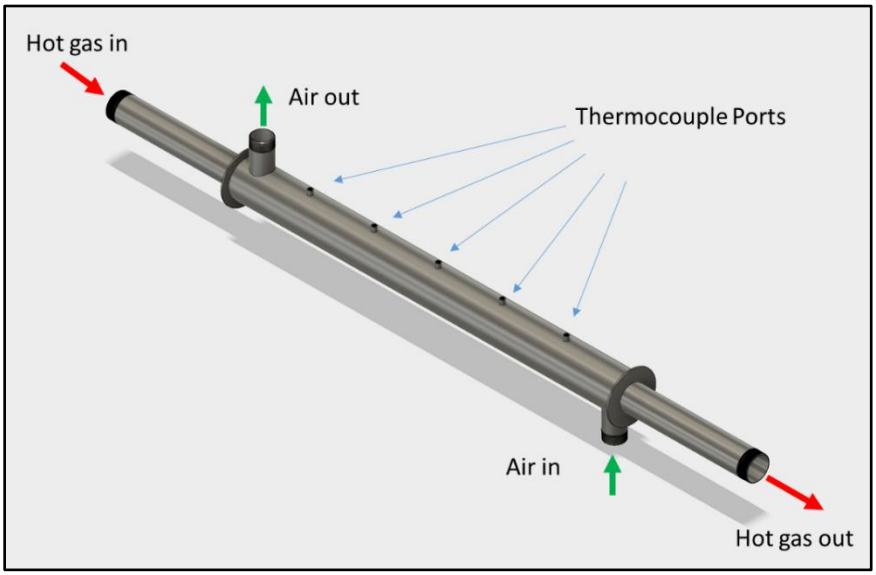

Figure 16. Design of large-scale heat exchanger for experimental evaluation. Thermocouples were placed in 0.3 m increments to measure temperature distributions.

Evaluation of the heat exchanger for model corrections was performed by conducting experiments similar to the small-scale heat exchanger for the pilot scale FBG (Figure 17). A compressor blower was used to supply air to a propane burner to generate hot exhaust gases for

the heat exchanger. Thermocouples were place at the inlet and outlet to measure the temperature differential of exhaust gases. A high pressure (HP) blower was used to supply ambient, cooling air through the heat exchanger to generate heated air. A LFE was used to measure the flow rate of air to the propane burner, while a pitot tube was used for the flow rate of ambient air. Seven thermocouples were used to measure the temperature distribution as ambient air was being heated. Pressure taps were located at the inlet and outlet of the heat exchanger to measure the pressure differential of air. The heat exchanger was insulated with ultra-high temperature ceramic fiber insulation to minimize heat losses of air to the environment.

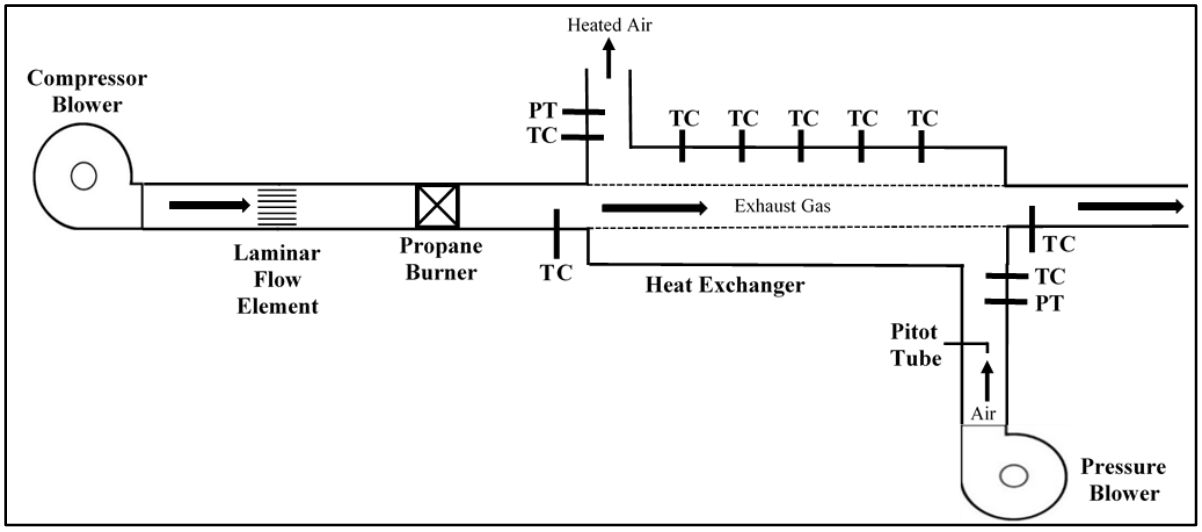

Figure 17. Experimental set up of large-scale heat exchanger for evaluation.

The propane burner used for heat exchanger experiments was a 146.5 kW_{th} (500,000 Btu hr^{-1}) Eclipse ThermJet Burner (TJ 0050, Honeywell-Eclipse, Rockford IL). Due to the configuration of the flame control unit for the burner, there was little flexibility in the control of

the combustion temperature at the outlet of the burner. The gas regulator was adjusted such that the pressure of the propane was at a minimum to sustain a reaction that produced exhaust temperatures similar to that of hot syngas at around 978°C (1300°F). This limited the flow rate of exhaust gases to a minimum flow; increasing the flow rate resulted in rapid increases of exhaust temperature reaching up to 1010°C (1850°F), which was deemed well beyond the acceptable temperature range for simulating syngas or generator exhausts.

Experimental procedure for heat exchanger testing was performed by first initiating the propane burner to preheat the system. Air supplied to the burner was set to a flow such that a constant, steady flame was sustained while maintaining a minimum exhaust temperature. Inlet and outlet temperatures of the exhaust gases through the heat exchanger were monitored and allowed to stabilize. Once steady state of exhaust temperature was achieved, ambient air flow was supplied by the HP blower and set to a target flow rate for each test. Each test consisted of 60 minutes, where data was collected every three minutes. At the completion of each test, ambient air flow was ceased in which only exhaust gases flowed through the heat exchanger for ten minutes. This removed any bias in between tests. At the completion of ten minutes, the next test was initiated and these steps were repeated.

Data collection during heat exchanger tests consisted of acquiring air pressures and temperatures to evaluate heat transfer of both exhaust gas and air. Flow rate of air supplied to the burner was measured by the pressure differential across a laminar flow element, where flow was calculated with equation 12.

$$\dot{V}_{burner} = 0.0001 * \Delta P_{LFE} - 0.0015 \quad (12)$$

where $\dot{V}_{burner}$ is volumetric air flow rate supplied to burner ($m^3\ s^{-1}$) and ΔP_{LFE} is pressure differential across the LFE (Pa). Ambient air was supplied by a type HP blower (1706S New

York Blower, Air Moving Equipment, Tomball, TX) connected to a variable frequency drive (VFD) (FRN005C1S-2U, Fuji Electric, Tokyo, Japan) to vary flow. Flow rate supplied by the HP blower was determined by measuring the total and static pressure from the pitot tube. The difference between the total and static pressure was the velocity pressure, which was used to determine the average velocity of air in the inlet duct. Flow rate was calculated by taking the product of air velocity and inlet duct area, illustrated in the following equation 13.

$$\dot{V}_{blower} = \sqrt{\frac{2*P_v}{\rho_{air}}} * A_{inlet} \quad (13)$$

where $\dot{V}_{blower}$ is volumetric air flow rate supplied by HP blower ($m^3\ s^{-1}$), P_v is velocity pressure (Pa), and A_{inlet} is cross sectional area of inlet duct (m^2). Volumetric flow rates of air were recorded in actual conditions.

Heat transfer to the air, or heat capture, was evaluated from the properties at the inlet and outlet of the heat exchanger. Mass flow rate of air was determined from the product of volumetric flow and density, while specific heat of air at the inlet and outlet temperatures of the heat exchanger was averaged. Heat transfer rate to the air was calculated with equation 9.

Pressure differential between the inlet and outlet of the heat exchanger was measured during testing to develop an empirical correlation with air flow rate. Energy losses experienced by air through the heat exchanger were at the inlet, straight section, and outlet, shown in Figure 18. Pressure differentials at the inlet (1-2) and outlet (3-4) of the heat exchanger were a consequence of inertial and constricting / enlargement losses, while straight section (2-3) pressure differentials were from friction losses. Potential and other kinetic energy losses were assumed negligible.

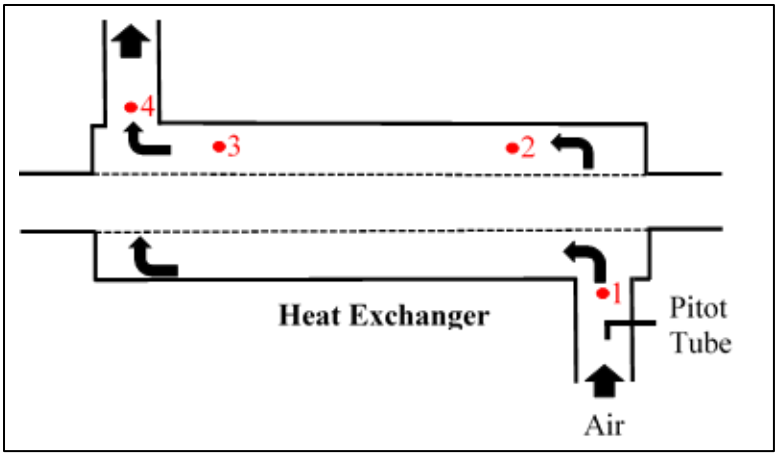

Figure 18. Regions of air energy losses within the heat exchanger.

Since length of heat exchangers for the HRS were one of the variables in the design, straight section losses were subtracted from the recorded total pressure differential. The resulting pressure differential was an estimation for losses at the inlet and outlet of the heat exchanger. Purpose of this method was to incorporate an empirical correlation between air flow rate and losses only at the inlet and outlet, while losses in the straight section could be estimated as a function of length. Straight section losses in the annulus, or $\Delta P_{straight}$, was estimated with Darcy's formula (Henderson et al., 1997), which predicts friction losses, shown in equation 14.

$$\Delta P_{straight} = f\left(\frac{L_{straight}}{D_H}\right)\left(\frac{V^2}{2g}\right) * \gamma \qquad (14)$$

where $\Delta P_{straight}$ is pressure drop in the straight section of the annulus (Pa), f is friction factor (dimensionless), $L_{straight}$ is length of straight section (m), D_H is hydraulic diameter of the annulus (m), V is air velocity (m s^{-1}), g is gravitational constant (m s^{-2}), and γ is specific weight (N m^{-3}).

Friction factor, *f*, is a function of both duct material and Reynolds number. Reynolds number is a dimensionless ratio of inertial to viscous forces that describes fluid flow as either laminar or turbulent (equation 15).

$$Re = \frac{\rho D_H V}{\mu} \tag{15}$$

where *Re* is Reynolds number (dimensionless) and μ is dynamic viscosity (Pa s). Assuming that the surfaces of the heat exchanger were of smooth conditions, *f* was estimated with the use of equation 16 (Bergman and Lavine, 2011) such that $3000 \leq \mathrm{Re} \leq 5\mathrm{x}10^6$ was satisfied.

$$f = (0.79 \ln Re - 1.64)^{-2} \tag{16}$$

Pressure losses at the inlet and outlet ($\Delta P_{i,o}$) of the heat exchanger were approximated by subtracting theoretical $\Delta P_{straight}$ from observed total pressure differential during heat exchanger tests. Volumetric flow rates of air ($\dot{V}_{blower}$) calculated from the pitot tube were reported in actual conditions and converted to standard flow ($\dot{V}_{std}$). Relationship between $\dot{V}_{std}$ and $\Delta P_{i,o}$ was established with a best-fit regression for a close approximation. Correlating $\Delta P_{i,o}$ to standard flow was done to provide a consistent relationship between the two parameters when designing heat exchangers for the overall HRS of the 250 kW_e FBG.

Design of heat exchanger experiments were of a single factor, randomized block design, where the ambient air flow rate was the single factor varied at 4 levels. As mentioned previously, the limitations of the propane burner's configuration constrained control of flow rate and temperature of the exhaust gases through the heat exchanger. Measured responses for each test was temperature at the various locations on the heat exchanger. Calculated responses were heat capture, heat exchanger effectiveness, overall conductance, air temperature distribution, and total pressure differential of air. Two replicates were performed for each air flow rate, resulting in a

total of 8 tests. Tests were randomized to reduce experimental variability, while each block represented each replicate. Analysis of variance (ANOVA) was executed with a significance level of 0.05.

During steady state for each heat exchanger test, heat exchanger performance was evaluated when heat capture was in steady state, or when change in overall heat capture was less than or equal to 1%. Tests were summarized by averaging responses during steady state, where air temperature distributions and overall heat captures were plotted with increasing length of heat exchanger. Overall effectiveness and UA were also summarized for each test.

Heat Transfer Model Corrections Procedure

The ε-NTU model developed from Chapter II was modified to estimate heat transfer by inputting dimensions of the larger heat exchanger, along with flow rates and temperatures of exhaust gases and ambient air. Overall conductance correction factor, or F_{UA}, for the model was calculated for each test by taking the ratio of actual to theoretical UA. Incorporating the correction to the model served to decrease relative errors of heat transfer such that the model provided relatively close approximations of heat capture and outlet temperatures of generator exhausts and air.

Heat Recovery System Design Process

The complete design of the 250 kW_e FBG system called for two 6 m (20 ft.) standard shipping containers. The first container was comprised of the control room, feeder, blower, gasifier, and cyclones, while the second container held the scrubber, generator, and any other additional equipment. Standard dimensions of each container were 2.4 m (8 ft.) wide by 6 m

long. Due to space limitations within each container, heat exchangers were determined to be placed above each container, where heat recovery from syngas would be above the gasifier components (container 1), while heat recovery from generator exhausts would be above the generator (container 2). This method was beneficial to allow versatility of configuration of heat exchangers, such as placement and length.

Objective of the HRS was to generate a constant stream of hot air that would be available for cotton gins to utilize as needed. Heated air supplied by the HRS does not become limited to only cotton drying, but to any process that requires heated air at gins. By providing a constant stream of heated air, gins could either reduce fuel usage by using air for direct cotton drying to replace fuel usage or preheated air for burners to reduce fuel usage. Examples of other potential processes include utilizing the heated air for battery condensers and for turbulent dryer traps. Providing a constant stream of hot air was deemed the most practical approach, especially since the thermal energy demand at gins can fluctuate significantly in short periods of time. This is a consequence of the incoming seed cotton's moisture content (MC); in any given moment, seed cotton can go from being relatively dry to being extremely wet.

Design of the HRS was comprised of two separate heat recoveries for each hot gas stream, which were generator exhaust and syngas heat recoveries. Each recovery consisted of multiple heat exchangers, in series, where the exiting hot gas stream from one heat exchanger would enter a subsequent heat exchanger. Each heat exchanger was determined to contain its own HP blower to supply ambient air. Heat recovery from the syngas was implemented immediately downstream of the cyclones such that the cooling of syngas would not negatively affect the separation efficiency of biochar particulates from syngas. Also, syngas would remain

at relatively high temperatures after the cyclones, allowing for greater heat capture potential. Heat recovery from the generator exhausts was incorporated at the outlet of the generator.

In addition to heat transfer, additional parameters were incorporated into the ε-NTU model to develop the HRS model. These additional parameters included estimating total pressure differential through each heat exchanger (ΔP_{total}) based upon a given flow rate of air, and calculating enthalpy of heated air. Total pressure differential was to utilized estimate power consumption of each blower, while enthalpy was to calculate temperature of mixed air. In order for these parameters to be used, ambient air was assumed to be dry and at standard conditions of 25°C and 1 atm.

The HRS model incorporated the estimation of power consumption of blowers that supplied air through each heat exchanger. Power consumption was a function of both volumetric air flow rate and total pressure differential through each heat exchanger. Total pressure differential through each heat exchanger was estimated by summing $\Delta P_{i,o}$ and $\Delta P_{straight}$. A fan curve was acquired (Tim Johnson, Air Moving Equipment, Personal Communication, 25 June, 2018) where static pressure and input power were plotted with flow (Appendix B). Efficiency of the blower (η_b) was calculated given certain operating points along each curve, which was approximately 34% for this particular blower. Therefore, power consumption for each blower in the HRS was estimated with equation 17.

$$P_b = \frac{\dot{V}_{blower} * \Delta P_{total}}{\eta_b} \tag{17}$$

where P_b is blower power (W), ΔP_{total} is total pressure differential of air through heat exchanger (Pa), and η_b is blower efficiency (decimal).

One aspect of the HRS design was to mix heated air from all heat exchangers, along with diluting ambient air. To estimate the temperature of a final mixture, both the conservation of mass and energy were applied. This approach incorporated the use of the enthalpy of dry air, where enthalpy was directly related to temperature. Volumetric flow rate was converted to mass basis in which the final mass flow rate was the summation from all heat exchangers. Enthalpy of air at the outlet of each heat exchanger was determined from the estimated temperature. Calculation of final enthalpy of mixed air (H_f) was performed with equation 18.

$$\dot{m}_f H_f = \dot{m}_1 H_1 + \dot{m}_2 H_2 + \ldots + \dot{m}_n H_n \quad (18)$$

where $\dot{m}$ is mass flow rate (kg s^{-1}), H is enthalpy (kJ kg^{-1}), and subscripts *f*, *1*, *2*, and *n* are final, first, second, and n^{th} streams, respectively. Once enthalpy of final air was calculated, temperature of the final mixture was determined.

Initial evaluation of the HRS was executed by cooling both generator exhausts and syngas to temperatures below 204°C (400°F) through as many heat exchangers as necessary. This design was done by utilizing the results from generator exhaust experiments, the corrected ε-NTU model for heat transfer, correlation between standard air flow rate and total pressure differential through each heat exchanger, and conclusions of tar thermal conductivity reported in Chapter II. Purpose of this approach was to overdesign the HRS such that a large majority of waste heat would be captured, allowing for optimization in the design.

In order to justify the large amount of waste heat capture from the initial design, an operational cost comparison was performed for electricity costs and natural gas costs. Electricity costs were to operate the blowers for heat exchangers, while natural gas costs were the costs to match the heat provided by heat exchangers. From the Texas Cotton Ginners' Association (TCGA) annual energy surveys for years 2010 to 2017 (TCGA, 2010-2017), average electricity

and natural gas costs were \$0.083 kW-hr^{-1} and \$4.56 GJ^{-1}, respectively. Typically gins use either natural gas or propane as fuel for burners, but for a conservative approach, natural gas was selected since it's generally cheaper than propane. Comparison of costs were compared with number of heat exchangers to determine a break-even point, demonstrating economic feasibility from an operational standpoint.

The final evaluation for optimizing the HRS design was to match the total air flow rate to the seed cotton drying requirements. Required drying air was estimated with equation 19.

$$\dot{V}_{req} = \frac{(bph)*(HM)*(A/C)}{3600} \quad (19)$$

where $\dot{V}_{req}$ is required standard flow rate of drying air (Nm^3 s^{-1}), *HM* is harvest method (kg$_{cotton}$ bale^{-1}), and *A/C* is air-to-cotton ratio (m$^3_{air}$ kg$_{cotton}^{-1}$). From the TCGA surveys for years 2010 - 2017, an average electricity usage of 42 kW-hr bale^{-1} was calculated which equated to a ginning capacity of about 6 bph for the 250 kW FBG. Assuming a stripper gin, *HM* was estimated to be about 900 kg$_{cotton}$ bale^{-1} (2000 lb$_{cotton}$ bale^{-1}). Lummus Corporation generally suggests an *A/C* ratio of 1.56 Nm$_{air}^3$ kg$_{cotton}^{-1}$ (25 ft$_{air}^3$ lb$_{cotton}^{-1}$). With these input parameters, the estimated required flow rate of drying air was determined to be 2.34 Nm^3 s^{-1} (5000 scfm). A stripper gin was selected for the air flow requirement as this provides a more conservative approach to the HRS design. In addition, a majority of gins located in Texas are stripper gins (Kelley Green and Aaron Nelson, TCGA, personal communication, 13 April 2016).

RESULTS AND DISCUSSION

Generator Exhaust Experimental Results

Experimental set up of generator tests is shown in Figure 19. Ultra-high ceramic fiber insulation was used to insulate the piping downstream of the muffler. Although insulation was used, temperature readings were assumed to be lower than temperatures exiting the engine, resulting in conservative values. Operation of the generator was achieved by manually controlling the flow of syngas such that the engine operated sustainably. Throughout all tests, there were instances when the engine would stutter and in some cases cease operation. This was a consequence of fluctuations in the heating value and flow of the syngas. In these instances, syngas was mixed with methane to get the engine operating sustainably. All data was collected when the engine was fueled solely by syngas.

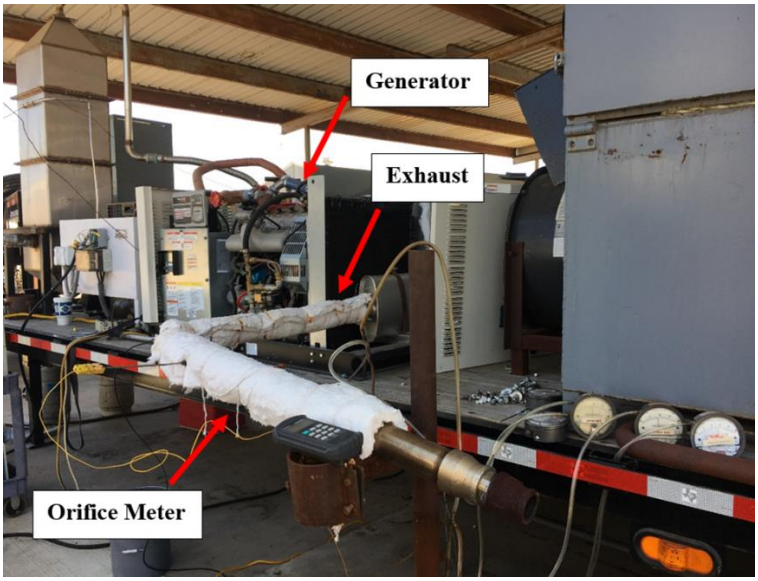

Figure 19. Set up of generator exhaust tests.

The average electrical loads for low and high load were 2059 and 8263 W, respectively, which corresponded to average %loads of 6.9% and 27.5%, respectively. Results of exhaust gas temperature and flow with the progression of time are illustrated in Figure 20. At high load, both responses were noticeably greater than no load and low load. Since low load was relatively similar to no load, there may have not been enough variation of electrical load to distinguish differences in exhaust flow. In addition, the manual control of syngas flow was varied such that the engine operated sustainably, rather than being set for optimal engine efficiency. Lastly, the fluctuation of heating value of syngas also affected the responses and operation of the generator.

Average exhaust gas temperatures and uncertainties with varying load are displayed in Figure 21. An increase in electrical load resulted in a near-linear increase in average exhaust gas temperature with an R^2 value greater than 0.99. Through extrapolation of this linear trend, the projected temperature at rated load was calculated to be approximately 593°C (1100°F), which was higher than the initial estimation of 538°C. The reported exhaust temperature from the generator manufacturer with natural gas as the fuel was 610°C (1130°F) at rated load.

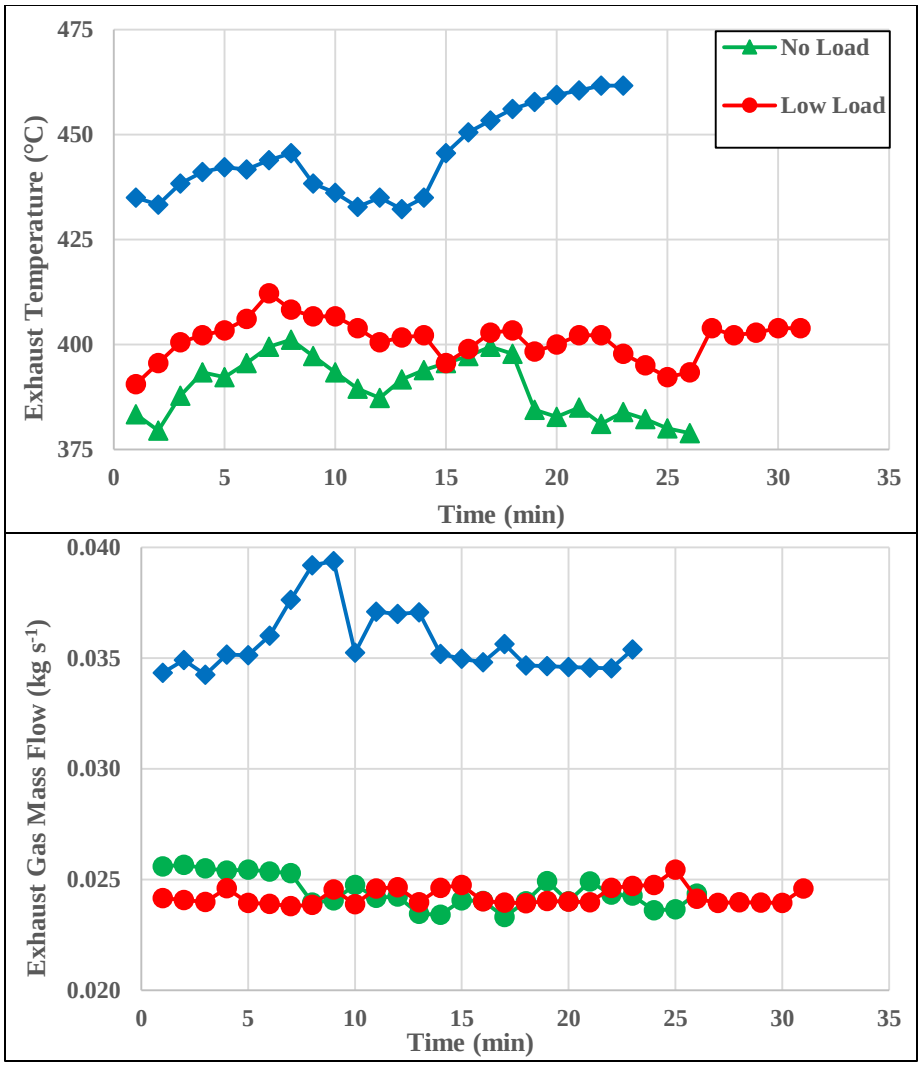

Figure 20. Results of exhaust temperature and flow rate by varying electrical load. At high load, both temperature and flow rate were noticeably higher than low load and no load.

Average ER and uncertainties with varying load are illustrated in Figure 22. Large fluctuations were observed within each test; standard deviations for no load, low load, and high load were 0.05, 0.04, and 0.1, respectively. This is also shown in the uncertainty error bars. Again, these large fluctuations were a consequence of the manual control and variation in heating value of syngas. The average ER from the three loads was determined to be

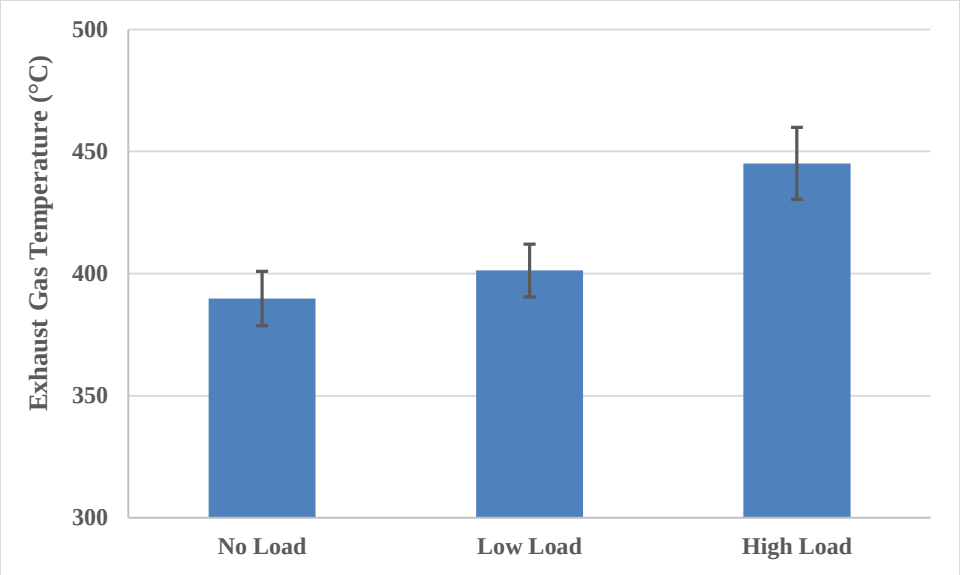

Figure 21. Average exhaust temperatures with varying electrical load. Increasing load resulted in a near-linear increase in temperature.

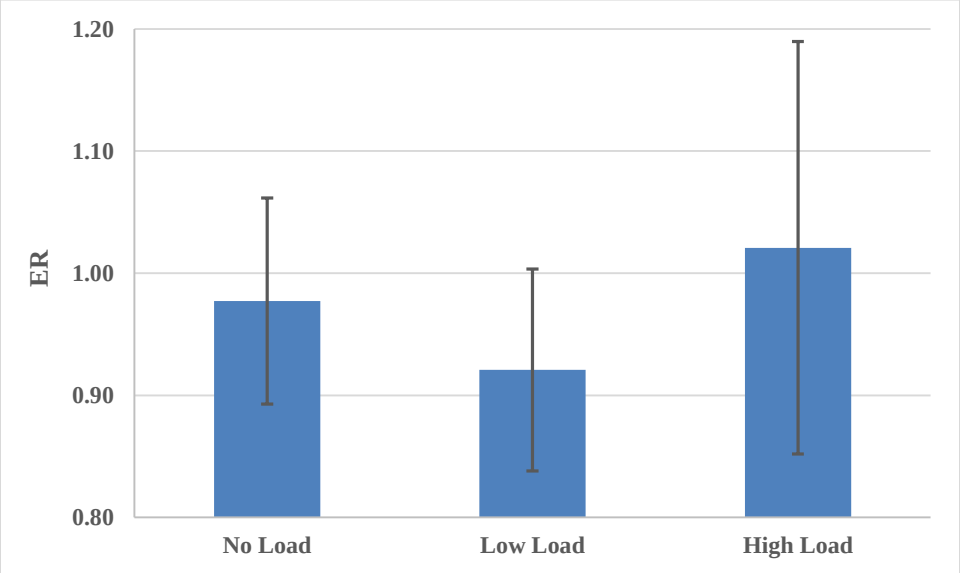

Figure 22. Average ER with varying electrical load. Between no load and high load, ER was insignificantly affected by load, where overall average ER was 0.97.

approximately 0.97. Compared to natural gas, the ER of the generator at rated load was 0.78. Average ER of 0.97 was estimated to be constant with varying load since the engine operated sustainably around this value for all three loads. However, common trends of ER with varying load in literature have somewhat bell shaped curves where peak power was achieved at ER's of around 0.77 (Li et al., 2016) and 1.0 (Al-Baghdadi, 2004).

Design Expert revealed that no transformation of exhaust temperature or ER data were recommended from Box-Cox plots. Normal plot of residuals showed relative normality with some scattering. Studentized residuals showed constant variance assumption to be true. Low p-values of <0.001 were calculated for exhaust temperature and ER between the three levels of no load, low load, and high load, which indicated that load significantly affected responses. Although ER was significant, a single factor ANOVA was performed between no load and high load. A p-value of 0.065, which was greater than α=0.05, indicated that ER was insignificantly affected between the two loads. Therefore, the null hypothesis for ER that means between no load and high load failed to be rejected. Exhaust temperature's null hypothesis was rejected. A detailed summary of ANOVA results for exhaust temperature and ER are shown in Table 6 and Table 7, respectively. Results of 99% confidence intervals for exhaust temperature and ER with varying load are displayed in Table 8 and Table 9, respectively. A majority of observed data for both parameters were within the range of intervals.

Results from generator tests were used to estimate the initial properties of exhaust gases for the design of the HRS. Assuming the generator for the 250 kW_e FBG system operated at rated load, the exhaust temperature was expected to be 593°C. Assuming an ER of 0.97, $(A/F)_{act}$ was about 1.0 $kg_{air}\ kg_{syngas}^{-1}$, which was the estimation in the preliminary analysis from Figure 13. At this $(A/F)_{act}$, mass flow of exhaust gases were approximately double that of syngas.

Table 6. ANOVA results for exhaust temperature from generator tests. Low p-value indicated that temperature was significantly affected by electrical load.

Source of Variation	SS	df	MS	F	p-value	F crit
Between Groups	122245.6	2	61122.8	330.6054	4.08E-35	3.135918
Within Groups	12202.17	66	184.8814			
Total	134447.8	68				

Table 7. ANOVA results for ER from generator tests. Low p-value indicated that ER was significantly affected by load.

Source of Variation	SS	df	MS	F	p-value	F crit
Between Groups	0.143863	2	0.071932	14.38158	6.54E-06	3.135918
Within Groups	0.330108	66	0.005002			
Total	0.473972	68				

Table 8. Confidence intervals (99%) for exhaust temperature with varying electrical load.

Load Type	Average Exhaust Temperature [°C]	Lower Bound [°C]	Upper Bound [°C]
No Load	390	386	393
Low Load	401	399	403
High Load	445	440	451

Table 9. Confidence intervals (99%) for ER with varying electrical load.

Load Type	Average ER	Lower Bound	Upper Bound
No Load	0.978	0.950	1.005
Low Load	0.921	0.904	0.968
High Load	1.021	0.968	1.074

Therefore, a mass flow of 0.66 kg s^{-1} and temperature of 593°C were used as the initial properties of exhaust gases for the HRS model.

Heat Exchanger Experimental Results

Heat exchanger experiments were conducted by varying the ambient air flow rate for each test, while maintaining a relatively constant flow and temperature of exhaust gases. Setup of the heat exchanger tests is illustrated in Figure 23. Four ambient air flow rates of 0.05, 0.07, 0.09, and 0.10 m^3 s^{-1} (100, 150, 200, and 220 ft^3 min^{-1}) were selected for what the HP blower was capable of supplying. Two replicates were performed for each flow rate. Ambient air temperatures between 26°C and 35°C (79°F and 95°F) were observed between all tests. An average mass flow of exhaust gases for all tests was 0.03 ± 0.0005 kg s^{-1}, where the addition of propane, by mass, was assumed negligible. As mentioned previously, flow of exhaust gases were configured to produce temperatures relatively similar to that of syngas.

Eight tests were performed to evaluate performance of the heat exchanger, which included evaluating air temperature distribution, heat capture, effectiveness, and overall conductance. A summary of inlet parameters for each test is described in Table 10. Since there was little control in exhaust temperature, each replicate of air flow rate was evaluated as its own test for model corrections. For example, tests #3 and #4 had the same air flow rate, but exhaust inlet temperature was 751°C and 792°C (1384°F and 1457°F), respectively.

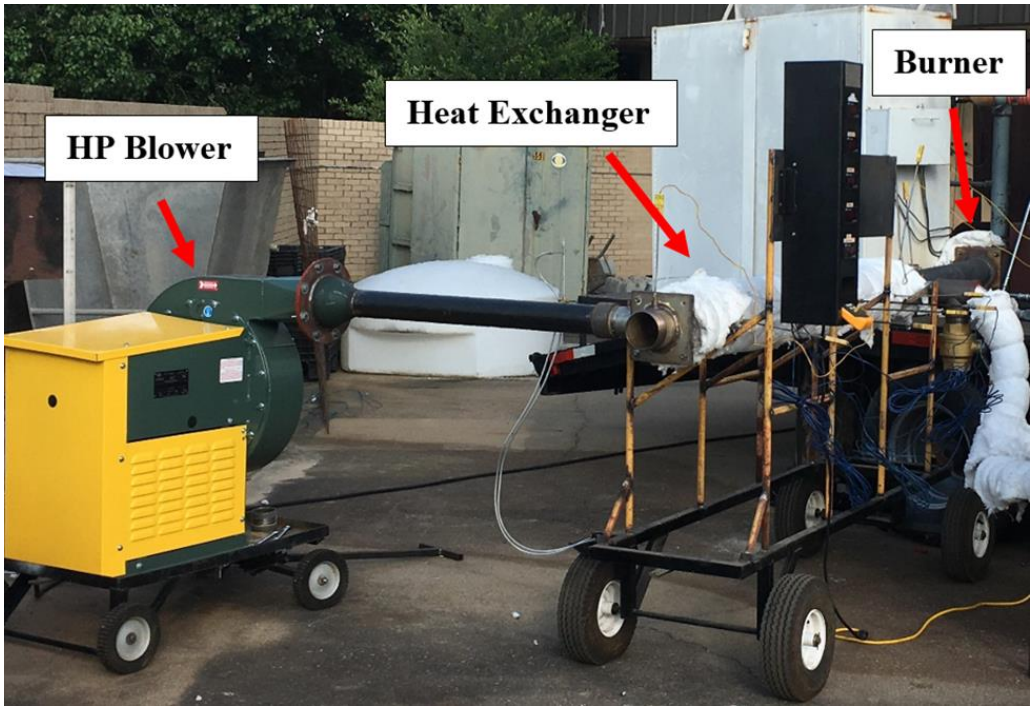

Figure 23. Set up of heat exchanger tests.

Table 10. Summary of ambient air flow rate, air inlet temperature, and exhaust inlet temperature for large-scale heat exchanger tests.

Test [#]	Ambient Air Flow [$m^3 s^{-1}$]	Air Inlet Temperature [°C]	Exhaust Inlet Temperature [°C]
1	0.05	34	755
2	0.05	27	731
3	0.07	35	751
4	0.07	30	792
5	0.09	28	741
6	0.09	28	734
7	0.10	31	772
8	0.10	26	725

For each test, air temperature distributions within the heat exchanger were plotted with increasing length, displayed in Figure 24. From the data, air temperature was generally higher at lower flow rates of air, which agreed with conclusions from Chapter II. A direct relationship was not observed with the data since there was fluctuation of exhaust temperature between tests. Temperature distributions for all tests displayed a common relationship; a rapid increase in air temperature between the air inlet and first thermocouple, gradual increase to fourth thermocouple (1.2 m), then another rapid increase to the fifth thermocouple and outlet. Both regions of rapid temperature increases were a consequence of the heat exchanger's inlet and outlet, where the air experienced turbulence. These turbulent regions induced pressure differentials of the air, resulting in increased heat exchange. This is a common tradeoff for heat exchangers.

Results of heat capture with increasing length of heat exchanger are presented in Figure 25. Again, conclusions from Chapter II were observed where increasing air flow rate increased heat transfer but decreased outlet temperature. Trends of heat capture were similar to that of air distributions where turbulence of the inlet and outlet increased heat capture. Overall heat capture between replicates for each flow rate were relatively similar, with the exception of test #7 where heat capture had an irregular spike to about 10 kW. A similar spike can be seen in the temperature distribution in Figure 24. Further inspection of the data revealed that recorded temperatures for test #7 were fairly consistent throughout the test with the exception of the outlet air temperature. The conclusion was made to classify test #7 as an outlier since tests #5-8 had similar flow rates, with heat captures at around 7.5 kW for three tests. Therefore, test #7 was removed for model corrections due to the irregular high heat capture, even though higher heat capture was desired.

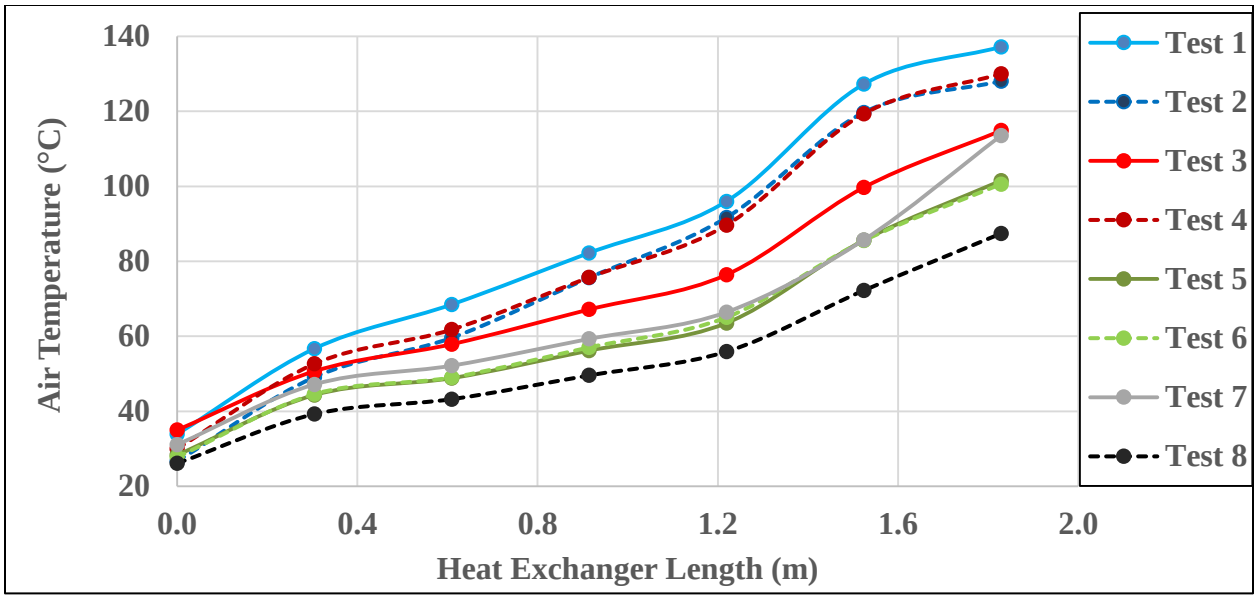

Figure 24. Heat exchanger air temperature distributions. Rapid increases in heat capture were observed at the inlet and outlets of the heat exchanger, while gradual increases in heat capture were observed in the straight section.

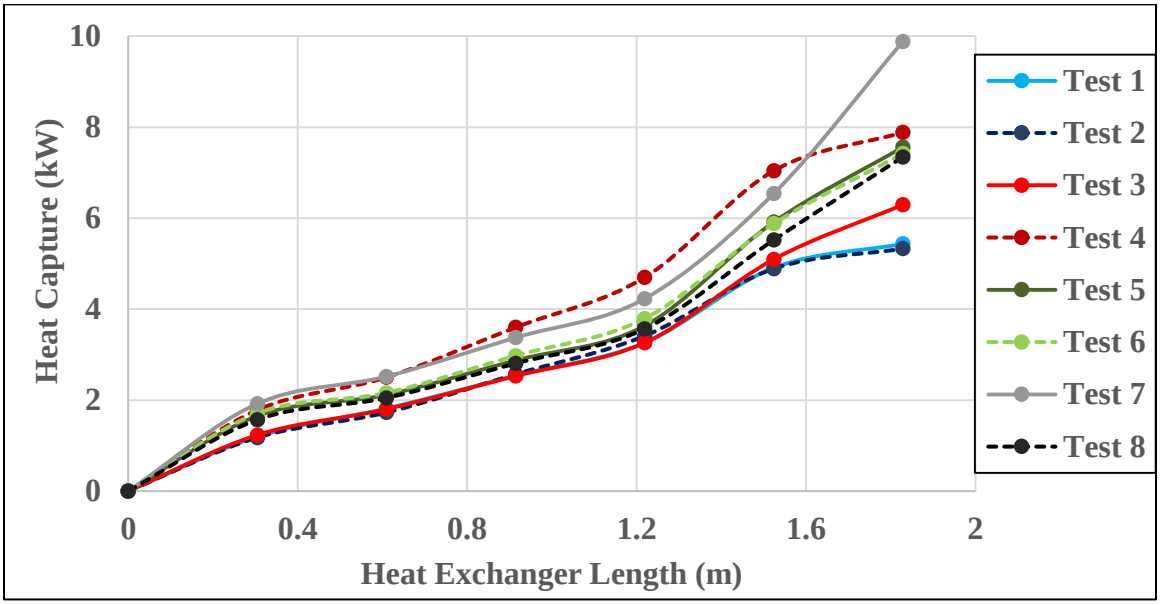

Figure 25. Results of heat capture by varying length of heat exchanger. Test #7 revealed an irregular spike in heat capture which resulted in the removal for model corrections.

Performance results of the large heat exchanger is displayed in Table 11, where overall heat exchanger effectiveness and UA are reported for each test. Overall effectiveness and UA generally increased between tests, indicating that increasing air flow rate positively increased the performance of the heat exchanger. Again, test #7 displayed irregularly high values of effectiveness and UA, which were removed from model corrections.

Table 11. Results of overall effectiveness and conductance from large-scale heat exchanger tests. Effectiveness and UA increased with increasing air flow rate.

Test [#]	**Overall Effectiveness**	**Overall Conductance [W K^{-1}]**
1	0.22	9.2
2	0.22	9.2
3	0.26	10.8
4	0.30	13.2
5	0.31	13.4
6	0.30	13.2
7	0.39	18.0
8	0.30	13.1

Actual air flow rate was converted to standard and plotted with $\Delta P_{i,o}$, displayed in Figure 26. Low uncertainties of $\Delta P_{i,o}$ were observed throughout tests, which ranged between 0 and 19 Pa. An empirical correlation between standard air flow and $\Delta P_{i,o}$ was established with a 2nd order polynomial regression, shown in equation 20.

$$\Delta P_{i,o} = 164797 * \dot{V}_{std}{}^{2} - 5313.3 * \dot{V}_{std} + 317.82 \quad (20)$$

where $\Delta P_{i,o}$ is pressure differential of the inlet and outlet of heat exchanger (Pa) and $\dot{V}_{std}$ is

volumetric air flow rate of standard air ($m^3\ s^{-1}$). The polynomial regression was the best-fit relationship, which had a reported R^2 of about 0.99. When compared to an exponential relationship, R^2 value was slightly lower at around 0.95. Since higher air flow rates at around 0.2 $m^3\ s^{-1}$ were expected for the HRS for the 250 kW_e FBG, the polynomial fit was selected.

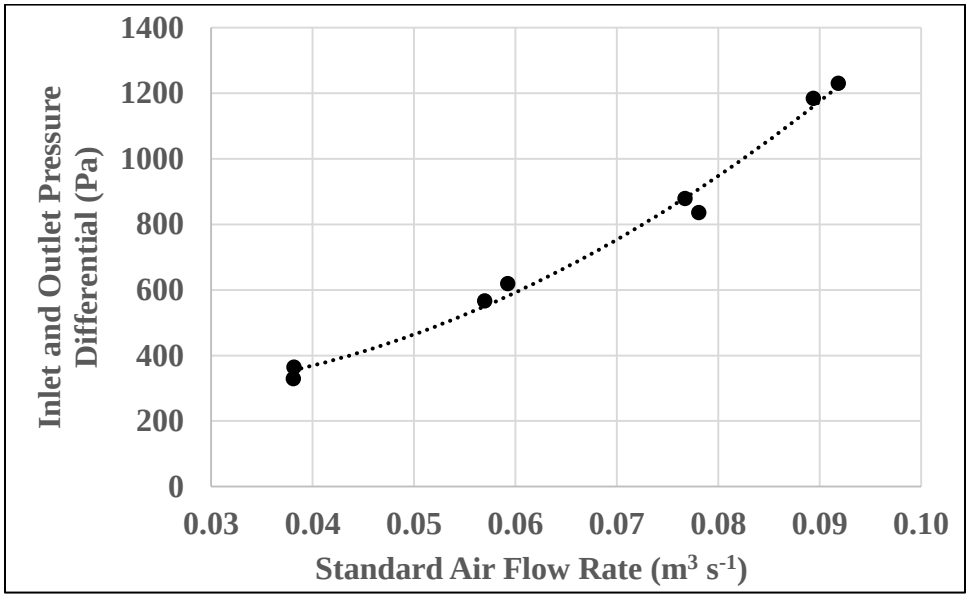

Figure 26. Heat exchanger inlet and outlet air pressure differentials and best fit polynomial regression with R^2 of 0.99.

Heat Transfer Model Corrections Results

Corrections to the ε-NTU model were performed by correcting theoretical UA with a correction factor, F_{UA}. Parameters for each test were input into the initial model (uncorrected) and the results of theoretical and actual UA are presented in Table 12. For all tests, theoretical UA was less than actual UA, which indicated that the initial model under-estimated heat

exchanger performance. Actual UA for test #7 was more than double theoretical UA. Therefore, average F_{UA} for all tests, except test #7, was calculated to be 1.54 and was applied to the ε-NTU model.

Table 12. Comparison between initial theoretical and actual UA from large heat exchanger tests. The UA correction factor was calculated as 1.54 by averaging ratios of actual to theoretical UA for each test.

Test [#]	Theoretical UA [W K^{-1}]	Actual UA [W K^{-1}]
1	6.8	9.2
2	6.8	9.2
3	7.5	10.8
4	7.7	13.2
5	8.1	13.4
6	8.1	13.2
7	8.3	18.0
8	8.3	13.1

Incorporating F_{UA} to the ε-NTU model was validated by evaluating the relative errors of heat capture. Values of heat capture between actual data, initial model, and corrected model are displayed in Table 13. Relative errors between actual heat capture and theoretical heat capture from the initial model ranged between 29% and 56%. However, relative errors of heat capture between actual data and the corrected model were reduced to below 10%, down to as low as 2.3%. This reduction indicated that the correction factor significantly reduced relative errors, where the corrected model provided for a more accurate estimation of heat capture.

Table 13. Comparison of heat capture between initial model and corrected model. Relative errors were reduced from up to 56% down to below 10% by incorporating a correction factor.

	Actual	Initial Model		Corrected Model	
Test [#]	**Heat Capture [kW]**	**Heat Capture [kW]**	**Relative Error [%]**	**Heat Capture [kW]**	**Relative Error [%]**
1	5.4	4.2	29%	6.0	9.3%
2	5.3	4.1	29%	5.9	9.6%
3	6.3	4.6	36%	6.6	4.7%
4	7.9	5.0	56%	7.2	9.8%
5	7.6	5.0	52%	7.1	6.9%
6	7.4	4.9	51%	7.0	5.8%
8	7.3	5.0	46%	7.2	2.3%

HRS Design

The first step of the HRS was to determine the dimensions of heat exchangers. Similar to the experimental heat exchanger, the inner and outer pipe sizes were selected to be 4 inch pipe and 6 inch pipe, respectively. The 250 kW_e FBG system was comprised of two standard 6 m (20 ft) shipping containers, therefore, length of each heat exchanger was determined to be 5.5 m (18 ft). This was beneficial to the overall HRS design since length was maximized while number of heat exchangers was reduced. By reducing number of heat exchangers, not only would the number of blowers be reduced, but also the amount of inlets and outlets to heat exchangers where a majority of losses (pressure differentials) would be experienced.

With dimensioned heat exchangers, the next step was to determine the maximum allowable air flow rate through each heat exchanger. Assuming dry standard air, maximum air flow rate through each heat exchanger was determined to be 0.24 $Nm^3\ s^{-1}$ (500 scfm) with an estimated ΔP_{total} of 9700 Pa, resulting in a blower power of about 7.0 kW_e. At this combination

of air flow rate and pressure differential, a HP blower was capable of supplying the air flow with a sufficient margin of maximum static pressure. Through subsequent heat exchangers, ΔP_{total} slightly decreased as a consequence of decreasing $\Delta P_{straight}$. Since less heat was transferred through following heat exchangers, air temperature decreased which resulted in decreasing velocity. Therefore, maximum blower power was experienced through the first heat exchanger of each heat recovery stream.

The first evaluation of the HRS for the 250 kW_e FBG system was to cool both generator exhaust gases and syngas to below 204°C (400°F). To achieve this, a minimum of 17 heat exchangers were required. Six heat exchangers were required to cool the generator exhausts while 11 were required for the syngas. Two reasons account for why a large number of heat exchangers were needed for the syngas: syngas had a lower flow rate and the fouling layer of biochar and tars significantly reduced heat transfer. Table 14 displays the heat capture and air outlet temperature for each heat exchanger for each hot gas heat recovery. Since the heat exchangers were placed in series, heat capture decreased for each succeeding heat exchanger, illustrated in Figure 27.

The next evaluation of the HRS was to compare operational costs of utilizing the HRS. Operational costs of electricity and natural gas were compared, illustrated in Figure 28. Regions where electricity costs were lower than natural gas costs demonstrated that gins would save money if a HRS were utilized at those number of heat exchangers. A break-even point was observed immediately after heat exchanger #12. Therefore, five heat exchangers were removed from the first HRS design such that system would be more economically beneficial for gins from an operational standpoint.

Table 14. Heat capture, air outlet temperature, and blower power consumption with varying number of heat exchangers from HRS model.

	Heat Exchanger [#]	Heat Capture [kW]	Air Outlet Temperature [°C]	Fan Power [kW]
Exhaust Gas Heat Recovery	1	78.6	294	7.0
	2	62.9	240	6.9
	3	50.3	198	6.8
	4	40.2	163	6.7
	5	32.2	136	6.7
	6	25.8	114	6.7
Syngas Heat Recovery	1	28.1	122	6.7
	2	24.9	111	6.7
	3	22.0	101	6.6
	4	19.5	92	6.6
	5	17.2	84	6.6
	6	15.2	77	6.6
	7	13.4	71	6.6
	8	11.8	66	6.6
	9	10.4	61	6.6
	10	9.1	56	6.6
	11	8.0	53	6.5

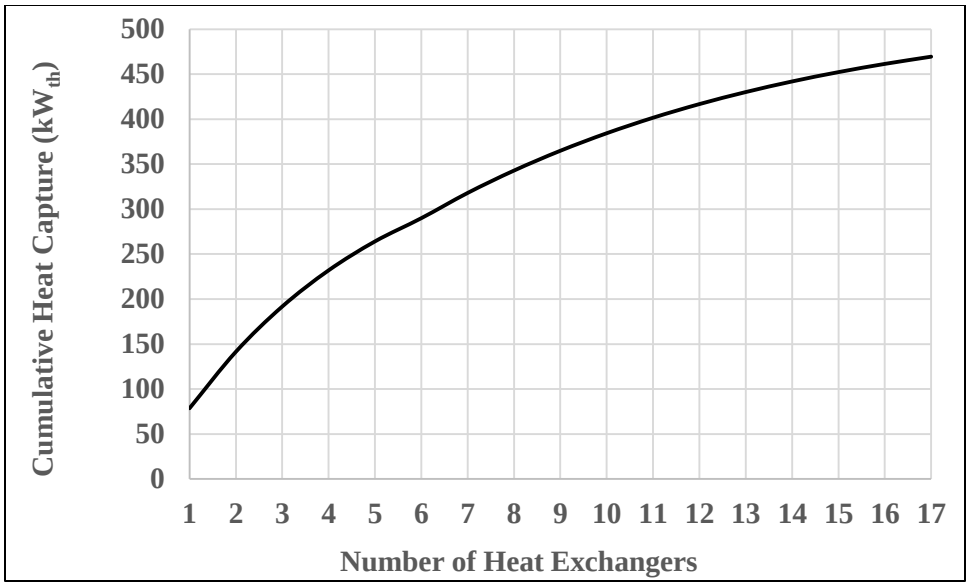

Figure 27. Cumulative heat capture from HRS model.

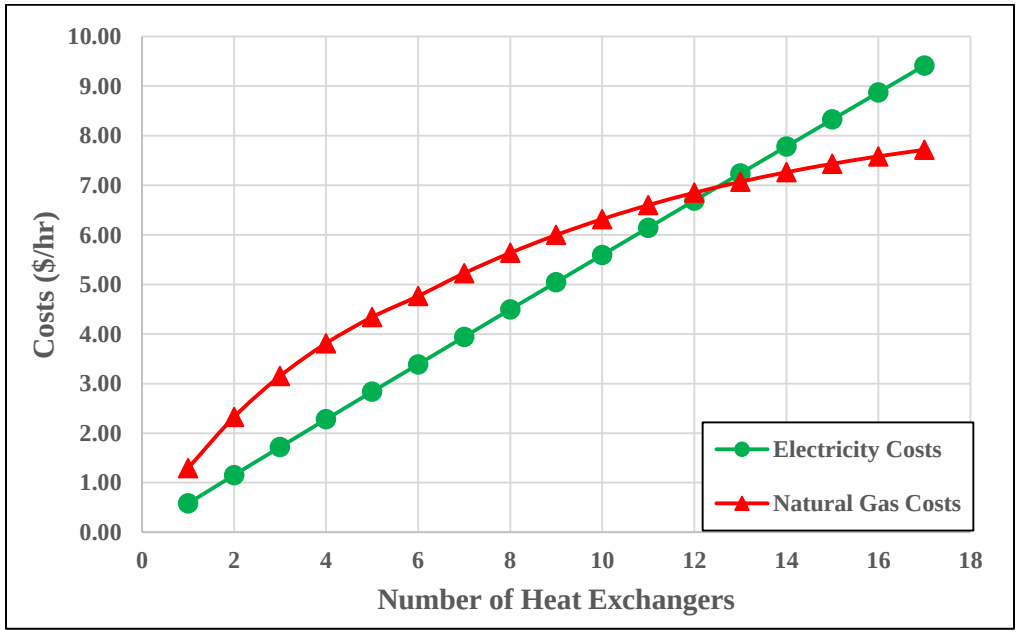

Figure 28. Cost comparison of natural gas and electricity by varying number of heat exchangers. A break-even point was observed at 12 heat exchangers, which revealed that operating up to 12 heat exchangers was economically beneficial for gins than purchasing natural gas.

The last evaluation for optimizing the HRS design was to match the total air flow rate to the seed cotton drying requirements while constraining the air temperature to a maximum of 150°C (300°F). With ten heat exchangers, the drying air flow rate requirement was met. However, the outlet temperature needed to be evaluated such that the temperature constraint was met. From the HRS model, final air outlet temperature for ten heat exchangers was 430K (315°F). At this point, reducing the number of heat exchangers would result in an increase in air temperature and decrease in air flow rate. To accommodate lower air flow rate from the HRS to match the gin requirement, ambient diluting air was used to increase air flow and decrease temperature. For nine heat exchangers, the temperature of heated air was 151°C (304°F), which still did not satisfy the temperature constraint. The initial design of the HRS consisted of eight heat exchangers that would generate 1.88 $Nm^3 s^{-1}$ (4000 scfm) of air at 172°C (342°F), with an estimated total heat capture of 343 kW. By incorporating diluting air to increase air flow rate to required, final conditions of the air stream was 2.33 $Nm^3 s^{-1}$ (5000 scfm) at approximately 143°C (290°F).

The initial design of eight heat exchangers for the HRS comprised of six heat exchangers for cooling generator exhausts and two for syngas. From Table 14, the sixth heat exchanger from generator exhausts heat recovery was 25.8 kW. If an additional generator exhaust heat exchanger were incorporated, then heat capture from the seventh heat exchanger was 20.7 kW, which was lower than the first two heat exchangers from the syngas heat recovery. Therefore, two heat exchangers from syngas heat recovery were selected which resulted in higher overall heat capture. Placement of the heat recovery for syngas would be above the gasifier (container 1), while the generator exhaust heat recovery would be above the generator (container 2), as shown in Figure 29.

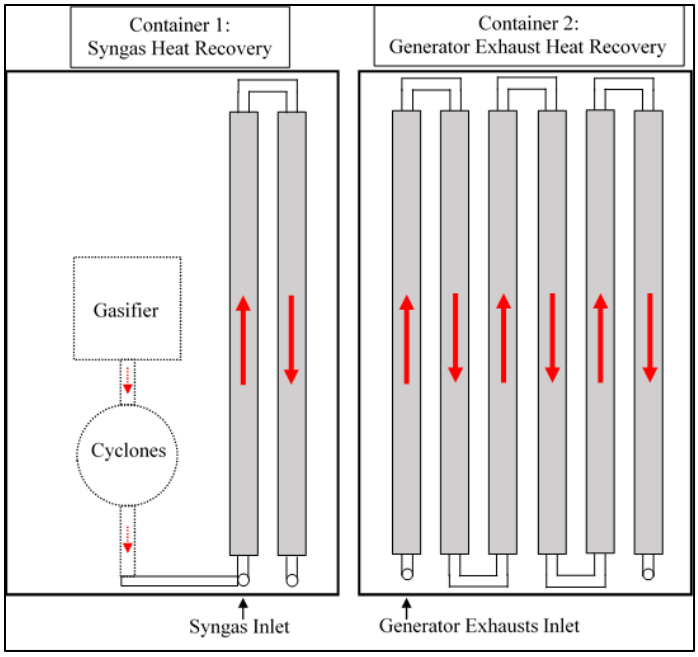

Figure 29. Placement of heat exchangers for the initial HRS design of eight heat exchangers. Two heat exchangers for syngas heat recovery would be placed above container 1, while six heat exchangers for generator exhaust heat recovery would be placed above container 2.

CONCLUSIONS

An HRS composed of multiple heat exchangers was proposed as the initial design for the 250 kW_e FBG system. Initial design of the HRS consisted of eight heat exchangers, which would generate approximately 1.88 $Nm^3\ s^{-1}$ of air at 445K (342°F), with an estimated heat capture of 343 kW. If diluting air were required to increase flow to 2.33 $Nm^3\ s^{-1}$, final temperature of air was estimated to be about 143°C (290°F). This design was to match the drying air requirement for a stripper gin and restricting the air temperature to a maximum of 149°C (300°F). The initial design was developed in part from experimental evaluation of a generator, where syngas was combusted to generate electricity. At rated load, exhaust temperature was estimated to be about 593°C (1100°F) with an A/F ratio of 1.0 $kg_{air}^{1}\ kg_{syngas}^{-1}$. In addition, an experimentally

determined average F_{UA} of 1.54 was applied to each heat exchanger in the HRS model. Overall, varying number of heat exchangers in the HRS allowed for an estimation of heat capture, final heated air temperature, and blower power consumption. The HRS model revealed that waste heat from cooling syngas and generator exhausts can be captured and converted to useful thermal energy for cotton gins. The ability to vary number of heat exchangers becomes beneficial when designing the HRS for specific gins, especially since several factors vary for each gin. These factors include drying method, thermal demand, target MC of dried cotton, type of fuel, etc. Determining the optimal number of heat exchangers based upon gin specifications will be described in the following chapter.

CHAPTER IV

HEAT RECOVERY TECHNICAL AND ECONOMIC ANALYSES

INTRODUCTION

Initial design of the heat recovery system (HRS) for the 250 kW_e fluidized bed gasification (FBG) system presented at the conclusion of Chapter III was composed of eight heat exchangers, where generator exhaust heat recovery comprised of six heat exchangers and syngas heat recovery of two. The HRS model predicted an air flow of 1.88 $Nm^3\ s^{-1}$ (4000 scfm) at a temperature of 172°C (342°F) with an estimated heat capture of 343 kW_{th}. If diluting air were required to increase flow to 2.33 $Nm^3\ s^{-1}$ (5000 scfm), final temperature of air was estimated to be 143°C (290°F). This configuration was selected to supply useful thermal energy for a stripper cotton gin. However, there were still aspects that needed to be investigated before a final design of the HRS could be established. These included estimating how much moisture could be removed from incoming seed cotton, assessing sensitivity of input parameters to the overall performance of the HRS, and evaluating economic feasibility of the HRS.

In addition to the Texas Cotton Ginners' Association's (TCGA) annual energy surveys, data was acquired from the United States Department of Agriculture (USDA) Agriculture Research Services (ARS). Purpose of the data set was to evaluate fuel usage and thermal efficiency of cotton drying at a Texas gin. For confidentiality reasons, location and gin name was not specified. From the set, data was collected in approximately 83 minute intervals. Fuel usage through a burner, heated air temperature, air flow rate, bales per hour (bph), seed cotton bale weight, and initial moisture content (MC) were some of the parameters measured during cotton drying. A summary of the data can be seen in Table 15. For the six intervals, an average stripper

seed cotton bale weight was about 780 kg $bale^{-1}$, which demonstrated that the estimated value of 900 kg $bale^{-1}$ was a conservative assumption. Average fuel usage was calculated to be 0.43 GJ $bale^{-1}$, approximately 2.6 times as much as the average reported from TCGA annual surveys. Air-to-cotton ratio was calculated by manipulating the air flow requirement from equation 19. An average value was determined as 1.6 m_{air}^3 kg_{cotton}^{-1}, which was relatively similar to the suggested value of 1.56 m_{air}^3 kg_{cotton}^{-1} by Lummus. Lastly, average heated air temperature was 116°C (240°F), ranging between 108°C and 136°C (226°F and 277°F). These temperatures were measured prior to the mix-point of seed cotton and heated air, which revealed that heated air from the HRS design would be sufficient for this particular gin. The major advantage of utilizing this data set was to illustrate the benefits of implementing a HRS to reduce fuel usage.

Method of cotton drying ranges significantly by gin for a number of reasons, such as region or location, harvest method of cotton, and season of ginning. Typically, gins use a variety of driers to increase turbulence and retention time that cotton gets exposed to heated air. Tower driers are an example, illustrated in Figure 30. The shelves within the dryer act as baffles, resulting in additional mixing between heated air and cotton. Drying times within driers can range from 10 to 15 seconds (Anthony and Mayfield, 1994). Target MC of seed cotton is typically around 5% (wet basis), but this value generally ranges between 4%-6% depending on a gin operator's experience. Drying cotton to this moisture range and below results in better separation efficiency of foreign matter. However, drying below around 5% can begin to cause cotton to stick to duct surfaces due to static electricity and cause fibers to become too brittle.

The Texas ginning data set from USDA ARS also contained some measurements for initial cotton MC. Minimum, average, and maximum initial cotton MC's (Appendix C) were measured during intervals of cotton drying. Sampling was performed for a duration of at least 60

Table 15. Summary of cotton drying data from a Texas gin from USDA ARS. Burner usage and heated air temperature data revealed an HRS would benefit the gin by replacing fuel usage.

Interval [#]	Cotton Type	Duration [min]	Seed Cotton Bale Mass [kg/bale]	Average Burner Power [GJ/bale]	A/C Ratio [m^3/kg]	Heated Air Temperature [°C]
1	Stripped	83	777	0.33	1.66	116
2	Stripped	83	777	0.34	1.66	116
3	Stripped	83	777	0.58	1.45	135
4	Stripped	83	777	0.39	1.68	108
5	Stripped	83	777	0.38	1.71	108
6	Stripped	83	777	0.57	1.48	135
		Average	**777**	**0.43**	**1.61**	**120**

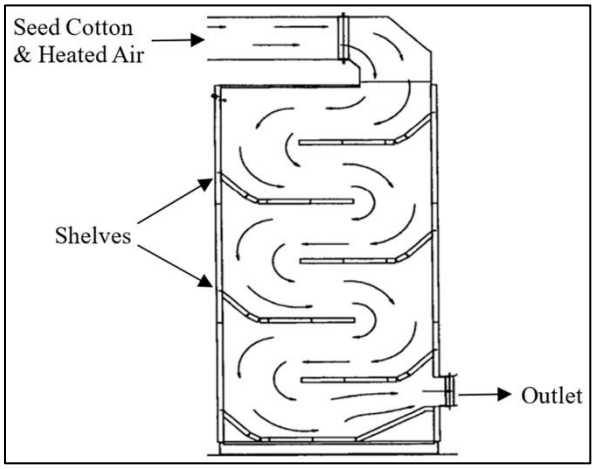

Figure 30. Tower dryer for cotton drying.

min for all three intervals. Minimum and maximum MC, in dry basis, had a wide range of values, from as low as 5.5% to as high as 12.2% for all data points, shown in the histogram in Figure 31. This clearly illustrated the spectrum of dry and wet cotton. Although 12.2% was the maximum, an upper limit of 11% was more likely. Most frequent MC were observed at around 8.5%, with a majority between 6% and 9.5%. Overall average from the data was 7.8%.

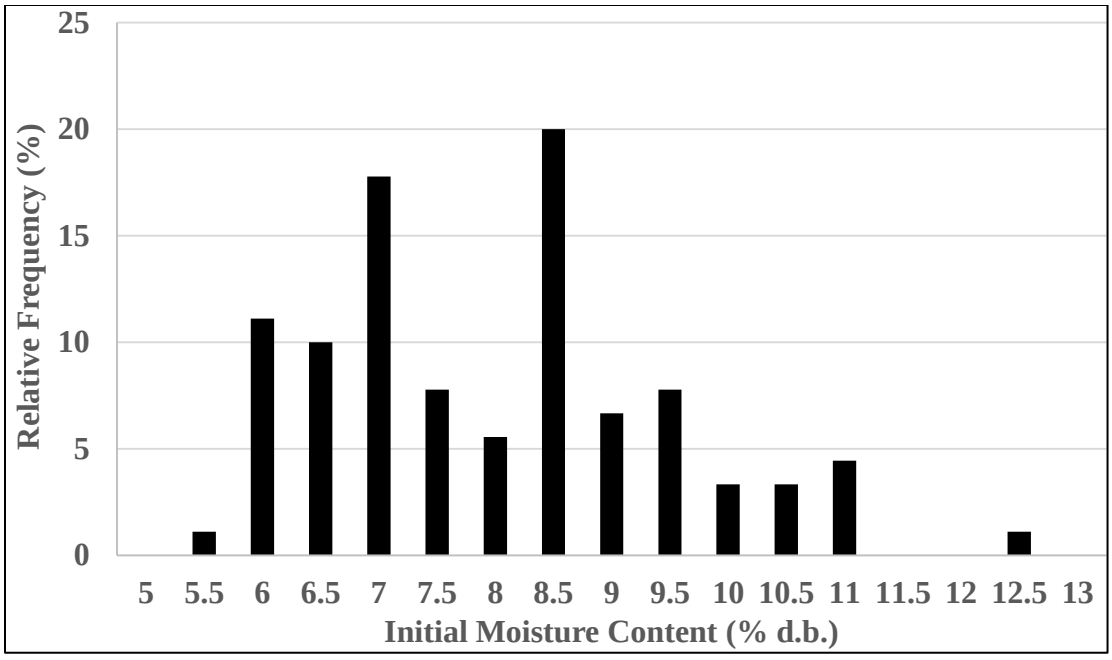

Figure 31. Relative frequencies of initial moisture content of incoming cotton from a Texas gin from USDA ARS data.

A drying model proposed by Barker and Laird (1993) was adopted to predict final MC of seed cotton with heated air from the HRS. The model predicted final MC of cotton based upon heated air temperature, initial MC, and drying time. Essentially, the model was capable of developing a drying curve, similar to the one shown in Figure 32. One limitation was that the model was developed from drying cotton lint, rather than drying all components of seed cotton. These components include lint, seed, and foreign matter (gin wastes). Fortunately, a majority of drying occurs from the lint rather than the other constituents (Laird and Barker, 1995), which is beneficial from an energy perspective. Seed cotton has an average seed-to-fiber ratio of around 1.4 (Dowd et al., 2018), by mass, while foreign matter content varies by harvest method. Picker

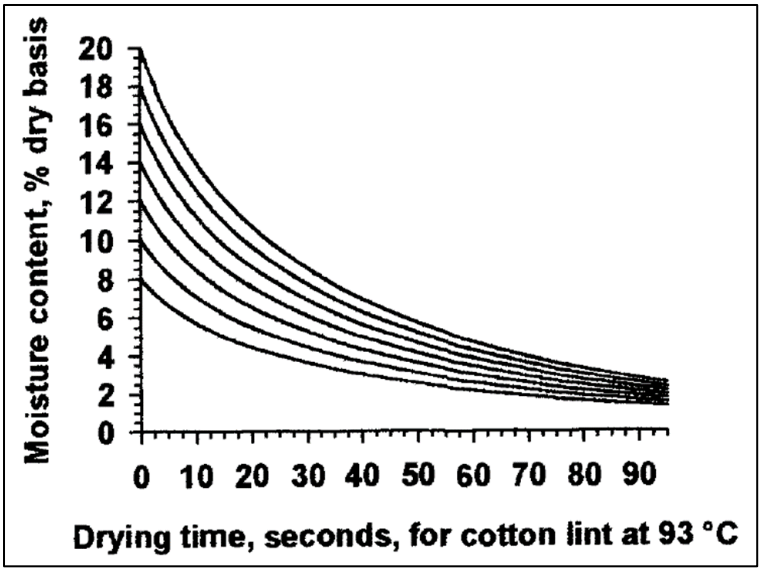

Figure 32. Cotton drying curves with varying initial moisture contents. Reprinted from Laird and Barker (1995).

cotton contains around 68 kg bale^{-1} (150 lb bale^{-1}), while stripper can range between 140 and 320 kg bale^{-1} (300 and 700 lb bale^{-1}) (Thomas et al., 2018).

A drawback to the HRS model was that input parameters were assumed constant. Evaluating a variety of these parameters was necessary to demonstrate confidence in the overall performance of the HRS. A selection of input parameters that were suspected to have greatest impact on HRS performance were ambient air temperature, F_{UA}, syngas mass flow, syngas initial temperature, actual A/F ratio of syngas combustion, generator exhaust initial temperature, tar thermal conductivity, and tar thickness. All of these parameters were varied by ± 10% to evaluate sensitivity on heat capture and thermal efficiency. Evaluating the sensitivity of input parameters provided insight as to which parameters most significantly affected HRS performance.

Richardson et al. (2016) reported the feasibility of implementing multiple 250 kW_e FBG systems at cotton gins, where a Monte Carlo model was developed and analyzed for an average gin (40 bph) and a large gin (100 bph). Both scenarios were concluded to have a better than 95% chance of being an economic success, where the optimal number of 250 kW_e gasifiers for the 40 bph and 100 bph gins were five and 11, respectively. Figure 33 illustrates the cumulative probability of net present value (NPV) for both gins. The average gin and large gin had a 90% chance of having a NPV of $8 million and $15 million, respectively. Project life was 20 years and NPV had a discount rate of 10%.

An economic analysis was performed in this study to determine feasibility of implementing a HRS to the 250 kW_e FBG. The HRS was evaluated as an independent system, separate from the FBG, to reveal economic benefits for cotton gins. Equipment for the HRS increases overall capital cost of the FBG system, along with incurring yearly variable costs such as repair and maintenance. Heated air supplied by the HRS would displace fuel usage, resulting in annual economic savings. However, annual savings must be greater than yearly costs for investors to consider investing. If feasible, the FBG system would be much more attractive for cotton gins by providing electrical energy, thermal energy, and a solution to gin waste disposal.

Typical indicators for economic feasibility include internal rate of return (IRR), investor's rate of return (IROR), payback period (PBP), and NPV (Riggs, 1968). Economic life of projects generally span between 10 and 20 years, which prompts the incorporation of the time value of money. Common methods are to apply interest to the project and a discount factor to yearly cash flows of the project. Future values of money are generally converted to present time to give investors an indicator of whether to invest in a project. High IRR, IROR, and NPV, with short PBP, incentivize investors to risk their money for a high return on their investment.

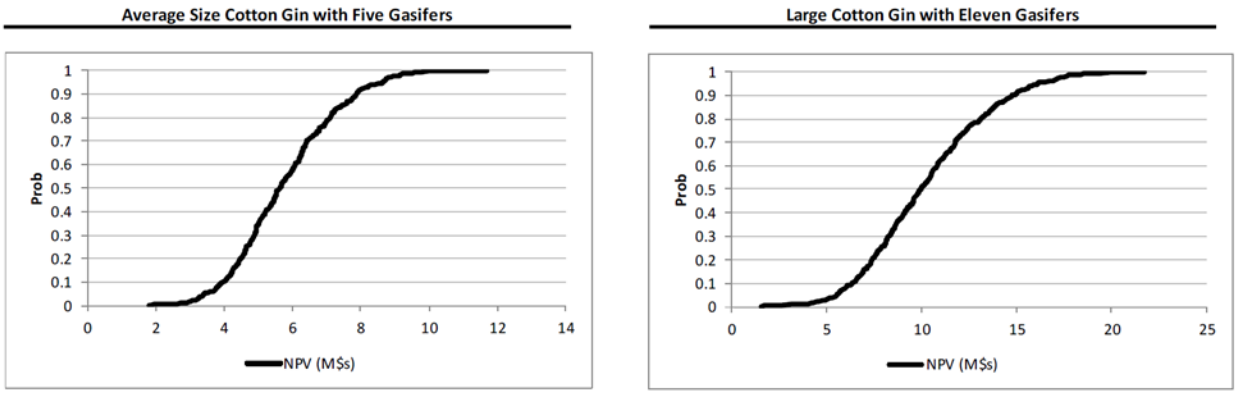

Figure 33. Cumulative probability of NPV for gasifiers at average and large cotton gins. Reprinted from Richardson et al., 2016.

Objectives

The objectives of this chapter were to evaluate the practicality of the HRS designs for the 250 kW_e FBG system such that a final design could be established. Specific objectives were to:

- Incorporate a drying model to estimate final MC and quantity of moisture removed per unit time from incoming seed cotton,
- Perform a sensitivity analysis of the intial HRS to evaluate and quantify effect of input parameters to the overall performance of the HRS, and
- Perform an economic analysis to evaluate the feasibility of the HRS by varying number of heat exchangers to determine an optimal number.

MATERIALS AND METHODS

Cotton Drying Model

The drying model presented by Barker and Laird (1993) was utilized to predict final MC of incoming seed cotton if heated air were used from the HRS. Ultimately, the amount of moisture removed was estimated. The benefit of the model was that theoretical values of final MC of cotton were compared to target values of 4%-6%. Since the drying model was developed from drying cotton lint, the assumption was made that the model would adequately predict final MC of seed cotton. The foundation of the model was the classical three dimensional diffusion differential equation presented by Newman (1932), but simplified to equation 21.

$$\frac{M_f - M_e}{M_o - M_e} = \beta\left(\frac{1}{\lambda}e^{-\lambda D_i \theta} + \frac{1}{\pi}e^{-4\pi D_i \theta} + \frac{1}{\omega}e^{-\omega D_i \theta}\right) \quad (21)$$

where M is dry basis MC (percent), β, λ, π, and ω are constants (dimensionless), D_i is diffusivity term (s^{-1}), θ is drying time (s), and *f*, *o*, and *e* are subscripts for final, initial, and equilibrium, respectively. Constants β, λ, π, and ω were solutions to Newman's spherical model with values of 0.7346, 1, 4, and 9, respectively. Spherical solutions were selected since the model better represented the data with higher R^2 values when compared to flat plate and cylindrical solutions.

Diffusivity term (D_i) is a measure of diffusion through the air space of a sample of cotton fibers, which included a diffusion coefficient ($m^2\ s^{-1}$). The data examined by Barker and Laird showed that D_i linearly increased with increasing temperature between 5°C and 90°C, with an R^2 value of 0.94. Therefore, D_i was approximated with equation 22.

$$D_i = -0.00157 + 0.0002 * T_{air} \quad (22)$$

where T_{air} is temperature of heated air (°C). Although the temperature of heated air from the HRS was around 140°C (290°F), it was assumed that equation 22 was valid for temperatures above 90°C.

Methods of calculating equilibrium MC, M_e, of cotton at elevated temperatures was presented by Abernathy et al. (1994). Similar to Barker and Laird, models were compared to data and evaluated for accuracy. Again, models were only compared up to an air temperature of 90°C. Therefore, when heated air temperatures were above 100°C from the HRS, M_e was assumed to be zero. This assumption was validated by observing humidity ratios at elevated temperatures; standard air at 50% humidity ratio that was sensibly heated to 140°C had less than 2% humidity.

Moisture contents measured from the USDA ARS data set, along with calculation of final MC of cotton from equation 21, were reported as dry basis. Dry basis MC is defined as the ratio of weight of moisture to dry matter, while wet basis is the ratio of moisture weight to total weight. In order to estimate the amount of moisture removed from drying cotton, MC was converted to wet basis, shown in equation 23 (Henderson et al., 1997).

$$m = \frac{M}{M+1} = \frac{W_m}{W_m+W_D} \tag{23}$$

where m is wet basis MC (decimal), W_m is weight of moisture (kg bale^{-1}), and W_D is weight of dry matter (kg bale^{-1}). Note: M was converted from a percentage to decimal when used for equation 23. Utilizing a seed cotton bale weight of 900 kg bale^{-1}, initial total weight (weight of moisture and dry matter) was calculated from the initial MC. Final moisture weight was calculated from the weight of dry matter and final MC. Difference between initial and final moisture weight was defined as the moisture removed during drying.

Barker and Laird's drying model was applied to evaluate cotton drying from the initial HRS design of eight heat exchangers. The design was evaluated by varying both drying time and initial MC. Response to the evaluation was final MC of cotton, which produced a drying curve similar to Figure 32. Initial MC's were the minimum, average, and maximum MC from the Texas ginning data, which were 5.5%, 7.8%, and 12.2%, respectively. A drying time of 15 seconds was assumed when varying initial MC, which was an estimated drying time reported by Anthony and Mayfield (1994).

In addition to the evaluation of the eight heat exchanger design, varying the number of heat exchangers between four and ten heat exchangers was also conducted. Cotton drying responses were final MC of cotton and weight of moisture removed. Drying times of 15 seconds were assumed, while minimum, average, and maximum initial MC from Texas ginning data were used. Stripper cotton was also assumed where bale weight was about 900 kg $bale^{-1}$.

Configurations of heat exchangers were selected to generate maximum thermal energy. For example, six heat exchangers consisted of five heat exchangers for generator exhaust heat recovery and one for syngas heat recovery (refer to Table 14 in Chapter III). Heated air temperature from each HRS configuration was estimated from the HRS model described in Chapter III, where diluting air was incorporated to increase air flow to the drying requirement of 2.33 $Nm^3\ s^{-1}$. For example, six heat exchangers generated heated mixed air at 192°C (378°F) and 1.41 $Nm^3\ s^{-1}$, but with diluting air, the final air temperature was 126°C (258°F). Heated air temperatures for each HRS configuration is displayed in Table 16, where temperatures ranged between 105°C and 157°C.

Table 16. Estimated final temperatures of mixed air by varying number of heat exchangers.

Number of Heat Exchangers [#]	Air Temperature [°C]
4	105
5	116
6	126
7	135
8	143
9	151
10	157

Sensitivity Analysis

A technical analysis was performed by evaluating the sensitivity of input parameters to the overall performance of the initial HRS design. Selected input parameters were ambient air temperature, F_{UA}, syngas mass flow, initial syngas temperature, actual A/F ratio of syngas combustion in the generator, generator exhaust initial temperature, and k_{tar}. All of these parameters were varied by ±10%, where range of values are shown in Table 17. Responses to variations in input parameters were overall heat capture and thermal efficiency from the HRS. Thermal efficiency was calculated as the ratio of heat capture to energy input of the FBG. Input energy was determined as the product of mass flow and higher heating value (HHV) of cotton gin trash (CGT). Evaluating the sensitivity parameters was done one at a time, where values for remaining parameters were held constant at their base values.

When evaluating sensitivity of syngas mass flow, necessary adjustments were made to corresponding process characteristics of the 250 kW_e FBG. Referring to Figure 13 from Chapter III, mass flow of CGT to the reactor was adjusted accordingly assuming a constant syngas yield

Table 17. Range of values for input parameters for sensitivity analysis of HRS model with eight heat exchangers. Base values were varied by 10%.

Input Parameter	Units	Minimum Value	Base Value	Maximum Value
Ambient Air Temperature	K	268	298	328
F_{UA}	-	1.38	1.54	1.69
Syngas Mass Flow	kg s^{-1}	0.3	0.33	0.36
Actual A/F Ratio	kg_{air} kg_{syngas}^{-1}	0.9	1	1.1
Initial Syngas Temperature	K	880	978	1075
Initial Generator Exhaust Temperature	K	780	866	953
Tar Thermal Conductivity	W m^{-1} K^{-1}	0.027	0.03	0.033
Tar Thickness	mm	0.9	1	1.1

of 2.03 Nm_{syngas}^3 kg_{CGT}^{-1}. Correcting mass flow of CGT also corrected the energy input to the FBG, which varied thermal efficiency of the system. In addition, varying syngas flow resulted in varying generator exhaust flow, assuming constant A/F ratio of 1 kg_{air} kg_{syngas}^{-1}, which affected overall heat capture.

Quantifying sensitivity of each input parameter to overall heat capture from the HRS was achieved by calculating a relative sensitivity coefficient, shown in equation 24 (Haan, 2002).

$$S_r = \frac{\Delta O}{\Delta I}\frac{I}{P} \tag{24}$$

where S_r is relative sensitivity coefficient (dimensionless), I is input parameter, O is input parameter, and ΔO and ΔI are change in values of output and input parameters, respectively. Absolute values of S_r indicated how sensitive a particular input parameter was to heat capture, where higher values revealed higher sensitivity.

Economic Analysis

An economic analysis of the HRS for the 250 kW_e FBG system was performed to evaluate the economic benefits of supplying thermal energy to cotton gins. In contrast to the sensitivity analysis, the economic analysis of the HRS was evaluated by varying the number of heat exchangers, which directly corresponded to varying thermal energy supplied. The analysis consisted of estimating yearly cash flows where cost of fuel displaced or saved was treated as the income. Three scenarios of cotton gins were developed for the economic model: one base case (BC) for natural gas (NG) usage, one BC for propane usage, and one for a Texas gin. The two base case scenarios were developed utilizing average TCGA data (Appendix C), while the Texas gin scenario utilized the Texas ginning data (Table 15).

Average fuel usage for the NG and propane BC scenarios were 0.16 and 0.11 GJ $bale^{-1}$, respectively, while costs were $4.56 and $15.23 per GJ, respectively. The Texas gin scenario had a natural gas usage of 0.43 GJ $bale^{-1}$, where cost was assumed the same as the NG BC scenario. From TCGA energy surveys between 2010 and 2017, fuel prices for both NG and propane fluctuated but did not display obvious increasing or decreasing overall trends. Therefore, the average costs were assumed constant for every year of the economic analysis. Constant average thermal demand for each gin scenario was also assumed for every year.

Thermal energy demands for the three scenarios were scaled according to the electrical power supplied by the 250 kW_e FBG system. Assuming an electrical usage of 42 kW-hr $bale^{-1}$, the FBG system was expected to supply sufficient electricity for a ginning capacity of about 6 bph. This equated to an average fuel usage for the NG BC, propane BC, and Texas gin scenarios of 0.97, 0.63, and 2.38 GJ hr^{-1}, respectively.

Varying number of heat exchangers for the three scenarios ranged between one and ten, which correlated to cumulative thermal energy from the HRS shown in Table 18. Values of thermal energy were acquired from the HRS model described in Chapter III. The assumption was made that electricity generated from the 250 kW_e FBG would power the blowers for heat exchangers. Displaced fuel was estimated as the thermal energy supplied by the HRS. When thermal energy supplied by the HRS exceeded average fuel usage, excess thermal energy was assumed to be wasted and not included as additional savings. Total energy of displaced fuel, in GJ, was calculated as the product of fuel usage and total hours of ginning, which was assumed as 2200 hours per season (Richards et al., 2016).

Capital costs of the HRS were estimated by correlating a parts list to varying number of heat exchangers. Each heat exchanger consisted of a base part list, which included an inner pipe, outer pipe, air inlet, air outlet, two stainless steel plates, and a high pressure (HP) blower. Increasing the number of heat exchangers resulted in additional piping, such as elbows and pipe nipples to connect heat exchangers in series for each heat recovery. A pricing list for each part is shown in Table 19. Prices for inner and outer pipes were acquired from Midwest Steel and Aluminum, HP blower from Air Moving Equipment, and remaining parts from McMaster-Carr. A detailed parts list is displayed in Appendix D. Capital costs for the HRS were conservative estimations since materials were individually priced at retail value. Therefore, capital costs can be expected to be lower when constructing heat exchangers, especially since Lummus is a manufacturing company.

Table 18. Estimated cumulative thermal energy, or heat capture, by varying number of heat exchangers from HRS model.

Number of Heat Exchangers [#]	Cumulative Thermal Energy Supplied [kW]
1	79
2	141
3	192
4	232
5	264
6	292
7	318
8	343
9	365
10	384

Table 19. Price list for heat exchanger components for the HRS.

Description	Price per Unit
Inner Pipe	$578
Outer Pipe	$945
Stainless Steel Plate	$32
Air Inlet / Outlet	$23
High Pressure Blower	$2,937
Stainless Steel Elbow	$118
Stainless Steel Pipe Nipple	$55

An example of first year cash flow calculations in the economic model are presented in Table 20. Total costs were a summation of annual tax / insurance, interest, and repair / maintenance costs. Each of these costs were estimated as 5% of the initial capital cost of the HRS. Difference between income and total costs was defined as net revenue. In order to

incorporate the time value of money, a discount factor was applied to annual net revenues to estimate yearly discounted revenues. A project life of 20 years and discount factor of 10% were assumed. Yearly discount factors were calculated from the discount rate using equation 25.

$$DF = (1 + DR)^{-t} \quad (25)$$

where *DF* is discount factor (decimal), *DR* is discount rate (decimal), and t is time (years).

Table 20. Example of first year cash flows for economic analysis.

Year	Total Costs	Income	Net Revenue	Discount Factor	Discounted Revenue
1	TC	I	NR = I - TC	0.91	NR*0.91

Four economic indicators, IRR, IROR, NPV, and PBP, were calculated for each of the three scenarios. Estimating PBP and IROR required the calculation of net average annual revenue, which was simply the average of discounted revenues for all 20 years. Payback period was calculated as the ratio of initial capital cost to net average annual revenue. Investor's rate of return was calculated as the ratio of net average annual revenue to initial capital cost, or the inverse of PBP. For each economic scenario, an accumulated value of the project was calculated each year where discounted revenue was added. For year 0, value of the project was negative and equal to the initial capital cost. Value for year 1 was initial capital cost plus year 1's discounted revenue. Value for year 2 was year 1's value plus year 2's discounted revenue. This was carried out until year 20. This method implied that negative yearly discounted revenues resulted in decreasing value of the project. The accumulated value at year 20 was defined as NPV. Finally,

IRR was calculated with the use of Microsoft Excel's function since solving IRR required complex numerical methods.

RESULTS AND DISCUSSION

Cotton Drying Results

Evaluation of cotton drying from the HRS of eight heat exchangers by varying initial MC is illustrated in Figure 34. As expected, quickest rate of drying occurs within around the first 5 seconds. At a drying time of 15 seconds for initial MC's of 5.5%, 7.8%, and 12.2% (wet basis), final MC's were 2.7%, 3.8%, and 6.0%, respectively. Since the minimum initial MC was within the suggested range before drying, ambient air would have sufficed to convey and slightly dry incoming seed cotton. Average initial MC was dried below the suggested range, which revealed that the HRS provided excess thermal energy that could completely replace fuel usage. Maximum initial MC was dried to the upper limit of the targeted final moisture range, indicating that if a gin operator decided to further reduce the MC, then a burner would be used and the HRS would have replaced a large portion of fuel.

Results of final MC by varying number of heat exchangers is presented in Figure 35. Drying time was 15 seconds. Difference in final MC between four and ten heat exchangers were 0.5%, 0.7%, and 1.0% for minimum, average, and maximum initial MC, respectively. Varying number of heat exchangers did not significantly affect final MC for the minimum and average initial MC's, however, maximum initial moisture had the greatest impact. Four heat exchangers would have insufficiently dried seed cotton, whereas eight to ten heat exchangers would have dried cotton to within the target range of 4%-6%. Therefore, these results demonstrated that four

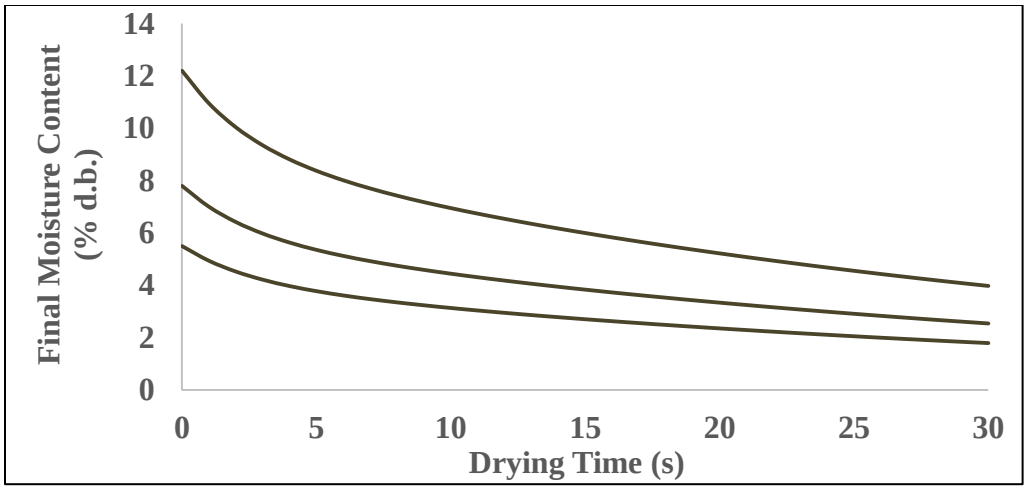

Figure 34. Final cotton moisture contents by varying drying time.

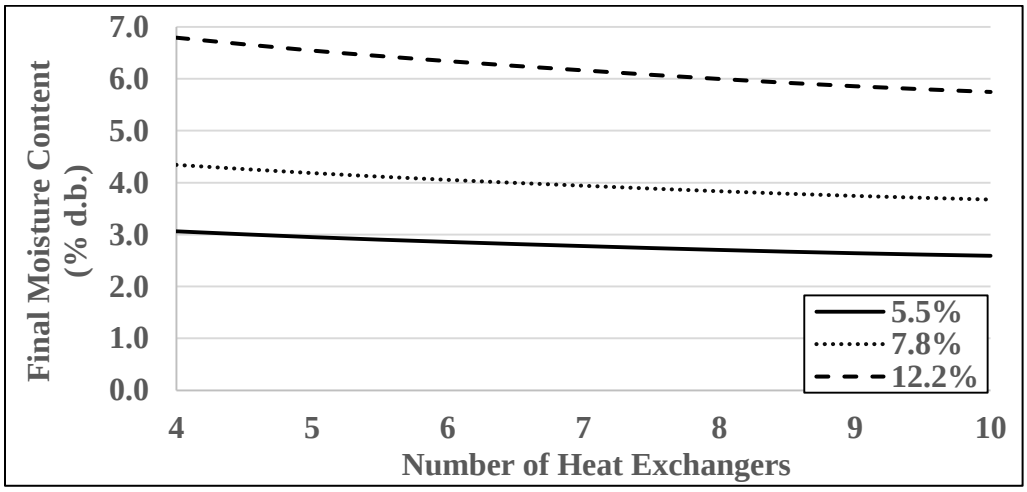

Figure 35. Final cotton moisture contents by varying number of heat exchangers.

heat exchangers would have been adequate for drying minimum and average initial MC's. More heat exchangers would be needed with increasing initial MC beyond average values, which is proportional to the gin's thermal demand.

Similar results can be seen in Figure 36, where moisture removed was estimated with number of heat exchangers. Moisture removed was relatively unaffected when initial MC's were minimum or average. Differences of moisture removed between four and ten heat exchangers were about 4 and 6 kg bale^{-1} for minimum and average initial MC's, respectively. Maximum initial MC had a difference of 8.5 kg bale^{-1}.

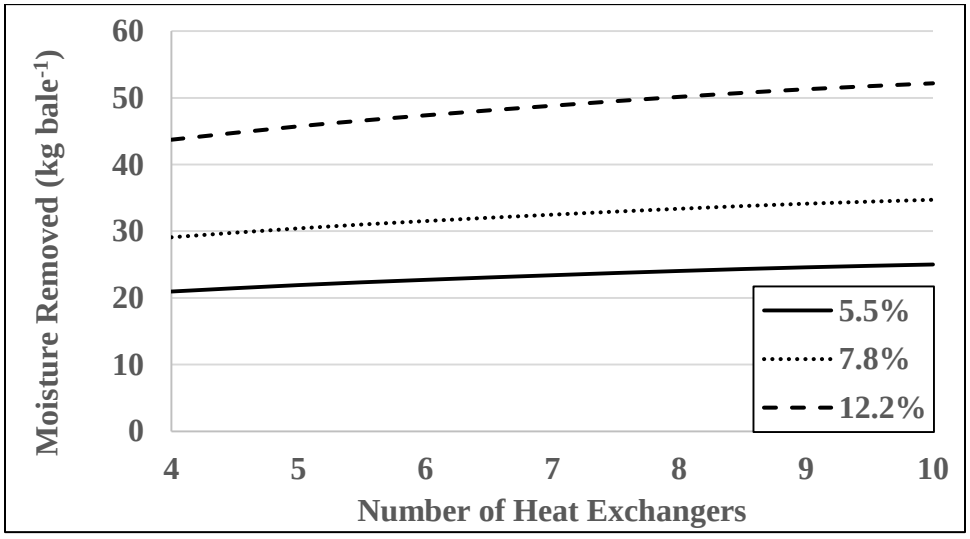

Figure 36. Moisture removed from cotton by varying number of heat exchangers.

Sensitivity Analysis Results

Sensitivity results of varying ambient air temperature, or heat exchanger air inlet temperature, are shown in Figure 37. Increasing ambient air temperature from 268K to 328K (23°F to 130°F) resulted in linear decreases in heat capture from 365 to 314 kW, respectively, and thermal efficiency from 15.2% to 13.1%, respectively. Higher heat exchanger inlet temperatures resulted in lower temperature differential between air and hot gas, which lowered

overall heat transfer. Therefore, gins that operate in cold / winter seasons can expect higher heat capture from the HRS.

Sensitivity of the overall conductance correction factor is illustrated in Figure 38. As expected, increasing F_{UA} resulted in a linear increase in both heat capture and thermal efficiency. Heat capture and thermal efficiency increased from 323 to 353 kW and 13.5% to 14.7%, respectively, between F_{UA} values of 1.38 and 1.69, respectively. A number of characteristics and properties affect F_{UA} when operating the FBG, such as ambient air temperature, hot gas temperatures and flow rates, and heat exchanger dimensions and material. Values of F_{UA} evaluated for the sensitivity analysis were within the range of experimentally determined values from the large-scale heat exchanger described in Chapter III.

Results of varying syngas mass flow are illustrated in Figure 39. Increasing syngas mass flow resulted in an increase of heat capture, but a decrease in thermal efficiency. Between syngas flow rates of about 0.30 and 0.36 kg s^{-1}, heat capture increased from 320 to 357 kW, respectively, while thermal efficiency decreased from 14.8% to 13.5%, respectively. Increasing syngas mass flow rate implied that feed rate of CGT was increased, resulting in higher energy input to the system. This method assumed the A/F ratio of air and CGT to the reactor was constant which did not affect reaction temperature. From this analysis, the flow of syngas of 0.33 kg s^{-1} corresponded to the optimal feed rate CGT, given a constant value for syngas yield. In addition, increasing syngas mass flow also increased flow of generator exhausts, resulting in higher heat capture from both heat recoveries.

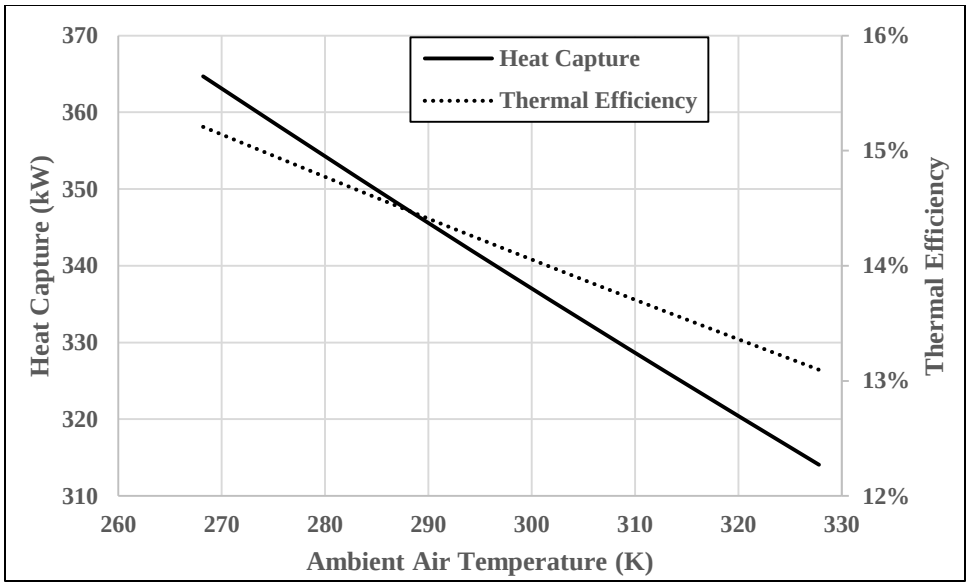

Figure 37. Sensitivity results of varying ambient air temperature.

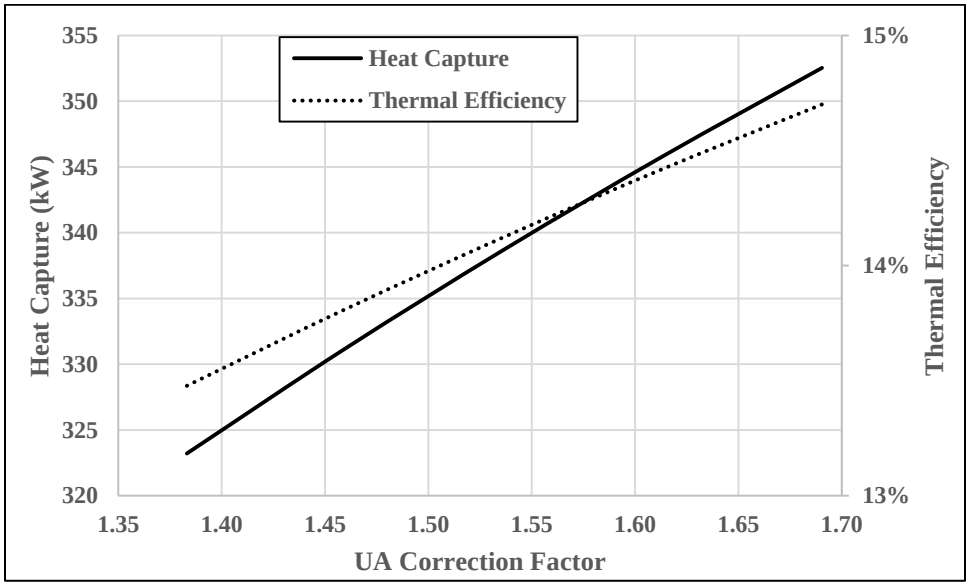

Figure 38. Sensitivity results of varying UA correction factor.

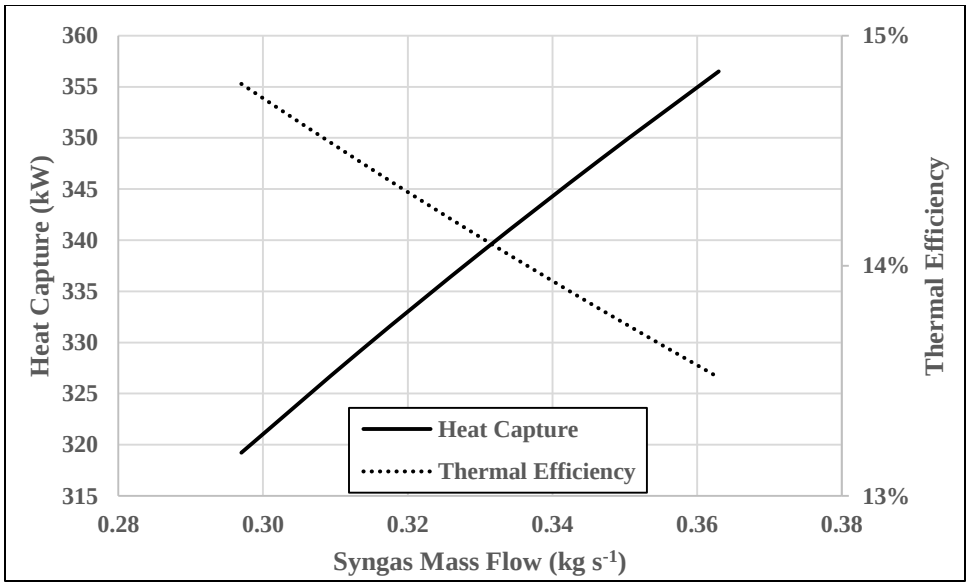

Figure 39. Sensitivity results of varying syngas mass flow.

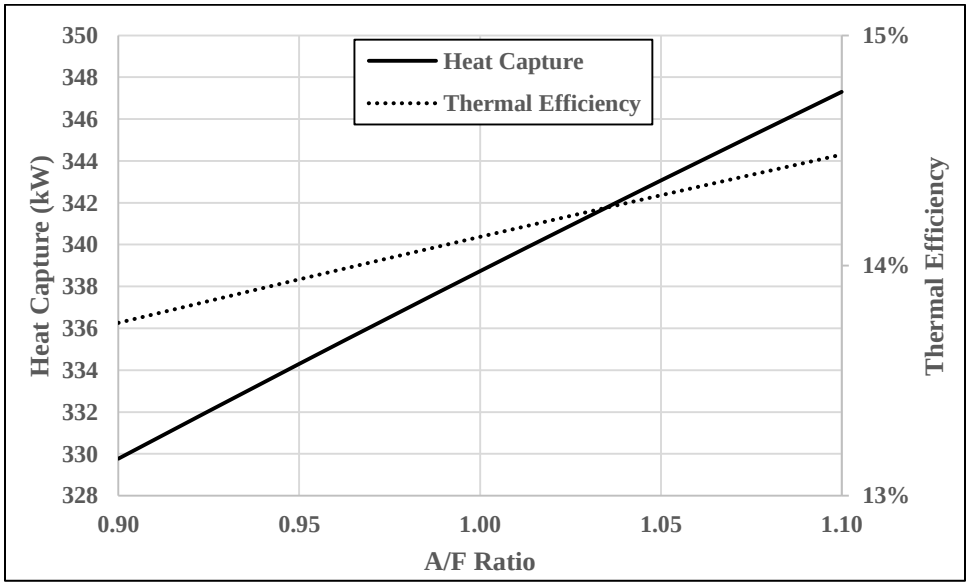

Figure 40. Sensitivity results of varying A/F ratio.

Sensitivity of varying generator A/F ratio is presented in Figure 40. Increasing A/F ratio of syngas combustion in the generator resulted in an increase in both thermal efficiency and heat capture, ranging between 330 to 347 kW and 13.8% to 14.5%, respectively. Variations in A/F ratio resulted in direct variations to flow of generator exhaust gases, or an increase in A/F ratio resulted in an increase in generator exhaust flow and vice versa. Flow of exhausts was directly related to available thermal energy for heat capture.

Sensitivities of initial syngas temperature and initial generator exhaust temperature are shown in Figure 41 and Figure 42, respectively. Increase in both hot gas temperatures resulted in an increase in both heat capture and thermal efficiency. Similar to A/F ratio, temperature was also directly related to available thermal energy for heat capture. Although initial syngas temperature can be controlled by varying the A/F ratio of CGT and air to the reactor, several uncontrollable factors can affect reaction temperature, such as MC of CGT along with humidity and temperature of ambient air. Similar characteristics can be acknowledged for generator exhaust temperature. Syngas temperatures evaluated for sensitivity were within the range of reaction temperatures typically experienced when operating a FBG. Generator exhaust temperatures between the minimum and base values were expected temperatures when the generator was running at rated load, but maximum temperature of about 677°C (1250°F) was an over approximation.

Lastly, sensitivities of tar thermal conductivity and tar thickness are presented in Figure 43 and Figure 44, respectively. Increasing k_{tar} resulted in slight increases to both heat capture and thermal efficiency. Heat capture and thermal efficiency were approximately 340 kW and 14.1%, respectively. Increasing tar thickness, or fouling layer, resulted in a slight decrease in both heat

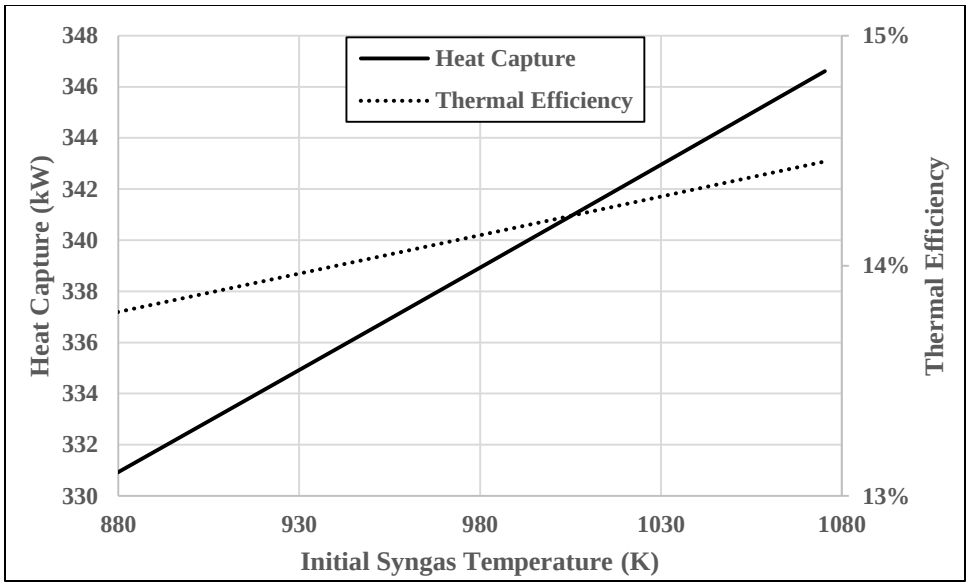

Figure 41. Sensitivity results of varying initial syngas temperature.

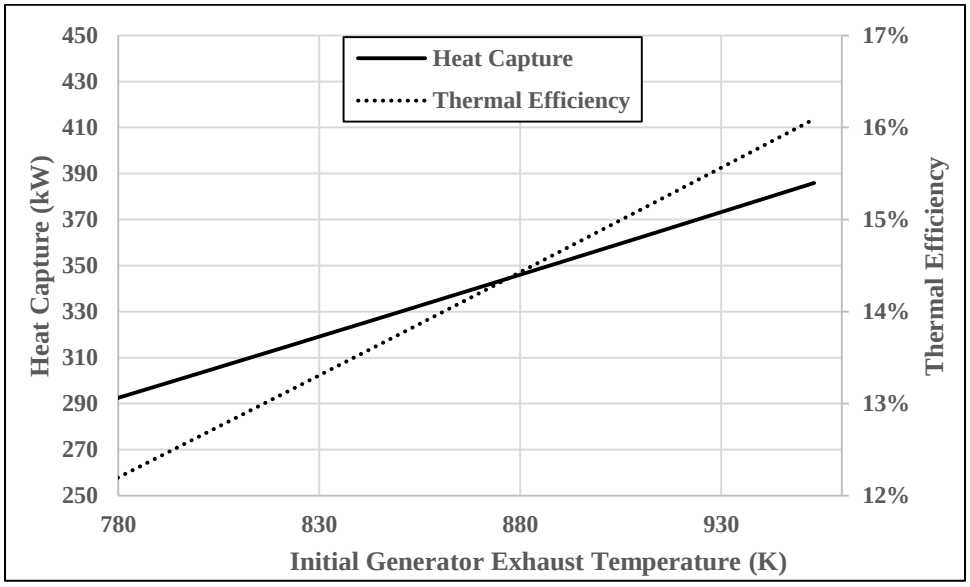

Figure 42. Sensitivity results of varying initial generator exhaust temperature.

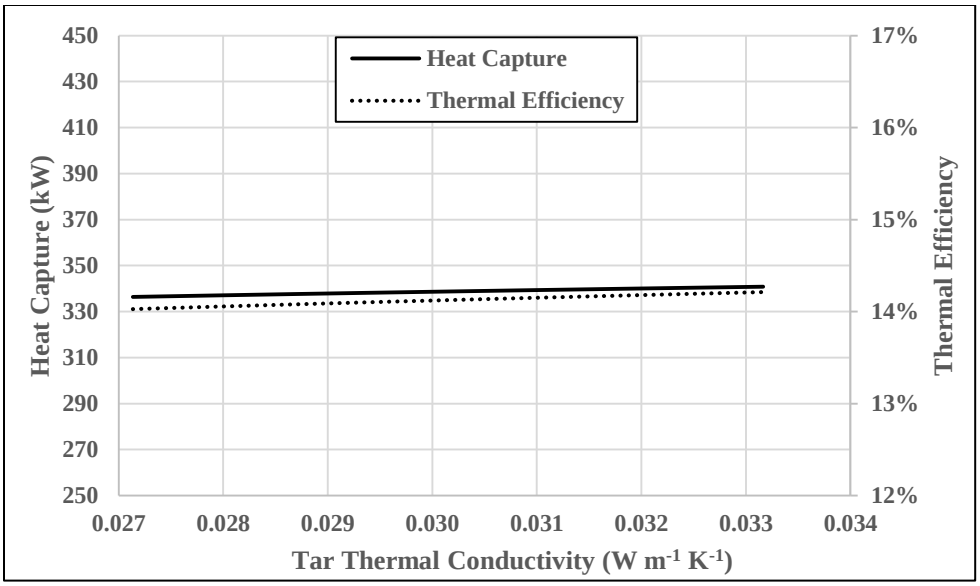

Figure 43. Sensitivity results of varying tar thermal conductivity.

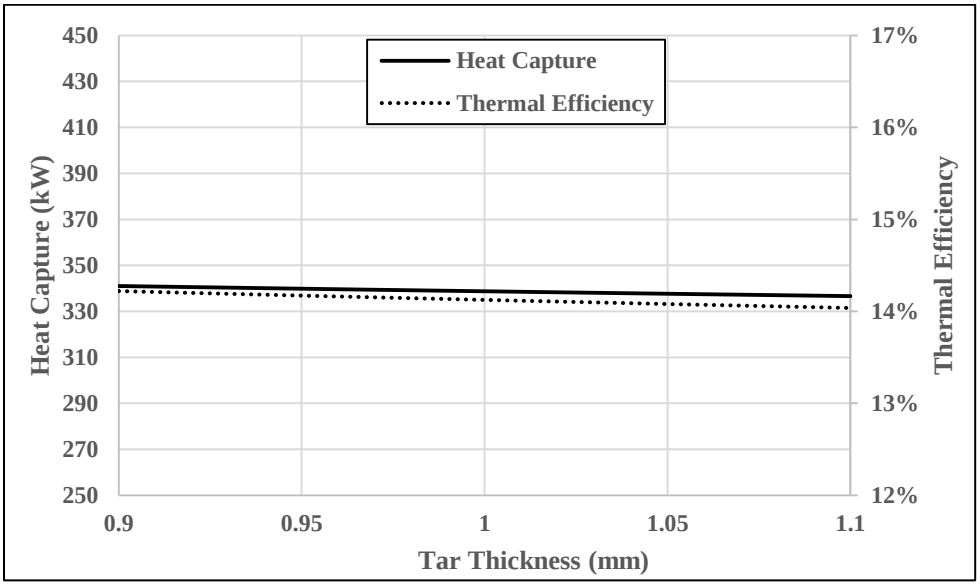

Figure 44. Sensitivity results of varying tar thickness.

capture and thermal efficiency. A constant thickness of biochar layer was assumed to be 1 mm, which was the other constituent of the fouling layer. Since the HRS was composed of only two heat exchangers for syngas heat recovery, k_{tar} and tar thickness had an insignificant effect on overall HRS performance.

A summary of S_r values for each input parameter can be seen in Table 21. Most sensitive input parameter was initial generator exhaust temperature, with a S_r value of 1.38. Least sensitive parameters were tar thermal conductivity and tar thickness (fouling layer) with values of 0.07 and 0.06, respectively. Variations in generator exhaust temperature were most sensitive since the HRS consisted of six heat exchangers for generator exhaust heat recovery. In contrast, sensitivity of the fouling layer was minimal since two heat exchangers were for syngas heat recovery.

Table 21. Relative sensitivity coefficient results for varying input parameters.

Input Parameter	Relative Sensitivity Coefficient, S_r
Ambient Air Temperature	0.75
F_{UA}	0.43
Syngas Mass Flow	0.55
Actual A/F Ratio	0.26
Initial Syngas Temperature	0.23
Initial Generator Exhaust Temperature	1.38
Tar Thermal Conductivity	0.07
Tar Thickness	0.06

Economic Analysis Results

Initial capital costs of the HRS was a function of number of heat exchangers for all three economic scenarios. Capital costs of the HRS is shown in Figure 45. Capital costs had a near-linear trend with number of heat exchangers, where a cost of about $4,600 and $48,000 were expected for one and ten heat exchangers, respectively. As stated previously, capital costs were a conservative assumption since parts were priced at individual retail value. For the NG BC, propane BC, and Texas gin scenarios, six, three, and 10+ heat exchangers were needed to supply sufficient thermal energy to meet demand of gins. Therefore, when number of heat exchangers exceeded thermal demand of the gin, additional capital and yearly costs negatively affected the economics for the gins.

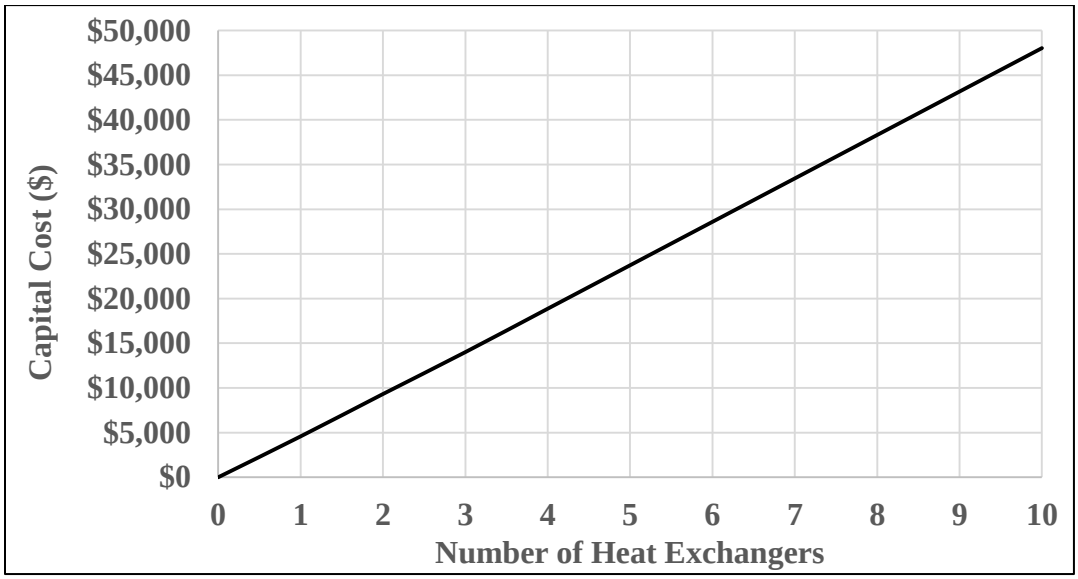

Figure 45. Initial capital cost of HRS by varying number of heat exchangers, which was around $4600 per heat exchanger.

Results of IRR for each scenario are illustrated in Figure 46. Highest IRR for NG BC, propane BC, and Texas gin were 33%, 166%, and 33%, respectively, for one heat exchanger. Increasing heat exchangers resulted in decreasing IRR for each scenario. Results between the BC NG and Texas gin scenarios were identical up to five heat exchangers. These similarities were a consequence of having the same price for NG. Also, beyond five heat exchangers, the Texas gin scenario had slightly better feasibility since increasing heat exchangers continued to supply useful thermal energy, which was not the case for the NG BC scenario. The propane BC scenario had positive feasibility up to ten heat exchangers, even though only three heat exchangers were needed to supply average thermal demand. Similar results were observed for IROR, shown in Figure 47.

Results for PBP are displayed in Figure 48. Increasing number of heat exchangers for all scenarios resulted in longer PBP. Shortest PBP for NG BC, propane BC, and Texas gin scenarios were five, one, and five years, respectively, at one heat exchanger. Differences between the NG BC and Texas gin scenarios were observed when number of heat exchangers exceeded five.

Results of IRR, IROR, and PBP for all scenarios suggested that one heat exchanger was the most economically feasible configuration of the HRS. However, the most valuable economic indicator from all scenarios was NPV, shown in Figure 49. Net present value directly correlated to useful thermal energy supplied by the HRS to meet gin demands for each scenario. Maximum NPV for the NG BC, propane BC, and Texas gin scenarios were $28,400, $148,800, and $28,400, respectively, at four, three, and four heat exchangers, respectively. Maximum NPV entailed that an optimal number of heat exchangers existed for the HRS. For NG BC and Texas gin scenarios, five heat exchangers resulted in a slightly lower NPV of $27,300, which indicated that either four or five heat exchangers were considered optimal.

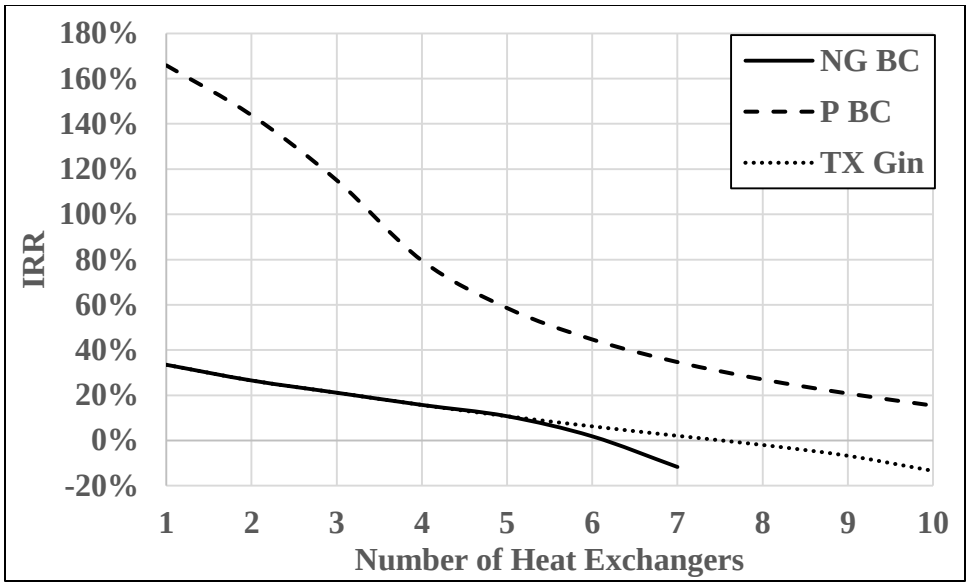

Figure 46. Results of IRR for each scenario by varying number of heat exchangers.

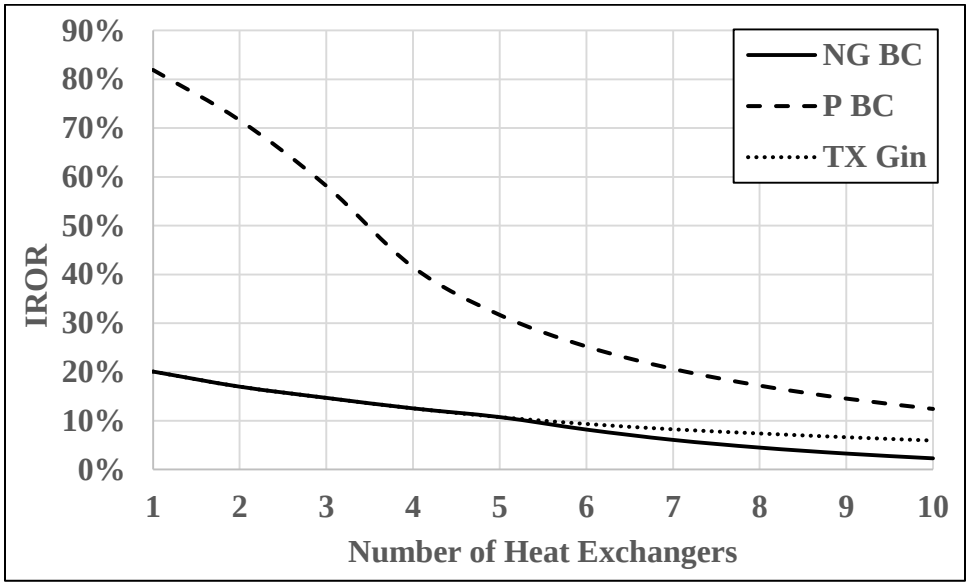

Figure 47. Results of IROR for each scenario by varying number of heat exchangers.

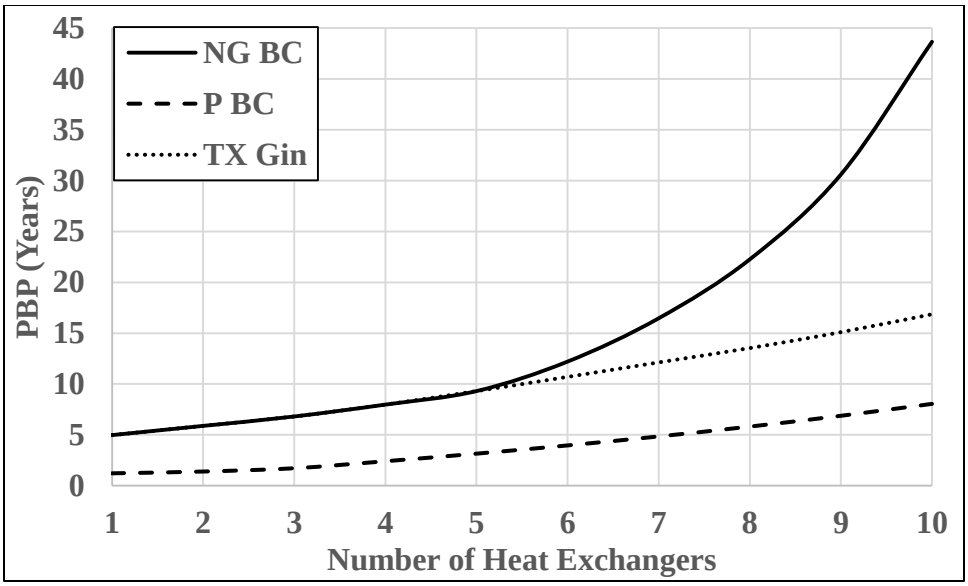

Figure 48. Results of PBP for each scenario by varying number of heat exchangers.

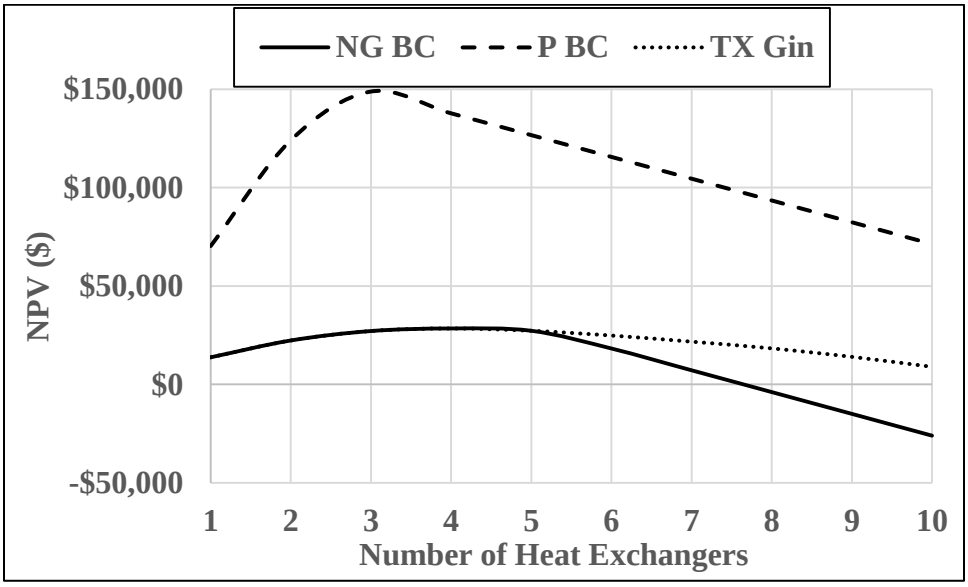

Figure 49. Results of NPV for each scenario by varying number of heat exchangers. At maximum NPV, optimal number of heat exchangers were observed at three, four and four for propane, natural gas, and Texas gins, respectively.

The propane BC scenario demonstrated very attractive economic benefits of implementing a HRS, which can be seen from all economic indicators. Cost of fuel significantly affected economic feasibility even though thermal demand for the propane BC was slightly lower than that of the NG BC scenario. Cost of propane, in terms of \$ GJ^{-1}, was more than triple compared to NG. Smaller gins, typically in rural areas, do not have access to natural gas and may not be able to get large quantity pricing. Therefore, gins that are restricted to using propane would benefit the most from a HRS.

Difference between the NG BC and Texas gin scenarios was the average thermal demand. The Texas gin scenario's demand was more than double that of the NG BC scenario, where increasing number of heat exchangers to ten continued to supply useful thermal energy. This equated to increasing yearly revenue for increasing number of heat exchangers between one and ten, but still provided the same conclusions. From this observation, a comparison between number of heat exchangers and NPV by varying thermal demand (GJ $bale^{-1}$) for natural gas was performed. Results are illustrated in Figure 50, where cost of natural gas was equal to that from the NG BC and Texas gin scenarios. At a thermal demand of 0.05 GJ $bale^{-1}$, an optimal number of heat exchangers was one, where investing in additional heat exchangers did not supply useful thermal energy. Increasing thermal demand from 0.05 to 0.11 GJ $bale^{-1}$ resulted in two to three optimal heat exchangers, while from 0.11 to 0.16 GJ $bale^{-1}$ resulted in four to five. Exceeding a demand of 0.16 GJ $bale^{-1}$ did not affect optimal number of heat exchangers, but rather demonstrated that investing in additional heat exchangers continued to provide useful thermal energy for yearly economic savings. Similar results were observed for propane gins shown in Figure 51.

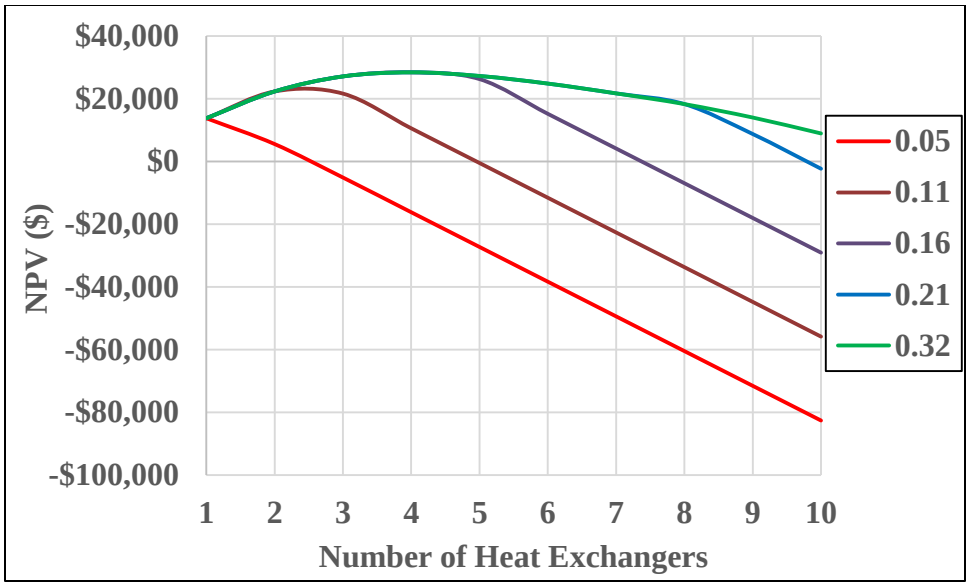

Figure 50. NPV by varying number of heat exchangers and thermal demand for natural gas gins.

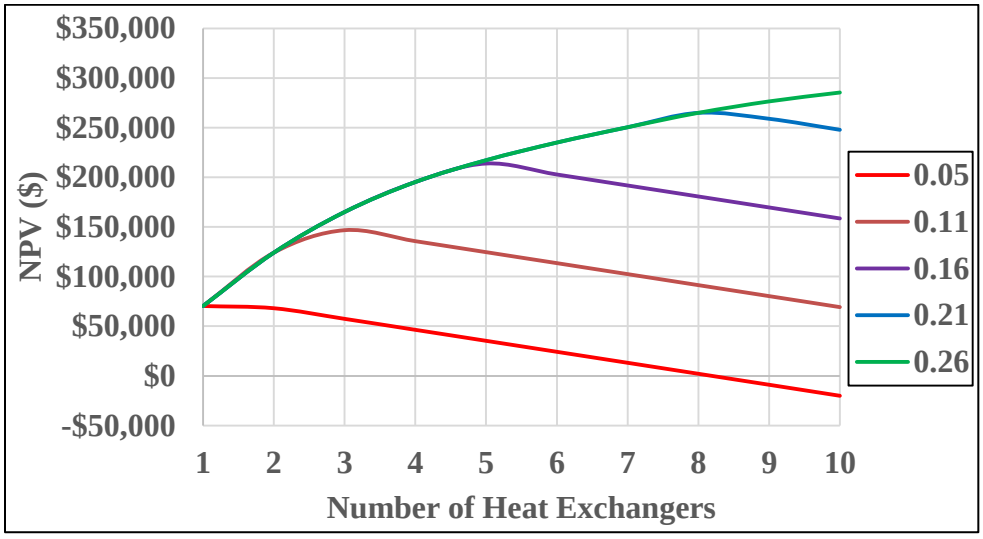

Figure 51. NPV by varying number of heat exchangers and thermal demand for propane gins.

CONCLUSIONS

Analyses of the HRS model were performed by evaluating cotton drying, sensitivity, and economics. Positive results were observed from all three sections that demonstrated beneficial implementation of a HRS for cotton drying at gins. At the conclusion of Chapter III, the initial design of the HRS was eight heat exchangers. However, both cotton drying and economic analyses revealed similar results that optimal number of heat exchangers depended on a gin's thermal demand, or how wet the cotton was. In terms of drying cotton to a targeted MC of 4%-6%, four heat exchangers were sufficient for the minimum and average initial MC's of 5.5% and 7.8%, respectively. The economics of varying number of heat exchangers contained similar results, where increasing thermal demand increased number of optimal heat exchangers. For natural gas gins, up to four or five heat exchangers were optimal beyond a demand of 0.16 GJ $bale^{-1}$. Propane gins had an increasing optimal number with increasing demand, but at an average demand of 0.11 GJ $bale^{-1}$, optimal number was three. Regardless of having an optimal number, propane gins would expect most economic benefits of investing in a HRS since price of propane was more than triple that of natural gas. Therefore, propane gins would be ideal candidates for implementing a HRS to supply their thermal energy.

The number of heat exchangers for the HRS should be evaluated case-by-case specifically for the gin where the 250 kW_e FBG would be implemented. Since the initial MC of seed cotton can vary by gin location and season, future thermal demands can have high uncertainty. Assuming an average thermal demand from TCGA annual energy surveys serves as a good approximation. Therefore, having five heat exchangers constitute as the basis of the HRS for the 250 kW_e FBG would significantly benefit cotton gins to either reduce or replace fuel usage, resulting in yearly economic savings. This recommended design of HRS would result in

about 260 kW_{th} of supplied thermal energy, thermal efficiency of 11%, and heat conversion of 1800 kJ kg_{CGT}^{-1}. Assuming an electrical efficiency of 10% from the preliminary analysis, overall efficiency of the 250 kW_e FBG system would be 21%.

CHAPTER V

CONCLUSIONS AND FUTURE RECOMMENDATIONS

Design and evaluation of a HRS specific to the 250 kW_e FBG system for cotton gins was accomplished. Five heat exchangers were recommended to capture waste heat from generator exhaust gases. This configuration served as a default for the HRS which matched the expected electricity supplied at about 6 bales per hour (bph), resulting in an expected heat capture of 260 kW_{th}, overall efficiency of approximately 21%, and heat capture conversion of 1800 kJ kg_{CGT}^{-1}. Heat recovery was only from generator exhausts since the effect of the fouling layer hindered heat capture from syngas cooling. Each of the five heat exchangers captured higher thermal energy than the initial heat exchanger from syngas cooling, which eliminated the maintenance concern of syngas heat exchangers in terms of both cleaning and corrosion. If additional heat exchangers beyond five were considered, it would be necessary to thoroughly investigate the characteristics of a particular gin, such as thermal demand and type of fuel. Implementing a HRS to the 250 kW_e FBG would classify the system as cogeneration, where gins can significantly reduce energy costs and eliminate cotton gin trash (CGT) disposal issues.

The HRS model predicted a mixed air temperature of about 116°C (240°F) for the five heat exchanger design. At this temperature, with an assumed drying time of 15 seconds, cotton drying performance was estimated with initial seed cotton moisture content (MC) from the USDA ARS data. For minimum (5.5%) and average (7.8%) initial MC, the five heat exchanger design sufficiently dried the cotton to acceptable final MC's within 4%-6%, indicating replacement of fuel usage. At maximum (12.2%) initial MC, the design significantly reduced fuel usage. Air flow from the HRS was designed for a stripper gin with an estimated bale weight of 907 kg $bale^{-1}$ (2000 lb $bale^{-1}$). The HRS can dry approximately 5400 kg hr^{-1} (12,000 lb hr^{-1}) of

cotton when initial MC is either minimum or average. When MC is maximum, heated air from the HRS could be used as preheated air for a burner, significantly reducing fuel usage.

Design of the HRS presented served as a recommendation for the configuration, operation, and number of heat exchangers for the 250 kW_e FBG system. The characteristics of heated air from the HRS were approximations developed from a heat transfer model that was corrected with actual data. Several assumptions were made for the HRS, which included dry standard ambient air, constant flow rates and temperatures of syngas and generator exhausts, no heat losses, and average fuel values reported by the Texas Cotton Ginners' Association (TCGA) surveys. However, gins may not experience these assumptions since a majority of them are uncontrollable, such as weather. One controllable factor is reducing heat losses of the HRS by insulating piping, which is highly recommended.

Heated air supplied by the HRS does not become limited to only cotton drying, but to any process that requires heated air at gins. Examples include utilizing the heated air for battery condensers and for turbulent dryer traps. By providing a constant stream of heated air, gins could either reduce fuel usage by using preheated air for burners, or completely replace fuel usage. Therefore, for a cotton gin to become completely energy independent, the long-term goal is to have multiple 250 kW_e FBG systems to supply the necessary electrical power along with thermal energy. From an economics standpoint, however, as reported by Richards et al. (2016), the optimal number of 250 kW_e FBG was to supply slightly less electricity than the gin's demand. This implied that gins would better benefit economically by purchasing small quantities of electricity from the grid.

Studies performed for this project revealed several characteristics that positively benefit the implementation of a HRS to supply thermal energy for cotton gins. Propane fuel, high fuel

costs, and high thermal demand economically favor the HRS. Winter ginning seasons and high generator exhaust temperatures increase heat capture of the HRS. Beyond the HRS, other characteristics include high disposal costs for CGT and high electricity costs.

Possible future work for the HRS could involve investigating modifications to heat exchangers. One example is type of material. From the HRS model, increasing thermal conductivity of pipes beyond the value for stainless steel did not significantly increase heat transfer. However, changing type of material might better be represented in the overall conductance correction factor, F_{UA}, which requires additional experimentation. The initial concern was that contaminants in syngas might corrode common heat exchanger materials, but this could also be true from generator exhausts. Once the FBG systems have been operated for long, continuous hours, deposits of contaminants from hot gases could be collected and analyzed. This would provide insight for candidate materials with higher thermal conductivity, such as copper, aluminum, and black iron alloys. Another modification to heat exchangers would be to investigate the addition of baffles to induce turbulence of the ambient air. The tradeoff would be between higher pressure differential of the heat exchanger, which equates to higher power consumption, and higher heat transfer.

Other future work would also be investigating methods of reducing the negative effect of the fouling layer from syngas cooling, and if present, generator exhausts. One method would be to implement catalysts in the reactor to reduce tar concentration, but the economic feasibility would also need to be evaluated. Cases where higher thermal energy is required would make this investigation more desirable. Reducing the effect of the fouling layer would increase efficiency of heat exchangers, resulting in increased heat transfer. Conclusions from this study indicated that cooling syngas may not be necessary for the cotton ginning industry due to the thermal

demand. However, other agricultural industries that have high thermal demands may be interested in FBG systems, where cooling syngas might be necessary. Each industry / facility would have to be evaluated independently.

One challenge of this project is to convince gin owners to invest in FBG systems. The major concern is that ginners do not want to take the risk as they are uncertain on the return of their investment. Informing ginners of the FBG technology and the solutions the systems provide should be done to show that cotton gins can become energy independent. In addition, several state and federal green energy incentives provide monetary support for investment in renewable energy technologies. One ideal example is the Rural Energy for America Program that provides loans and/or grants for rural agricultural facilities. Since CGT is a waste biomass, cotton gins investing in FBG systems are eligible to apply and get accepted.

REFERENCES

Al-Baghdadi, M. A. R. S. (2004). Effect of compression ratio, equivalence ratio and engine speed on the performance and emission characteristics of a spark ignition engine using hydrogen as a fuel. *Renewable Energy*, 29, 2245-2260.

Anthony, W. S., and Mayfield, W. D. (1994). *Cotton ginners handbook*. Washington, D.C: USDA ARS.

Baina, F., Malmquist, A., Alejo, L., Palm, B., and Fransson, T. H. (2015). Analysis of a high-temperature heat exchanger for an externally-fired micro gas turbine. *Applied Thermal Engineering*, 75, 410-420.

Barker, G. L., and Laird, J. W. (1993). Drying and humidification rates for cotton lint. *Transactions of the ASAE*, 36(6), 1555 – 1562.

Bergman, T. L., and Lavine, A. S. (2011). *Fundamentals of heat and mass transfer* (7th ed.). Danvers, MA: John Wiley and Sons.

Buffler, A. J. (1977). Three years' experience with a heat-recovering incinerator in north Alabama. Agro-industrial report, Cotton Incorporated. 4(8): 35-36.

Capareda, S. C. (1990). Studies on activated carbon produced from thermal gasification of biomass wastes. PhD diss. College Station, Texas: Texas A&M University, Department of Agricultural Engineering.

Capareda, S. C., and Maglinao, A. L. (2018). Pre-commercialization studies of the AgriLife Research fluidized bed gasification system using cotton gin trash. Beltwide Cotton Conf. Proc.

Dowd, M. K., Pelitire, S. M., and Delhom, C. D. (2018). Molecular biology and physiology: Seed-fiber ratio, seed index, and seed tissue and compositional properties of current cotton cultivars. *Journal of Cotton Science*, 22, 60-74.

Francois, J., Abdelouahed, L., Mauviel, G., Patisson, F., Mirgaux, O., Rogaume, C., . . . Dufour, A. (2013). Detailed process of modeling of a wood gasification combined heat and power plant. *Biomass and Bioenergy*, 51, 68-82.

Funk, P. A., and Hardin, R. G. (2017). Engineering and ginning: Energy utilization and conservation in cotton gins. *Journal of Cotton Science*, 21, 156-166.

Haan, C. T. (2002). *Statistical methods in hydrology* (2nd ed.). Ames: Iowa State Press.

Henderson, S. M., Perry, R. L., and Young, J. H. (1997). *Principles of process engineering* (4th ed.). St. Joseph, MI: American Society of Agricultural Engineers.

Hesselgreaves, J.E. (2002). An approach to fouling allowances in the design of compact heat exchangers. *Applied Thermal Engineering*, 22, 755-762.

Kiel, J. H. A., van Paasen, S. V. B., Neeft, J. P. A., Devi, L., Ptasinski, K. J., Janssen, F. J. J. G., . . . Bramer, E. A. (2004). Primary measures to reduce tar formation in fluidized-bed biomass gasifiers. Final report SDE project P1999-012.

Laird, J. W., and Barker, G. L. (1995). Time relationships for drying cotton. ASAE Annual Int. Meeting.

Laird, J. W., and Barker, G. L. (1996). Cotton gin drying time relationships. Beltwide Cotton Conf. Proc.

Lee, S., and Bae, C. (2008). Design of a heat exchanger to reduce the exhaust temperature in a spark-ignition engine. *Internal Journal of Thermal Sciences*, 47, 468-478.

LePori, W. A., and Soltes, E. J. (1981). Thermochemical conversion for energy and fuel. In *Biomass energy: a monograph* (pp. 9-74). College Station, Texas: Texas A&M University Press.

Li, W., Liu, Z., Wang, Z., Dou, H., Wang, C., and Li, J. (2016). Experimental and theoretical analysis of effects of equivalence ratio on mixture properties, combustion, thermal efficiency and exhaust emissions of a pilot-ignited NG engine at low loads. *Fuel*, 171, 125-135.

Maglinao, A. L. (2009). Instrumentation and evaluation of a pilot scale fluidized bed biomass gasification system. MS thesis. College Station, Texas: Department of Biological and Agricultural Engineering.

Maglinao, A. L. (2013). Development of a segregated municipal solid waste gasification system for electrical power generation. PhD Diss. College Station, Texas: Department of Biological and Agricultural Engineering.

Maglinao, A. L., Capareda, S. C., and Nam, H. (2015). Fluidized bed gasification of high tonnage sorghum, cotton gin trash and beef cattle manure: Evaluation of synthesis gas production. *Energy Conversion Management*, 105, 578-587.

McCaskill, O. L., Wesley, R. A., and Anthony, W. S. (1977). Progress of incineration research at Stoneville. Agro-industrial report, Cotton Incorporated. 4(8): 11-15.

NCC. (2018). 2018 Cotton economic outlook. Reports and publications. Memphis, Tennessee: NCC. Accessed April 13, 2018. Available at www.cotton.org

Newman, A. B. (1932). The drying of porous solids: Diffusion calculations. *Transactions of American Institute of Chemical Engineers*, 27, 310-333.

Nwokolo, N., Mamphweli, S., and Makaka, G. (2016). An investigation into heat recovery from the surface of a cyclone dust collector attached to a downdraft biomass gasifier. *Applied Thermal Engineering*, 98, 1158-1164.

Parnell, C. B. Jr. (1977). Methods of composting ginning waste. Agro-industrial report, Cotton Incorporated. 4(8): 37-40.

Parnell, C. B. Jr. (1996). Cyclone design for air pollution abatement associated with agricultural operations. Beltwide Cotton Conf. Proc.

Permatasari, R., and Yusuf, A. M. (1977). Material selection for shell and tube heat exchanger using computational fluid dynamics method. AIP Conf. Proc.

Richardson, J. W., Herbst, B., McGee, R., and Oosthuizen, W. (2016). Economic feasibility analysis for a cotton gin trash gasifier. Agricultural and Food Policy Center. Available at https://www.afpc.tamu.edu/

Riggs, J. L. (1968). *Economic decision models for engineers and managers*. New York: McGraw-Hill.

Schaafhausen, S., Borner, F. D., Chand, T., Lippmann, W., Hurtado, A., and Muller, M. (2015). Corrosion of laser joined silicon carbide in gasification environment. *Advances in Applied Ceramics*, 114, 350-360.

Sixto, J. M. C., Parnell, C. B. Jr., and LePori, W. A. (1999). Reducing nitrogen oxide emissions by staged combustion of low calorific value gas derived from agricultural wastes. *J. agric. Engng Res.*, 74, 111-120.

Skorek-Osikowska, A., Bartela, L., Kotowicz, J., Sobelweski, A., Iluk, T., and Remiorz, L. (2014). The influence of the size of the CHP (combined heat and power) system integrated with a biomass fueled gas generator and piston engine on the thermodynamic and economic effectiveness of electricity and heat generation. *Energy*, 67, 328 – 340.

TCGA. (2010 – 2017). TCGA gin operating cost survey. Austin, Texas: TCGA.

Thapa, S., Bhoi, P. R., Kumar, A., and Huhnke, R. (2017). Effects of syngas cooling and biomass filter medium on tar removal. *Energies*, 10, 349, 1-12.

Thomas, J. W., Cory, M. D., Rutherford, R. D., & Sutton, R. (2018). Bio-generation, a solution to gin waste disposal. Beltwide Cotton Conf. Proc.

USDA. (2016). Ginned cotton in United States: 2016. National Agricultural Statistics Database. Washington, D.C.: USDA National Agricultural Statistics Service. Accessed 27 July 2017. Available at: www.nass.usda.gov

Usowics, B., Lipiec, J., Lukowski, M., Marczewski, W., and Usowicz, J. (2016). The effect of biochar application on thermal properties and albedo of loess soil under grassland and fallow. *Soil & Tillage Research*, 164, 45-51.

Wang, J., Yang, K., Xu, Z., and Fu, C. (2015). Energy and exergy analyses of an integrated CCHP system with biomass air gasification. *Applied Energy*, 142, 317-327.

Winterton, R.H.S. (1998). Where did the Dittus and Boelter equation come from? *Int. J. Heat and Mass Transfer*, 41, 809.

APPENDIX A. GENERATOR ELECTRICAL AND EXHAUST SPECIFICATIONS

Table 22. Fuel usage at various loads of 30 kW Generac generator.

Electrical Output	Natural Gas (ft^3/hr)	Propane (gal/hr)
Exercise cycle	60	0.7
25% of rated load	240	2.6
50% of rated load	320	3.5
75% of rated load	400	4.4
100% of rated load	492	5.4

Table 23. Generator exhaust properties at rated load for 30 kW Generac.

Exhaust Property at Rated Load	Value	Units
Flow at rated output	237	$ft^3\ min^{-1}$
Temperature at muffler outlet	610	°C

APPENDIX B. FAN CURVE OF HP BLOWER FOR HRS

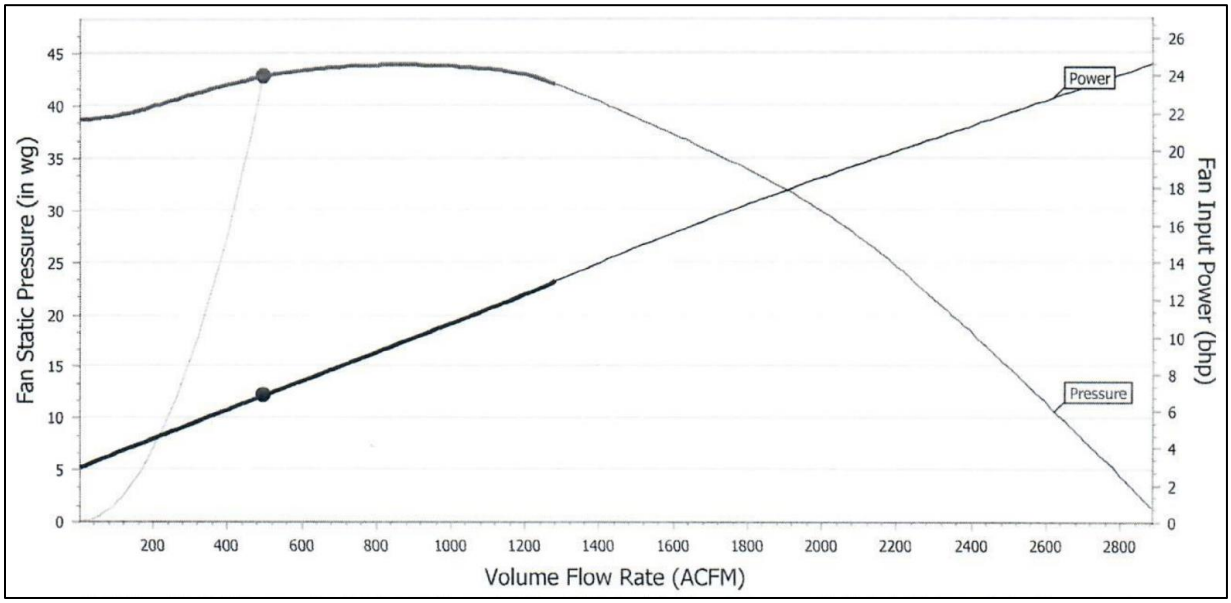

Figure 52. Fan curve for each HP blower for heat exchangers. Operating point of 500 acfm allowed sufficient static pressure for heat exchangers.

APPENDIX C. TEXAS COTTON GINNING INFORMATION

Table 24. Initial moisture contents of incoming seed cotton at a Texas gin from USDA ARS.

Interval [#]	Average Initial MC [% d.b.]	Minimum Initial MC [% d.b.]	Maximum Initial MC [% d.b.]	Std. Deviation MC [% d.b.]
1	8.2%	6.1%	12.2%	1.5%
2	6.3%	5.5%	7.2%	0.5%
3	8.8%	7.3%	10.9%	0.9%

Table 25. Summary of TCGA energy data for years 2010 to 2017.

	Electricity		Natural Gas		Propane	
Year	Average Usage per Bale [kW-hr/bale]	Average Cost per Unit [$/kW-hr]	Average Cost per Unit [$/GJ]	Average Usage per Bale [GJ/bale]	Average Cost per Unit [$/GJ]	Average Usage per Bale [GJ/bale]
2010	41.0	0.08	4.34	0.17	17.43	0.08
2011	40.9	0.09	4.82	0.13	18.99	0.05
2012	43.5	0.08	4.34	0.13	14.01	0.10
2013	44.8	0.08	4.83	0.18	19.72	0.11
2014	43.4	0.09	5.12	0.16	14.94	0.11
2015	40.3	0.08	3.73	0.20	10.38	0.13
2016	41.5	0.08	4.86	0.19	12.04	0.12
2017	41.7	0.08	4.46	0.16	14.32	0.15
Average	**42.1**	**0.08**	**4.56**	**0.16**	**15.23**	**0.11**

Table 26. Texas ginning seasons by region.

Region	Ginning Season
South Texas	July 15 - October 30
Blackland	August 15 - November 30
Rolling Plains	October 1 - January 30
Far West	October 1 - January 30
High Plains	September 15 - February

APPENDIX D. PARTS DESCRIPTION FOR HRS

Table 27. Part description for components of HRS.

Part	Description
Inner Pipe	4 in. pipe, 19 ft. long
Outer Pipe	6 in. pipe, 18 ft. long
Plate	8 in. x 8 in. x 1/4 in.
Air Inlet / Outlet	3 in. pipe, 3 in. long
Elbow	4 in. pipe, 90°
Pipe Nipple	4 in. pipe, 8 in. long